CAL Report No. UM-2929-E-1

RF PARAMETER STUDY IN SUPPORT OF STRUCTURES FOR ORBITING RADIO TELESCOPES (SORT)

Stephen N. Andre, Richard J. Blum and John O. Clark
Cornell Aeronautical Laboratory, Inc.
4455 Genesee Street
Buffalo, New York 14221

October 1970

Final Report January–October 1970

Prepared for

NATIONAL AERONAUTICS AND SPACE ADMINISTRATION
GODDARD SPACE FLIGHT CENTER
Greenbelt, Maryland 20771

TECHNICAL REPORT STANDARD TITLE PAGE

1. Report No.	2. Government Accession No.	3. Recipient's Catalog No.

4. Title and Subtitle

RF PARAMETER STUDY IN SUPPORT OF STRUCTURES FOR ORBITING RADIO TELESCOPES (SORT)

5. Report Date October 1970

6. Performing Organization Code

7. Author(s)

Stephen N. Andre, Richard J. Blum and John O. Clark

8. Performing Organization Report No.

CAL No. UM-2929-E-1

9. Performing Organization Name and Address

Cornell Aeronautical Laboratory, Inc.
4455 Genesee Street
Buffalo, New York 14221

10. Work Unit No.

11. Contract or Grant No.

NAS 5-21134

12. Sponsoring Agency Name and Address

National Aeronautics and Space Administration
Goddard Space Flight Center
Greenbelt, Maryland 20771

13. Type of Report and Period Covered

Final Report
28 January - 28 October 1970

14. Sponsoring Agency Code

15. Supplementary Notes

16. Abstract

The objective of this program was to provide a study of RF parameters of an orbiting 100-meter-diameter flight test model of a LOw Frequency Radio Telescope (LOFT) operating in the 15- to 150-MHz frequency band. The study included investigations of dual-polarized antenna feeds and the characteristics of the reflector grid. A tradeoff study to establish design parameters of the LOFT antenna was also performed. Computer programs were developed to investigate effects of both axissymmetric and ϕ-dependent reflector surface errors on the far-field radiation patterns.

The trapezoidal tooth antenna feed is recommended for the LOFT antenna application as a result of the feed study. The investigation of reflector grids resulted in a characteristic curve of grid performance versus grid mass.

Far-field antenna patterns at and near the mainlobe were determined by a surface current integral formulation. In the angular region far from the mainlobe and in the shadow region behind the reflector, Geometrical Diffraction Theory was used to determine the radiation characteristics of the reflector.

The tradeoff study to establish LOFT design parameters resulted in a recommended design. The LOFT performance characteristics for the selected design are also included.

17. Key Words	18. Distribution Statement
Reflector antennas Radio astronomy Reflector surface errors Antenna computer programs Antenna feeds	

19. Security Classif. (of this report)	20. Security Classif. (of this page)	21. No. of Pages	22. Price
UNCLASSIFIED	UNCLASSIFIED	150	

Form DOT F 1700.7 (8-69)

PREFACE

The objective of this program was to provide a study of RF parameters of an orbiting 100-meter-diameter flight test model of a LOw Frequency Radio Telescope (LOFT) operating in the 15- to 150-MHz frequency band. The study included investigations of dual-polarized antenna feeds and the characteristics of the reflector grid. A tradeoff study to establish design parameters of the LOFT antenna was also performed. Computer programs were developed to investigate effects of both axisymmetric and ϕ -dependent reflector surface errors on the far-field radiation patterns.

The trapezoidal tooth antenna feed is recommended for the LOFT antenna application as a result of the feed study. The investigation of reflector grids resulted in a characteristic curve of grid performance versus grid mass.

Far-field antenna patterns at and near the mainlobe were determined by a surface current integral formulation. In the angular region far from the mainlobe and in the shadow region behind the reflector, Geometrical Diffraction Theory was used to determine the radiation characteristics of the reflector.

The tradeoff study to establish LOFT design parameters resulted in a recommended design. The LOFT performance characteristics for the selected design are also included.

FOREWORD

This report was prepared by the Electronics Research Department of Cornell Aeronautical Laboratory for NASA-Goddard Space Flight Center under Contract No. NAS5-21134.

The suggestions of Mr. William Hibbard and Mr. Gay Hilton of NASA - GSFC, in establishing LOFT performance goals and tradeoffs are acknowledged. Data on the LOFT configuration and reflector surface errors was provided by Dr. John Hedgpeth of Astro Research Corporation.

The authors wish also to thank Mr. James Dearlove of CAL for his assistance in preparing the computer program for asymmetric reflectors. The contribution of Mr. B. Riley Tripp in preparing this report, and for his valuable suggestions, are also acknowledged.

TABLE OF CONTENTS

TABLE OF CONTENTS (Cont.)

LIST OF ILLUSTRATIONS

LIST OF ILLUSTRATIONS (Cont.)

LIST OF TABLES

Section 1
INTRODUCTION AND SUMMARY

1.1 INTRODUCTION

The objective of this program was to provide a study of RF parameters in support of a Structure for Orbiting Radio Telescope (SORT) research program in progress at NASA-GSFC. The SORT program has developed the technology necessary for the design of large-diameter space structures, the ultimate objective being a 1500-meter-diameter LOw Frequency Radio Telescope (LOFT) antenna. Placed in a high orbit above ionospheric noise and absorption, the LOFT would serve the needs of radio astronomy in the 0.5- to 10-MHz frequency region. The study performed by CAL was directed to a 100-meter-diameter LOFT flight test model with operation in the 15- to 150-MHz frequency region.

The LOFT overall structural configuration consists of a centrifugally suspended reflector grid of flexible filaments held in a parabolic shape by front and back tension stays (Figure 1). The stays emanate from either end of a deployable mast, which is extended along the spin axis to form a central compression column. A broadband antenna feed structure, which illuminates the reflector, is attached at the forward end of the column. Additional information on the LOFT configuration and potential applications is provided by References 1-4.

The three main areas of investigation were:

(1) Antenna feed definition

(2) Parametric study of the gridded reflector

(3) Reflector far-field patterns.

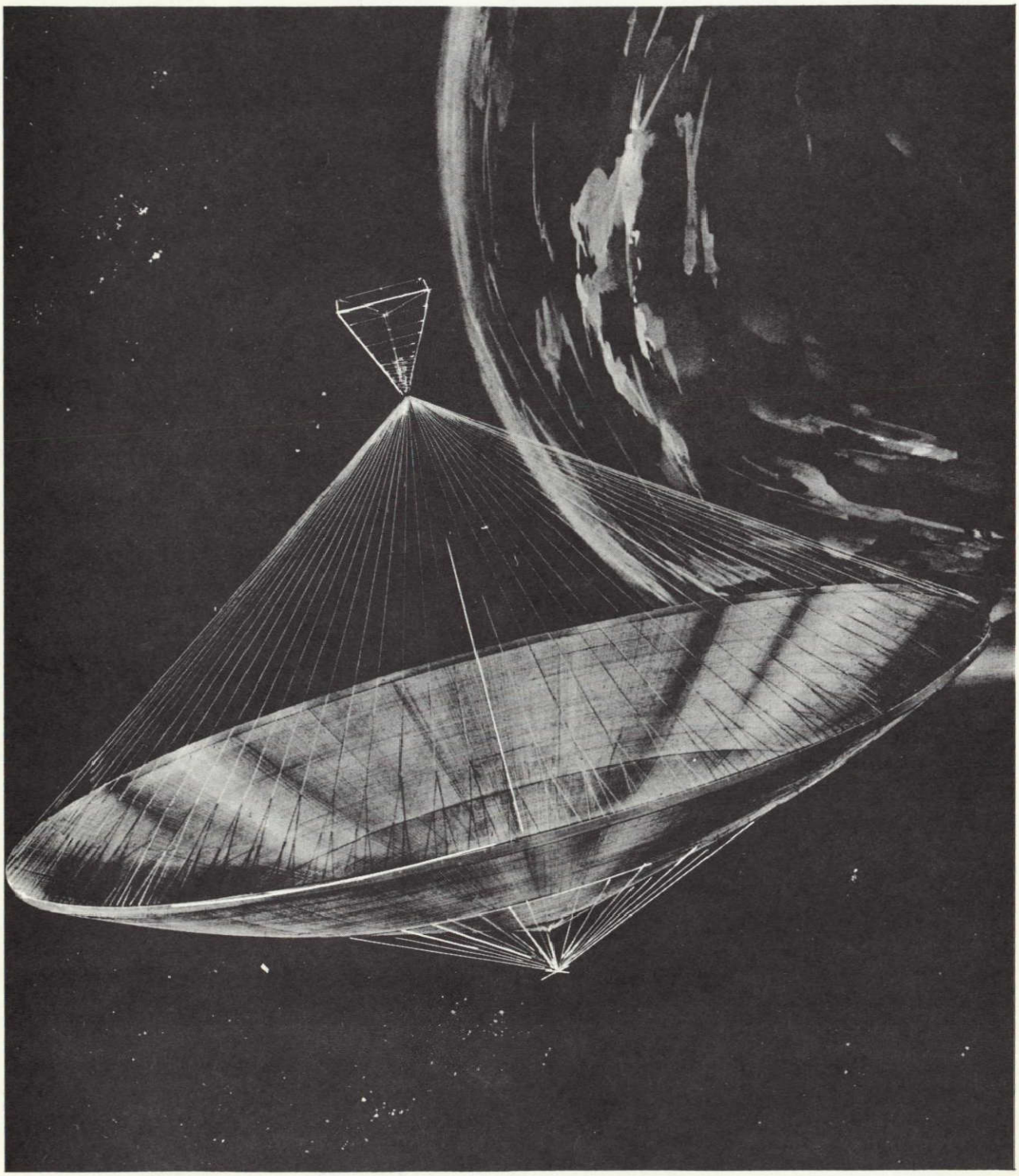

Figure 1 LOFT BASELINE CONCEPT (REFERENCE 4)

The key factors considered during performance of these studies are discussed below.

The antenna feed requirements called for continuous coverage over the 15- to 150-MHz frequency band and simultaneous dual-polarization capability (either two-axis linear or right-left circular). A wide variety of antenna feeds were considered and their applicability to LOFT was determined. As a result of this initial investigation, two feed antenna types (the log-periodic dipole and trapezoidal tooth) were selected as potential candidates and investigated in detail.

The reflector grid, comprised of conducting ribbons, was investigated to determine effects on the reflector far-field patterns as a function of the reflector weight. Three major effects were investigated: (1) RF leakage into the region behind the reflector, (2) antenna gain behavior with variations in grid reflection coefficient and ohmic loss, and (3) increases in near-sidelobe levels due to aperture phase errors caused by the reflector grid. The results are presented in Sections 3 and 4. Results of the grid-performance versus grid-weight investigation are reported in Section 3.

Computed reflector far-field patterns were used to quantify the effects of the antenna feed, reflector grid and reflector surface distortions on LOFT antenna performance. These patterns were calculated using surface current integrals, implemented in computer programs, for the angular region embracing the mainlobe and first few sidelobes. For the axisymmetric reflector (surfaces of revolution) cases, an existing computer program was modified to include the effects of the reflector grid. A second computer program, developed by CAL, was used to study asymmetric reflector cases. The latter program accounted for the surface distortions of the reflector attributable to thermal and torque effects. The radiation patterns far from the mainlobe and in the shadow region behind the reflector were calculated by the Geometrical Diffraction Theory (GDT) procedures previously developed at CAL. Results are given in Section 5.

Investigations were performed to determine the effects on LOFT far-field antenna patterns of

(1) displacement of the feed antenna phase center from the reflector focus

(2) feed antenna amplitude patterns

(3) variation of reflector F/D in the range of 0.3 to 0.5

(4) reflector grid electrical parameters

(5) approximation of a parabolic reflector by two conics in the central region of the reflector

(6) thermal and torque surface distortions

(7) feed antenna aperture blockage.

The effects of small-scale reflector surface irregularities were also determined using available theory for random surface errors.

A summary of the report is given in Section 1.2. Conclusions and Recommendations are included in Section 6.

1.2 SUMMARY

1.2.1 Antenna Feed

The results of the antenna feed investigation are given in Section 2. A summary of performance characteristics of the feeds investigated is given in Table 1. The trapezoidal tooth and log-periodic dipole feeds were selected for further detailed investigation and calculation of reflector antenna patterns. The trapezoidal tooth feed is recommended as a result of the antenna pattern studies.

Table 1
FEED INVESTIGATION SUMMARY

FEED TYPE[1]	10-dB BEAMWIDTH[2] (degrees) E	H	CROSS-POLARIZATION (dB)	PHASE[3] CENTER DISPLACEMENT (WAVELENGTHS)	SIDELOBE[4] LEVEL (dB)	APERTURE[5] EFFICIENCY (%)	COMMENTS
TRAPEZOIDAL TOOTH	110	110	10 TO 15	0.2 TO 0.4	20	60 TO 75	RECOMMENDED FEED AT PRESENT
TRIANGULAR TOOTH	110	110	12 TO 15*	0 3 TO 0.4*	20*	60 TO 75*	MAY HAVE LESS CROSS-POLARIZATION THAN TRAPEZOIDAL TOOTH FEED
ZIG-ZAG WIRE	100	110	12 TO 15*	0.85	20*	60*	LARGE PHASE CENTER DISPLACEMENT
LOG-PERIODIC DIPOLE	110	170	25	0.7	17	45 TO 55	SHOULD BE INVESTIGATED FURTHER IF CROSS-POLARIZATION OF TOOTH FEEDS IS TOO LARGE
SHORTENED-ELEMENT LPD	110	170	25	0.7 TO 1.2	17*	45 TO 55*	MECHANICAL POSITIONING REQUIRED WHEN OPERATING FREQUENCY IS CHANGED
VEE ELEMENT LPD	110	170	25	0.7	17*	45 TO 55*	CAN NOT EQUALIZE E- AND H-PLANE BEAMWIDTHS
CONICAL SPIRAL	110		LARGE	0.6	20*	60 TO 70*	CONTRAWOUND VERSIONS HAVE LARGE CROSS POLARIZATION
MULTITURN HELIX	30 TO 100		20	?	–	LOW*	BEAMWIDTH TOO NARROW AND VARIES WITH FREQUENCY
CONICAL TRANSMISSION LINE	NOT APPLICABLE		LARGE	0.0	15 TO 17	30	50 PERCENT SPILLOVER LOW GAIN. HIGH SIDELOBES

(1) FIRST SIX FEEDS PROVIDE ORTHOGANAL LINEAR POLARIZATION LAST THREE FEEDS PROVIDE DUAL-SENSE CIRCULAR POLARIZATION

(2) A 110^{o} BEAMWIDTH IS OPTIMUM, WHEN THE REFLECTOR F/D RATIO IS 0.5. H-PLANE BEAMWIDTH CAN BE MADE MORE OR LESS THAN 110^{o} WITH OTHER DESIGNS, BUT E-PLANE BEAMWIDTH OF THE LINEAR POLARIZED FEEDS CANNOT BE MADE LARGER THAN 110^{o}

(3) PHASE CENTER DISPLACEMENT RELATIVE TO FEED VERTEX

(4) SIDELOBE LEVEL OF LOFT REFLECTOR USING A PARTICULAR FEED. (NOT SIDELOBE LEVEL OF FEED ITSELF)

(5) APERTURE EFFICIENCY IS RATIO OF REFLECTOR ANTENNA GAIN USING A PARTICULAR FEED TO THE GAIN OF A UNIFORMLY ILLUNIMATED APERTURE ANTENNA HAVING NO SPILLOVER.

*ESTIMATE

1.2.2 Reflector Grids

Section 3 of the report describes the theory of reflecting grids and tradeoffs relative to the LOFT application. The results of the study show that the following guidelines should be used in the selection of a grid.

- It is not important whether the orthogonal conductors are connected at the junctions because the angle of incidence of the feed field onto the reflector is relatively small (less than 40 degrees for any reflector whose F/D ratio is 0.3 or greater).
- A square mesh should be used rather than a rectangular mesh to keep the polarization of the reflected field nearly the the same as that of the incident field.
- Conductor thickness and conductivity need only be large enough so that the term involving strip impedance, Z, is small relative to other terms. As shown in Section 3, stainless steel conductors only 6.35 microns thick will suffice and aluminum conductors could be even thinner.
- A uniform-size mesh should be used throughout the reflector surface to minimize phase error attributable to the grid.
- The grid must have continuity in orthogonal directions; a weave with poor contact between adjacent conductors is unsuitable.
- The grid has the most effect on radiation patterns at the highest operating frequency.

1.2.3 Radiation Near Mainlobe

Radiation characteristics of the LOFT antenna at and near the mainlobe are given in Section 4. Tradeoffs relative to antenna feed selection, reflector F/D ratio, effects of reflector surface errors, antenna feed aperture

blockage and the reflector grid are described in detail. Reflector far-field patterns illustrating the tradeoffs are provided. The following trends and conclusions were derived from the antenna pattern data:

- The conic surfaces degrade performance more at high frequencies than at low frequencies.
- Feed phase center displacement degrades performance more at low frequencies than at high frequencies. This occurs because phase displacement was deliberately minimized at high frequency.
- At 15 and 30 MHz, some of the tabulated sidelobe levels are not much higher when feed phase error is included. This occurs because the first one or two sidelobes blend into the mainlobe. The deleterious effect of feed phase error will then show up as a much wider mainlobe beamwidth at the 20-dB points.
- Feed phase center displacement relative to the reflector focal point should be less than 0.4 wavelengths. This can be accomplished with a fixed position, trapezoidal tooth antenna but not with a fixed position, log-periodic dipole antenna.
- The optimum reflector F/D ratio using a trapezoidal tooth feed is 0.5, if maximum gain is desired. When conic surfaces and feed phase center errors are included, the worst case sidelobe level is 19 dB. If F/D = 0.4 is used, gain is lower by 0.4 to 0.6 dB and the worst-case sidelobe level is 20 dB.
- The optimum reflector F/D ratio using a log-periodic dipole feed is 0.4. The worst case sidelobe level is 17 dB and the gain is 0.7 to 1.6 dB lower than the gain obtainable with a trapezoidal tooth feed.
- Patterns using a trapezoidal tooth feed are essentially axisymmetric. E-plane patterns using a log-periodic dipole feed have 10 to 15 percent wider beamwidth than the H-plane

patterns. Some radio astronomy applications require an axisymmetric mainlobe.

- Cross-polarization in the 45° plane is 1 to 2 dB worse using a log-periodic dipole feed as compared to a trapezoidal tooth feed. It is emphasized that cross coupling in the feed has been neglected. A small F/D ratio also degrades the cross-polarization.
- Surface errors due to thermal and torque effects will not seriously degrade antenna performance.

1.2.4 Radiation Far From Mainlobe

In Section 5, the radiation characteristics of LOFT in the region far from the mainlobe and in the shadow region behind the reflector are described. Far from the mainlobe, in the illuminated region in front of the reflector, the principal radiation components are direct radiation from the feed, scattering from the random perturbations of the reflector surface and diffraction from the reflector. Geometrical Diffraction Theory (GDT) is used to provide calculations of the pattern from the reflector in this region. In the shadow region, tradeoffs relative to leakage of feed radiation through the reflector grid are discussed. It was found that:

- In the illuminated region, direct feed radiation is the most significant radiation mechanism (for random surface error less than 0.03-m RMS).
- In the shadow region at the higher frequencies, feed leakage through the reflector grid for typical grid designs is larger than diffraction around the reflector.
- Reflector panel billowing should be kept below 0.03 meter RMS (0.1-m peak-to-peak) to keep far-out sidelobe level below that due to other radiation sources.

- A reflector grid with 8.6-dB transmission loss at 150 MHz gives feed leakage in the shadow region 40 dB below the mainlobe peak across the 15- to 150-MHz frequency band.
- The gain in the backlobe direction is -1.0 dB relative to isotropic, independent of frequency.
- An F/D of 0.4 instead of 0.5 can reduce sidelobe level only in the shadow region (due to reduced reflector edge illumination) but feed leakage through the reflector grid must be significantly reduced for a reduced sidelobe level to be realized.

Conclusions and recommendations derived from the study results are given in Section 6. Section 6 also presents the parameters and expected performance characteristics of an optimum 100-meter-diameter LOFT antenna configuration.

Section 2
ANTENNA FEED INVESTIGATION

The feed antenna is placed at the focal point of the parabolic reflector to receive the radio energy redirected from the reflector. The feed should meet the following requirements:

- Frequency: 15 to 150 MHz, preferably without electrical or mechanical tuning.
- Feed Amplitude Pattern: Proper beamwidth for illumination of a parabolic reflector with F/D ratio between 0.3 and 0.5. The pattern should be frequency independent and axisymmetric.
- Feed Phase Pattern: There should be a point on the feed antenna about which the feed phase is constant. This point (called the phase center) can be placed at the focal point of the parabolic reflector and thus minimize aperture phase error due to the feed. Ideally, the location of the feed phase center should remain stationary with frequency variations.
- VSWR: Low (e.g., < 3:1) over the entire frequency range, preferably without mechanical or electrical tuning.
- Polarization: Polarization diversity is required. The feed should provide either orthogonal linear or dual-sense circular polarization.
- Structural Requirements: The feed structure should be sufficiently simple to permit deployment in orbit.

The properties of feed antennas investigated on this program are described hereinafter.

The following antennas are discussed:

LINEAR POLARIZED FEEDS

Log-Periodic Dipole Array
Shortened Element Log-Periodic Dipole Array
Log-Periodic Vee Dipole Array
Trapezoidal Tooth Array
Triangular Tooth Array
Zig-Zag Wire Array

CIRCULAR POLARIZED FEEDS

Conical Spiral
Multiturn Cylindrical Helix

CONICAL TRANSMISSION LINE FEED

Table 1 provides a summary of the results of the antenna feed investigation. Two feeds were selected as providing the best match to the LOFT feed antenna requirements: the trapezoidal or triangular tooth feeds. These feeds, along with the log-periodic dipole array as an alternate, were investigated in greater detail. Results of these further investigations are given in Sections 4 and 5.

2.1 LINEAR POLARIZED FEEDS

2.1.1 Log-Periodic Dipole Array (Figure 2(A))

The log-periodic dipole array [5] has 3-dB and 10-dB E-plane beamwidths of about 60° and 110°, respectively, and this beamwidth is practically invariant (± 10 percent) for all designs which give a well-formed antenna pattern. The H-plane 3-dB beamwidth can be varied from 90° to 140° and the 10-dB beamwidth from 150° to 260°. The narrower beamwidth is achieved with a long array having a small expansion angle α and large adjacent dipole length ratio ($\tau = 0.97$). In all cases, the H-plane beamwidth is at least 1.5 times wider than the E-plane beamwidth. The phase center moves farther from the dipole array vertex (feedpoint) as the array is made with small

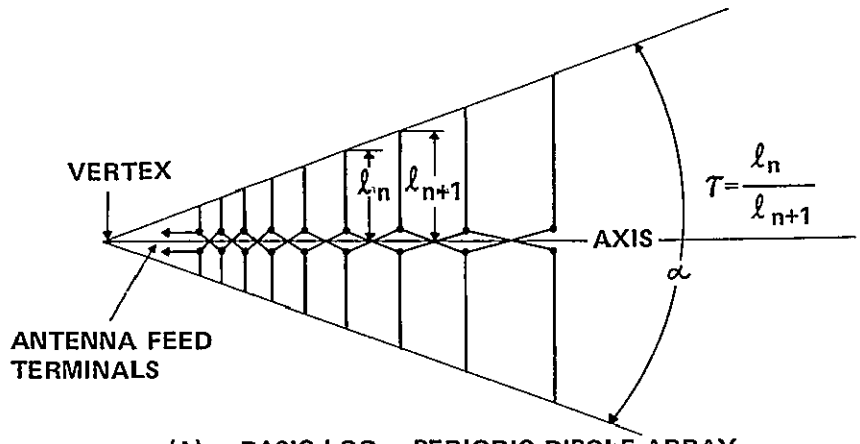

(A) BASIC LOG – PERIODIC DIPOLE ARRAY

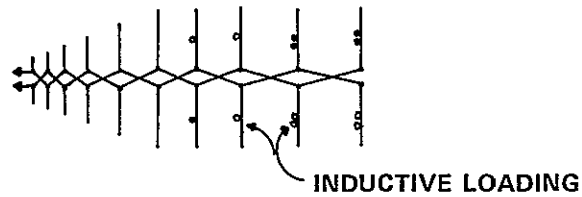

(B) SHORTENED – ELEMENT LOG – PERIODIC DIPOLE ARRAY

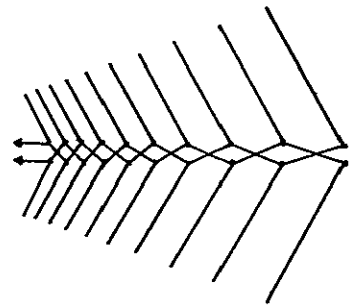

(C) LOG – PERIODIC VEE DIPOLE ARRAY

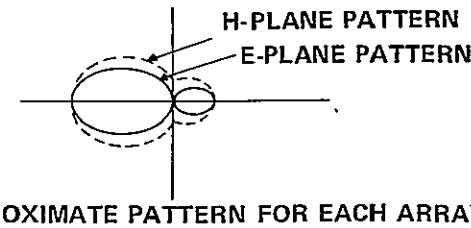

(APPROXIMATE PATTERN FOR EACH ARRAY)

Figure 2 LOG-PERIODIC DIPOLE ARRAY

expansion angle in an attempt to narrow its H-plane beamwidth. A dipole array with an H-plane 3-dB beamwidth of 107° has a phase center 0.72 wavelengths from its vertex. The phase center could be moved to 0.5 wavelengths from vertex by redesign of the array,but then the H-plane beamwidth would be more than twice as wide as the E-plane beamwidth.

The position of the feed phase center relative to the reflector focus governs the phase uniformity over the antenna reflector aperture. Referring to Figure 3, the phase center displacement, P, relative to the feed vertex is proportional to wavelength. When a fixed position feed is used for a 10:1 frequency range, the feed should be positioned such that the phase center at the upper frequency limit is slightly closer to the parabolic reflector than the focal point. At the low frequency limit, the phase center displacement to the focal point is then almost equal to the phase center displacement from the dipole array vertex.

The phase error (phase lead) at the edge of the reflector aperture relative to the center of the aperture as a function of reflector F/D ratio and displacement of the feed phase center from the reflector focus, S, is given in Table 2.

Serious degradation of the far-field patterns will occur for aperture phase error greater than 90°. The advantage of using a large F/D to minimize the effects of feed phase center displacement from the focus is illustrated in Table 2. It is also desirable to maintain the feed phase center displacement, S, as small as possible. A phase center displacement, S, of 0.36 wavelength can be obtained with a trapezoidal tooth antenna [6] and others.

To summarize, the log-periodic dipole array always has a wider H-plane beamwidth than E-plane beamwidth, which is essentially fixed at 60° (3 dB) and 110° (10 dB). The H-plane beamwidth can be minimized only at the expense of large phase center displacement. The advantages of the dipole array are that it can be constructed in one plane rather than two

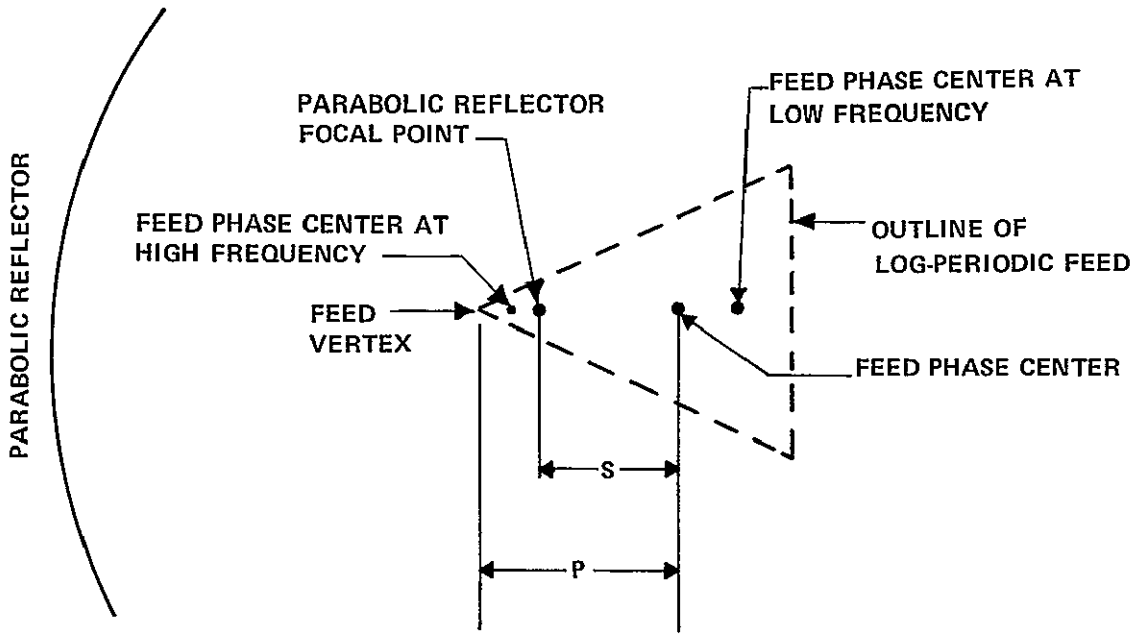

P: PHASE CENTER DISPLACEMENT RELATIVE TO FEED VERTEX $(P \sim \lambda)$
S: PHASE CENTER DISPLACEMENT RELATIVE TO FOCAL POINT AT LOWEST FREQUENCIES $(S \rightarrow P)$

Figure 3 FEED PHASE CENTER DISPLACEMENT

Table 2

APERTURE PHASE ERROR WITH PHASE CENTER DISPLACEMENT

F/D RATIO	S = 0.72 λ (degrees)	S = 0.36 λ (degrees)
0.30	179	96
0.35	147	80
0.40	122	66
0.45	104	56
0.50	87	47

inclined planes and that two orthogonal dipole arrays can be constructed on a common axis with little cross-coupling. Thus, crossed-linear or dual-sense circular polarizations can be achieved with less than 25-dB cross-coupling [7].

2.1.2 Shortened-Element Log-Periodic Dipole (Figure 2B)

The dipole elements can be shortened physically and tuned to resonance with inductive loading in each element [8]. An array whose longest dipole element has been shortened from the usual 0.5 λ_M (λ_M = wavelength at lowest operating frequency) to 0.25 λ_M and all preceding dipole elements of length 0.25 $\lambda_M < \ell < 0.5\lambda_M$ have also been shortened to 0.25 λ_M has been analyzed. This shortened-element dipole array is compared with a dipole array having full-length elements in Table 3.

The phase center displacement for the vertex, P, for operating wavelength $\lambda < 0.5\lambda_M$ is 0.75 λ for the shortened dipole array, because both arrays are identical over this wavelength range. However, when λ approaches λ_M, the phase center for the shortened-element array approaches 1.2 λ. It thus results that a shortened-element dipole array is not applicable to the LOFT antenna because (1) the phase center is too far behind the parabola's focal point at the low-frequency end of the band, (2) the array is 1.7 times longer, if the longest element lengths are halved, (3) more dipole elements are required and (4) approximately 20 loading coils with reactances ranging from 100 to 950 ohms [8] are required.

If any array having inductively loaded shortened elements is constructed with the same number of elements and the same array length as an array having full-length elements, it will have a degraded front/back ratio, wider H-plane beamwidth and higher VSWR at the lower operating frequencies.

Table 3

CHARACTERISTICS OF SHORTENED-ELEMENT AND FULL-LENGTH-ELEMENT LOG-PERIODIC DIPOLE ARRAYS

PARAMETER	FULL-LENGTH DIPOLE ARRAY	SHORTENED-ELEMENT DIPOLE ARRAY
E-PLANE BEAMWIDTH (3 dB)	62^{o}	62^{o}
E-PLANE BEAMWIDTH (10 dB)	109^{o}	109^{o}
H-PLANE BEAMWIDTH (3 dB)	107^{o}	107^{o}
H-PLANE BEAMWIDTH (10 dB)	190^{o}	190^{o}
FREQUENCY BANDWIDTH	10:1	10:1
PHASE CENTER DISPLACEMENT FROM VERTEX (P)	0.75λ	SEE TEXT
LONGEST DIPOLE ELEMENT LENGTH	$0.5\lambda_M$	$0.25\lambda_M$
TOTAL ARRAY LENGTH	$0.78\lambda_M$	$1.38\lambda_M$
TOTAL NUMBER OF ELEMENTS	18	24

2.1.3 Log-Periodic Vee Dipole (Figure 2C)

Higher gain dipole arrays have been achieved by operating the dipole elements in a 1.5 λ or 2.5 λ mode and tilting the dipole halves toward the boom-forming Vee dipole elements [9]. The performance of this antenna in the 0.5 λ mode [Reference 9, Figure 8] was examined to determine if a wider E-plane beamwidth could be obtained with the same H-plane beamwidth as compared to a straight dipole array. Such was not the case, however; the ratio of E- to H-plane beamwidths for the Vee dipole array was the same as that for the straight dipole array. Therefore, the problem of H-plane beamwidth's being much wider than E-plane beamwidth remains for any dipole array. Of course, two dipole arrays arranged onto inclined planes could be used to narrow the H-plane beamwidth until it equals the E-plane beamwidth, but simpler structures, which will be discussed next, are available.

2.1.4 Trapezoidal Tooth (Figure 4A)

Trapezoidal tooth arrays provide patterns suitable for illuminating a parabolic reflector [6, 10]. Like the dipole array, the E-plane beamwidth is almost invariant with different designs (67° at 3-dB points, 105° at 10-dB points). The H-plane beamwidth can be made equal to or wider than the E-plane beamwidth by varying the angle between the inclined planes containing each trapezoidal tooth structure, and/or by varying the adjacent tooth dimension ratio τ . The E- and H-plane phase centers are at different distances from the structure's vertex, but both can be made less than 0.4 λ [6].

Crossed-linear polarization can be obtained by arranging four trapezoidal tooth structures as sides of a pyramid. However, cross-coupling exists between orthogonal pairs resulting in some elliptical polarized radiation when only one pair is excited [11]. Even a single pair of trapezoidal tooth structures radiates cross polarization, which is only 15 to 20 dB below the desired polarization [10], probably due to direct radiation from the currents on the inclined booms.

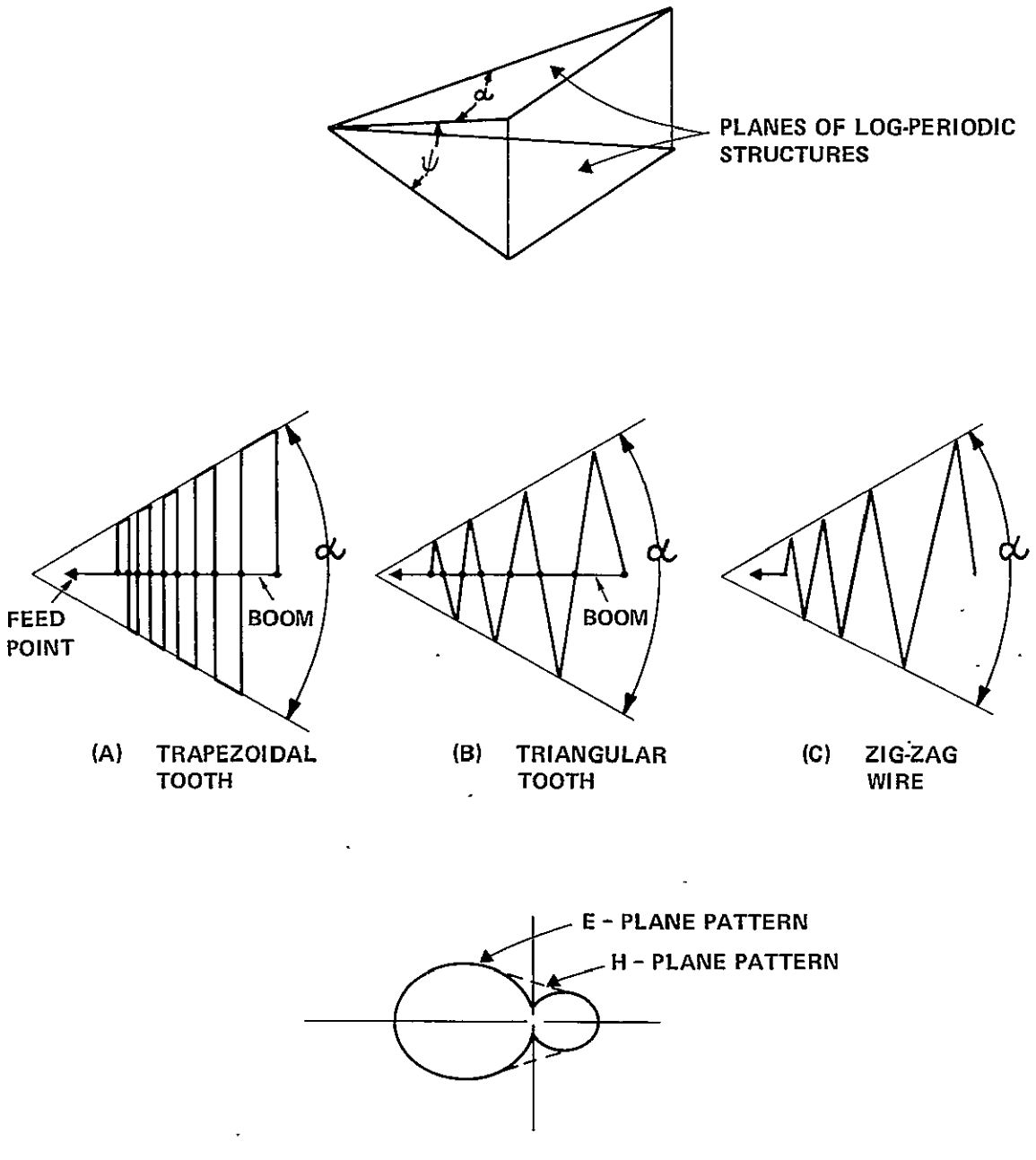

Figure 4 LOG-PERIODIC STRUCTURE PROVIDING AXISYMMETRIC PATTERNS

2.1.5 Triangular Tooth (Figure 4B)

Useful design data exist for this type of antenna [12]. It is similar in performance to the trapezoidal tooth. The triangular tooth structure might have less cross-coupling between orthogonal pairs in crossed-linear polarization feed system, because the longitudinal end pieces of the trapezoidal teeth are replaced by end points. No experimental verification of this expected reduced coupling is known at present, however.

2.1.6 Zig-Zag Wire (Figure 4C)

The Zig-Zag log-periodic antenna is similar in appearance to the triangular tooth structure; the difference being that the central booms are eliminated, leaving a pair of Zig-Zag wires lying in inclined planes. It has been reported that the expansion angle of each Zig-Zag structure and the angle between the inclined planes should both be less than 30°; otherwise, pattern breakup occurs [13]. Thus, the maximum attainable E- and H-plane 3-dB beamwidths are 60°, and the phase center is 0.85 λ from the vertex. Further experimentation with emphasis on obtaining clean, low-sidelobe, wide-beamwidth patterns is required to evaluate this antenna as a parabolic reflector feed.

2.2 CIRCULAR POLARIZED FEEDS

2.2.1 Conical Spiral (Figure 5A)

Much useful design data have been obtained by Dyson [14]. E- and H-plane beamwidths differ by less than 10°, and antennas can be designed with 3-dB beamwidths anywhere from 40° to 130°. The conical spiral is circularly polarized, with axial ratio less than 3 dB. The phase center will be from 0.4 to 0.7 wavelength behind the vertex for 3-dB beamwidths from 105° to 70° respectively. The conical spiral antenna has a cleaner pattern, with a smaller backlobe when wide spiral arms are used. Wide arms can be replaced with wires following the edges of each arm. Satisfactory patterns can also be obtained with thin-wire tight spiral angle arms, however.

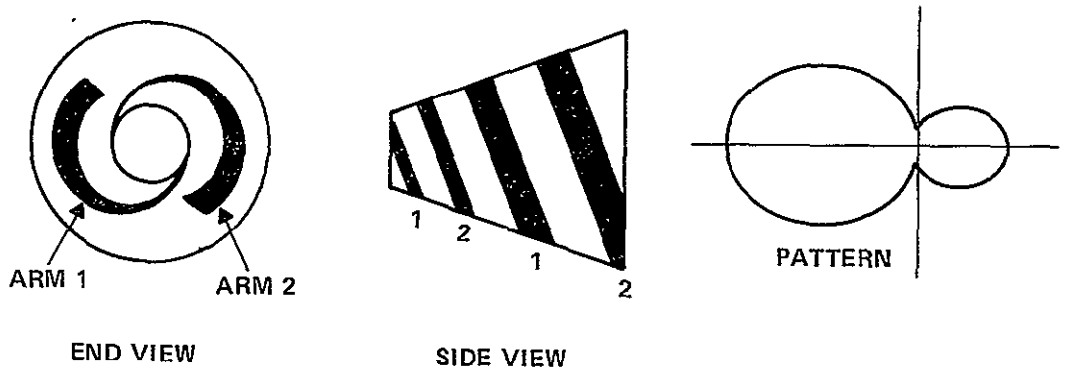

(A) CONICAL SPIRAL

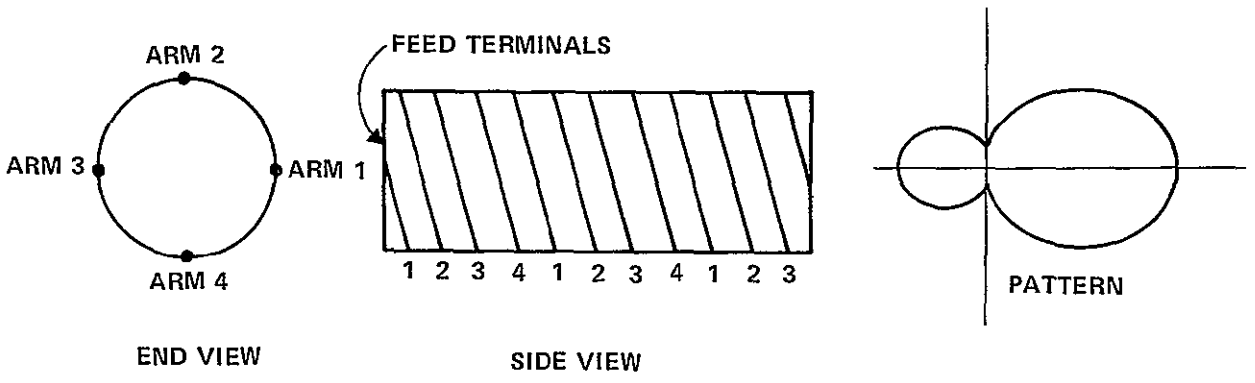

(B) MULTITURN CYLINDRICAL HELIX

Figure 5 CIRCULAR POLARIZED FEED ANTENNAS

Attempts have been made to obtain both senses of circular polarization by contrawinding another pair of conical spiral arms over the original pair of arms. Results were poor; the originally low axial ratio of a singly wound antenna was made very large by the addition of the contrawound arms [15].

The conical spiral antenna is one of the more difficult antennas to implement, but should be considered if only right or left handed circular polarization is suitable, because the pattern shapes are excellent for parabolic antenna feeds.

2.2.2 Multiturn Cylindrical Helix (Figure 5B)

All antennas considered above are backfire; maximum radiation is in the direction opposite to the transmission line wave propagation (toward feedpoint). The multiturn, cylindrical helix [16] is a broadband forward-fire antenna. Dual-sense circular polarization with axial ratios less than 2 dB has been obtained with contrawound versions [17]. Despite these advantages, the multiturn helix appears unsuitable for LOFT application because:

- The beamwidth is too narrow and decreases with increasing frequency. The widest beamwidth obtained varied from 30° to 70° over a 5:1 frequency band.
- A 9:1 frequency band requires 8 arms for each sense circular polarization (16 arms for dual sense). A relative phase of 45° is required from one arm to the next. The multiturn helix is considered relatively difficult to implement for LOFT.
- Sidelobes 3 dB below the main beam occur for narrow frequency ranges within the operational band [18].

2.3 CONICAL TRANSMISSION LINE FEED

A sketch of a parabolic reflector using a conical transmission line feed is shown in Figure 6. The feed consists of equispaced conducting strips

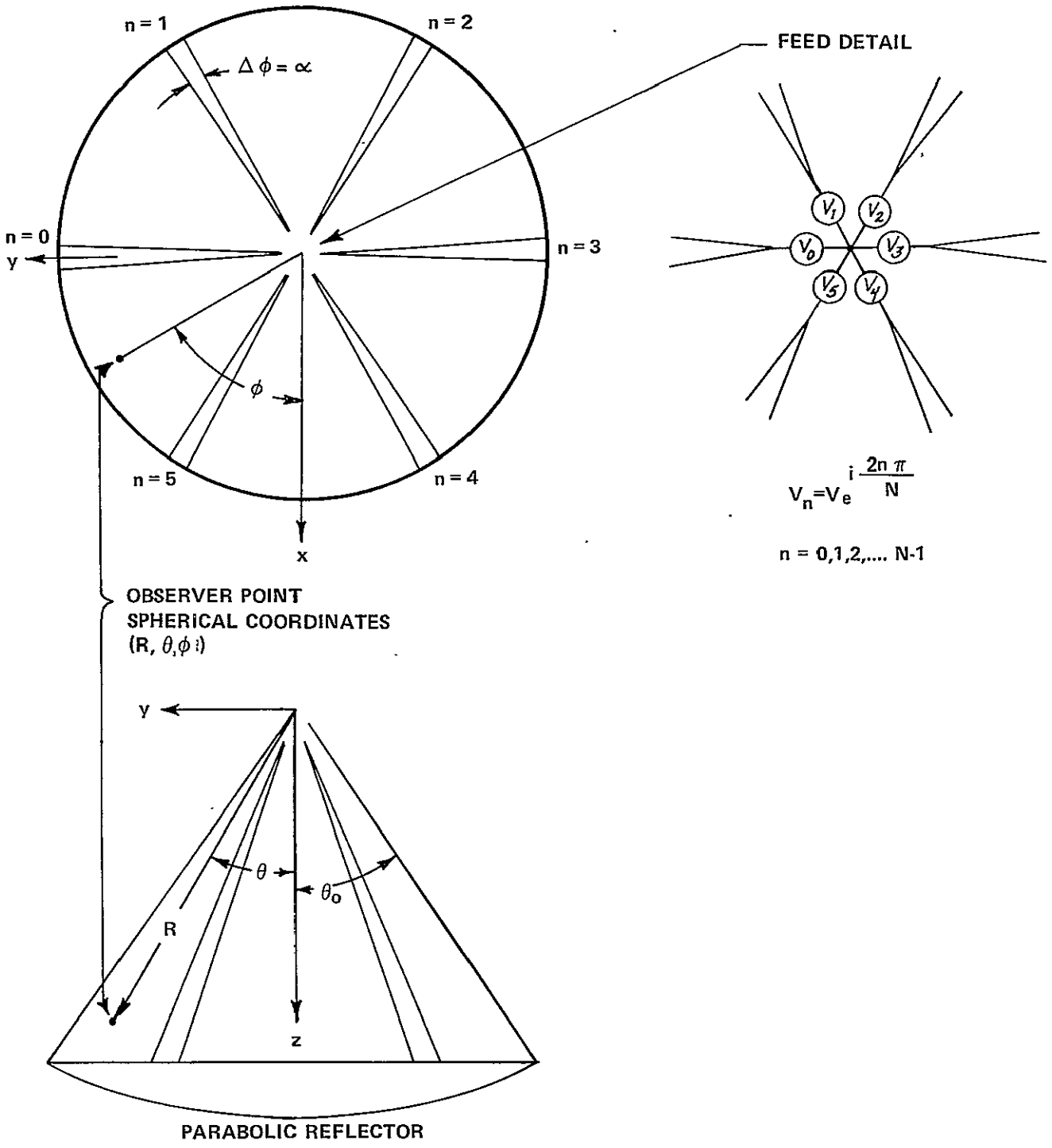

Figure 6 TRANSMISSION LINE FEED PARABOLIC ANTENNA

lying on a cone. These strips can be some of the front tension stays and therefore, no additional structure is required to implement this feed. In contrast, all feeds covered in Sections 2.1 and 2.2 require a separate structure at the end of the central support column.

The feed consists of an equispaced conducting strips lying on a cone. A six-conductor transmission line with 60° spacing between lines is shown in Figure 6, but N conductors with 360/N degree spacing can be used. The apex of the cone is at the parabolic reflector's focal point. The phase center of the conical transmission line is at this apex independent of frequency [19]. Therefore, this feed does not have phase error resulting from phase center shift as a function of frequency as experienced with log-periodic feeds. Each strip conductor is connected to the rim of the reflector because best antenna patterns are obtained with this configuration. The E_θ radial field component reverses direction at the surface of the cone, including the conductor strips and if the reflector extended outside the cone, there would be a 180° phase reversal of the aperture rield distribution for the E_θ component. This phase reversal reduces gain and increases sidelobes.

The multiconductor transmission line is excited with equal amplitude and a progressive phase shift of 360/N degrees from one conducting strip to the next as illustrated in Figure 6. This excitation gives a circularly polarized aperture field at the reflector center and nearly so over a large portion of the reflector surface. The six-conductor excitation can be realized with a network of 3 dB and 4.8 dB, 180° hybrids and 3 dB, 90° hybrids [20,21]. An eight-conductor excitation can be realized with a network of 3 dB, 180° and 90° hybrids. The 3 dB, 180° and 90° hybrids covering a 10:1 frequency band at VHF are available [22]. Broadband VHF 4.8 dB, 180° hybrids are not yet available.

Linear polarized reflector illumination can be obtained by combining in a 3-dB, 180° hybrid the mode having a progressive 360/N degree phase advance with the mode having a 360/N degree phase delay. The

resultant mode has a cosine (n π /N) amplitude distribution (n = 0, 1, ...N-1) whose phase is either 0° or 180° as given by this cosine function. Crossed-linear polarization can be provided with a sine (n π /N) excitation. These linear-polarized excitations could be implemented directly without generating the two circular polarized modes.

In Appendix A, the field equations for the transmission line feed are given and discussed relative to performance characteristics for LOFT. Also included in Appendix A is an analysis of aperture blockage effects for the case in which a transmission line feed is used as a backup to a feed antenna such as the trapezoidal tooth feed described in Section 2.1.4.

The aperture blockage effect of eight or less conductors is insignificant (as shown in Appendix A) if the width of each conductor is less than 0.1 meter. Therefore, up to eight conducting tension stays can be added to the front of the reflector if desired as a transmission line feed backup. It is not certain how close the conducting strips can be brought to the focal point without disturbing the feed fields incident on the reflector.

The disadvantages of the conical transmission line feed are:

(1) Only half the feed power illuminates the reflector; the other half is lost as spillover.

(2) Cross polarization is large at angles off the mainlobe peak.

(3) Close-in sidelobe level will be at best 18 dB below the mainlobe.

(4) Far-out sidelobe level is higher than that obtainable with trapezoidal tooth feeds, because edge illumination, and hence edge diffraction, will be greater and feed-back radiation will be higher.

(5) Gain is 2 to 3 dB lower than the gain obtainable with a log-periodic feed.

(6) The transmission line feed excitation network for a polarization diversity antenna is relatively complicated.

The advantages of the conical transmission line feed are:

(1) No phase error due to feed phase center shift as a function of frequency as experienced with log-periodic-type feeds.

(2) Ease of deployment in the LOFT application when compared to other type feeds.

At present, the disadvantages appear to outweigh the advantages. Therefore, the conical transmission line feed is not recommended as a primary feed antenna but could be used as a backup feed.

Section 3

REFLECTOR GRIDS

The reflecting surface of the LOFT antenna is comprised of a conducting mesh. It is desirable to reduce the mass of the reflector as much as possible, while retaining high grid reflectivity and low transmissivity. Therefore, grids with conductor spacings much larger than conductor widths were studied extensively during the program. Flat strip conductors are preferred over round wire conductors, because their mass is less for the same reflection coefficient and they are more immune to meteorite damage [4]. Strip thickness was so thin (0.0005 inch or less) that the finite conductivity of the material had to be taken into account.

3.1 DESCRIPTION OF GRID

The reflector grid investigated consisted of orthogonal conducting strips lying in a flat plane (Figure 7). Strip spacing, width, and thickness need not be the same in the orthogonal directions. The orthogonal strips may or may not be connected at the junctions. The finite conductivity of the metal strips has been taken into account. Flat plane analysis is applicable to a parabolic reflector, provided the radius of curvature of its surface is large compared to a wavelength and provided the grid spacing, width, and thickness do not change appreciably over distances comparable to a wavelength.

3.2 ANALYSIS OF REFLECTING GRIDS

The procedure for finding the reflection coefficient for arbitrary angle of arrival and arbitrary polarization of the incident field is given in Reference 23. In general, the procedure is very complicated, and the polarization of the reflected wave is not simply related to the polarization of the incident wave. The only case considered in this study was: the plane of incidence (plane containing normal to the grid and the incident ray, Figure 7) parallel to one of the conductor sets, and the polarization either

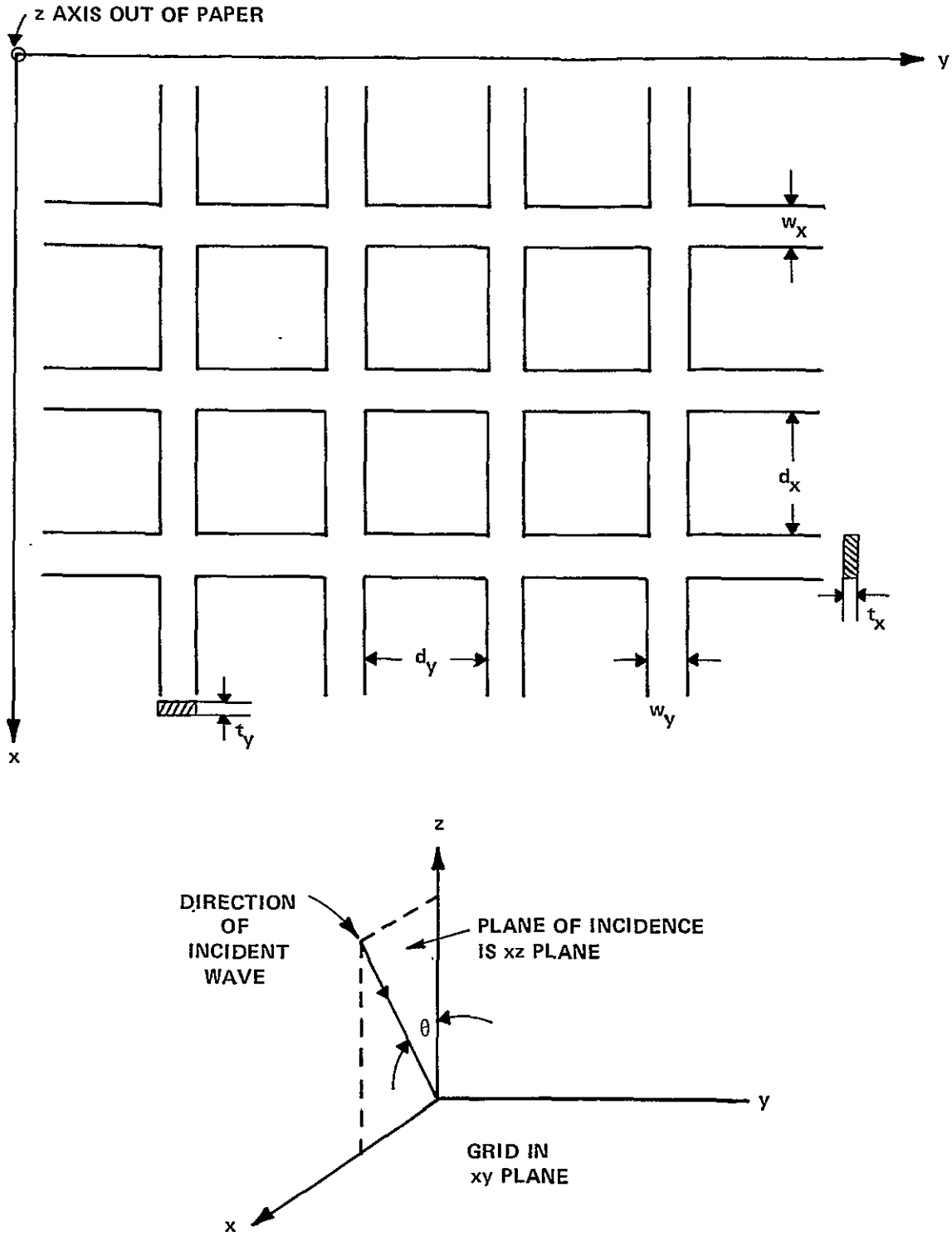

Figure 7 STRIP CONDUCTOR GRID

perpendicular or parallel to the plane of incidence. Arbitrary polarization can be handled by resolving the incident field into perpendicular and parallel components. The case analyzed is applicable to antenna reflector grids consisting of radial and circumferential strips. The following equations assume strip spacing is much larger than strip width, which is the case of interest here.

The voltage reflection coefficient $R_\perp$ for perpendicular polarization (only a E_y component) is

$$R_\perp = \frac{-1}{1 + i\,\frac{2d_x}{\lambda}\cos\theta \ln\frac{2d_x}{\pi w_x} + \frac{Z_x d_x}{60\pi}\cos\theta} \qquad (1)$$

i = $\sqrt{-1}$

λ = wavelength

d_x = strip spacing defined in Figure 7

w_x = strip width defined in Figure 7

θ = angle of incidence

Z_x = impedance of strips of width w_x and thickness t_x

The strip impedance Z_x is given by

$$Z_x = \frac{1+i}{2\sigma\delta w_x}\coth\frac{(1+i)\,t_x}{2\delta}$$

where σ is the conductivity of the strip material and δ is the skin depth given by [24]

$$\delta = \frac{1}{2\pi\sqrt{\sigma f \times 10^{-7}}} \quad \text{meters}$$

σ mho/meter
f frequency in hertz

Equation (1) is valid whether the orthogonal strips are connected at the junctions or not: In fact, the strips parallel to the X-axis have no effect (under the assumption of large spacing relative to strip width) for perpendicular polarization.

The voltage reflection coefficient $R_{\parallel,o}$ for parallel polarization (only a E_θ component) with the strips unconnected at the junctions is:

$$R_{\parallel,o} = \frac{-1}{1 + i\,\dfrac{2d_y \cos\theta}{\lambda}\,\ln\dfrac{2d_y}{\pi w_y} + \dfrac{Z_y d_y}{60\pi\cos\theta}} \tag{2}$$

where

$$Z_y = \frac{1+i}{2\sigma\delta w_y}\,\coth\frac{(1+i)t_y}{2\delta}$$

The voltage reflection coefficient $R_{\parallel,s}$ for parallel polarization with the strips connected at the junctions is

$$R_{\parallel,s} = \frac{-1}{1 + i\,\dfrac{2d_y}{\lambda\cos\theta}\left(1 - \dfrac{d_x \sin^2\theta}{d_x + d_y}\right)\ln\dfrac{2d_y}{\pi w} + \dfrac{Z d_y}{60\pi\cos\theta}} \tag{3}$$

where

$$Z = \frac{1+i}{2\sigma\delta w}\,\coth\frac{(1+i)t}{2\delta}$$

The x and y subscripts on w and t are omitted because equation (3) is valid only when the orthogonal strips have the same width and thickness. At normal incidence, $\theta = 0°$, equations (2) and (3) are identical and the reflection coefficient is the same, whether the strips are connected at the junctions or not.

In all cases, the voltage transmission coefficient T is

$$T = 1 + R \tag{4}$$

When strip conductivity is infinite, the strip impedance Z is zero and:

$$|R|^2 + |T|^2 = 1$$

or the sum of reflected and transmitted power equals incident power. For finite conductivity, equations (1), (2), or (3) with (4) yield

$$|R|^2 + |T|^2 < 1$$

as expected, because some of the incident power is dissipated in the strip conductors.

If the grid conductors are round wires of radius r, rather than flat strips, replace w with $4r$, and impedances Z_x and Z_y with appropriate round wire impedances [25].

Equations (1) and (3) were incorporated into the surface integral computer program, which computes antenna gain and pattern (Appendix B). Both equations are needed, because the incident polarization of the feed onto the reflector surface has in general both parallel and perpendicular components relative to the plane of incidence. The coordinate system used for equations (1) and (3) and shown in Figure 7 was transformed to the coordinate system used in the surface integral computer program.

A weaved grid (Figure 8) without electrical connection between adjacent conductors is unsatisfactory for fields polarized transverse to the conductors (X-direction). Fields in the X-direction induce currents in the X-direction, but the weaved grid shown cannot support such currents, thus its reflection coefficient is low. A weaved grid therefore must have good and reliable connections at the junctions to provide high reflectivity for arbitrary polarization.

3.3 COMPUTED RESULTS FOR CONDUCTING GRIDS

Some results on grid performance relative to the LOFT application are given in this section. Grid performance is governed by operation at the highest frequency of interest, where the reflection coefficient is lowest.

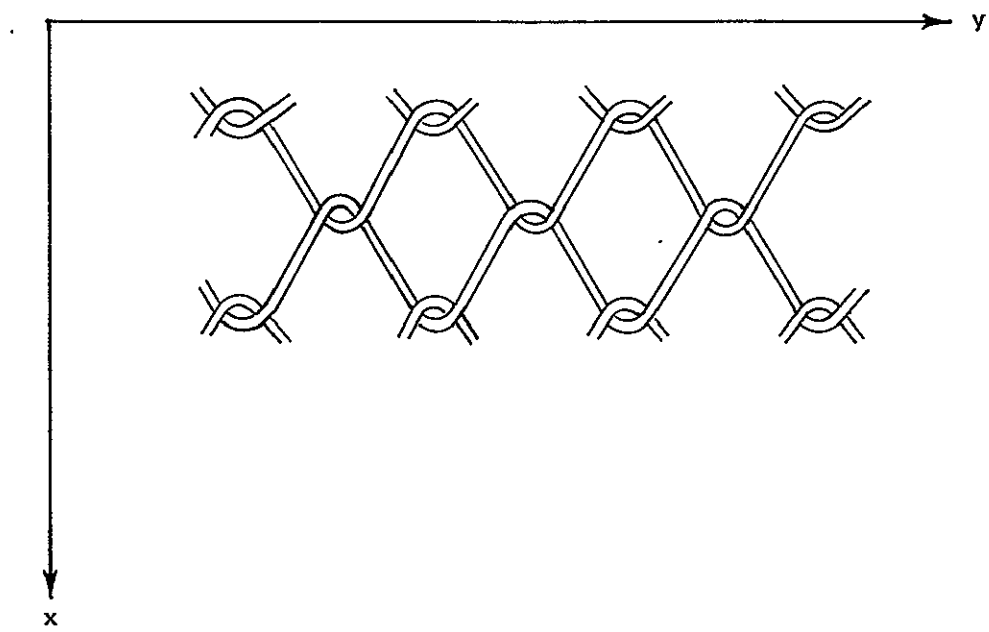

Figure 8 WEAVED GRID

The magnitude of the reflection and transmission coefficients as functions of grid spacing are given in Figures 9 and 10 for the following conditions:

Frequency	f = 150 MHz (highest frequency in band)
Normal Incidence	$\theta = 0^\circ$
Square Mesh Grid	$d_x = d_y = d$ $3 < d < 20$ centimeters
Equal Strip Widths	$w_x = w_y = w$ w = 0.3, 1, 3 and 10 millimeters
Equal Strip Thicknesses	$t_x = t_y = t$ = 6.35 microns
Strip Material	Aluminum $\sigma = 3.72 \times 10^7$ mho/meter Stainless Steel $\sigma = 1.43 \times 10^6$ mho/meter

The thickness used was the practical minimum which can be fabricated [4]. The conductivities are handbook values [26]. The measured conductivity of a sample stainless steel strip conductor was 1.6×10^6 mho/meter. Reflection and transmission coefficients for infinite conductivity strips are within 0.5 percent or less of the values shown for aluminum. Even 6.35-micron-thick stainless steel has sufficiently low impedance, when the strip width is 3 millimeters or greater, that the effect of conductivity is relatively small.

There are many combinations of strip widths and spacings which give the same reflection and transmission coefficients. Several values of w and d for 6.35-micron-thick stainless steel conductors resulting in $|R| = 0.93$ at 150 MHz (0.6-dB reflection loss) are given in Table 4. Also tabulated is the mass of stainless steel required for a 100-meter-diameter reflector grid.

The mass reduction obtainable by using narrow strip widths can be seen to be appreciable.

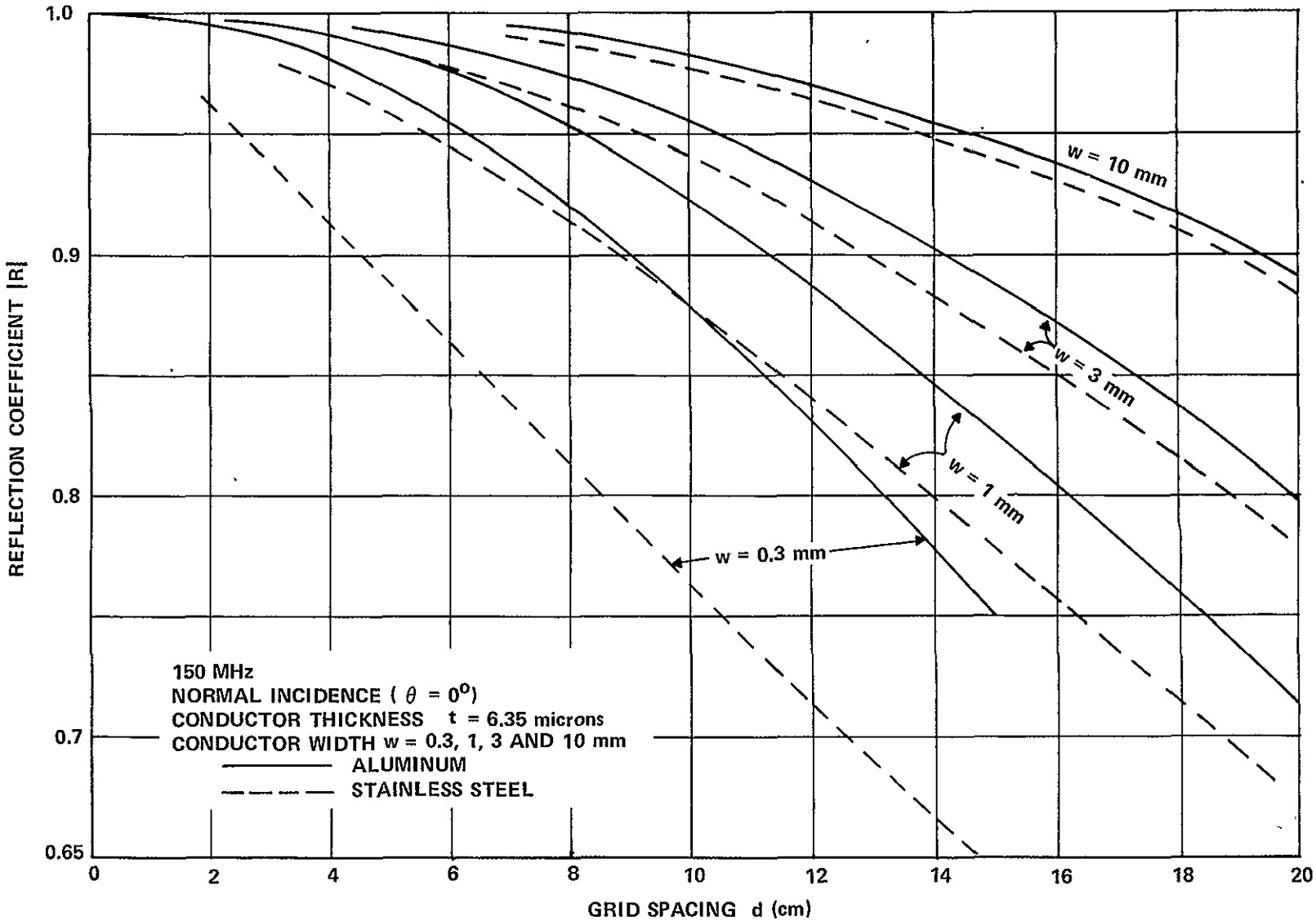

Figure 9 GRID REFLECTION COEFFICIENT

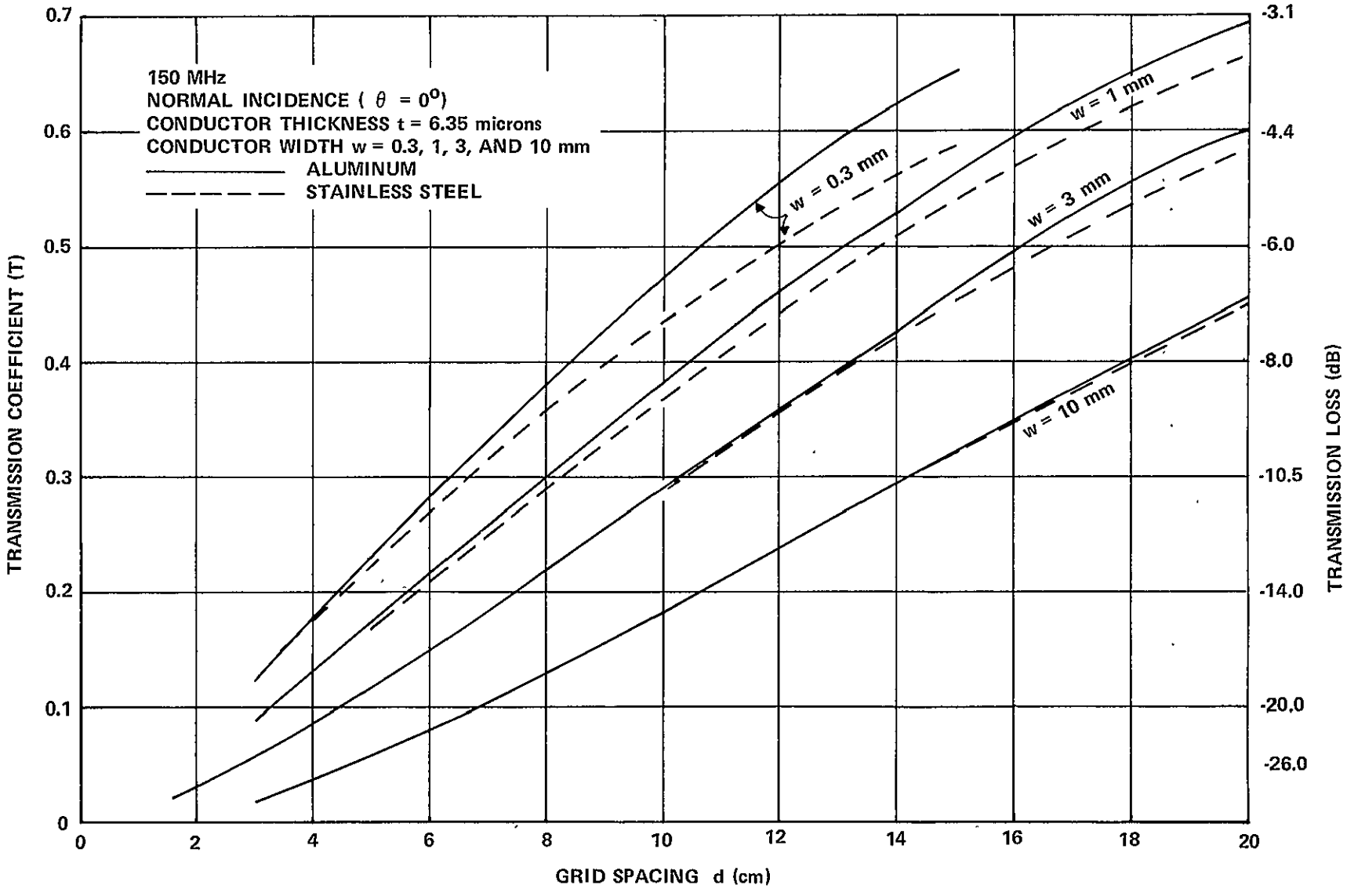

Figure 10 GRID TRANSMISSION COEFFICIENT

Table 4

GRID PARAMETERS FOR 0.93 REFLECTION COEFFICIENT
(STAINLESS STEEL, 6.35 microns THICK)

STRIP SPACING d (cm)	STRIP WIDTH w (cm)	MASS* (kg)
6.9	1.0	11.6
10.8	3.0	22.2
17.0	10.0	46.8

*FOR 100- meter-diameter REFLECTOR

Strip spacing and reflector mass, which provide a given transmission coefficient at 150 MHz, are given in Table 5. Stainless steel strips 6.35 microns thick and 3 millimeters wide are assumed. Also tabulated is the resulting reflection loss in dB for each grid configuration.

A small transmission coefficient minimizes leakage of the feed fields through the grid into the shadow region of the reflector. It is desirable to reduce this leakage to a level lower than the shadow region fields due to edge diffraction. It will be shown in Section 5 and Figure 35 that the reflector transmission coefficient at 150 MHz must be -10 dB to reduce the leakage field to the level of the backlobe (180° away from mainlobe), and -25 dB to reduce the leakage field to the level of the edge diffracted fields in the shadow region exclusive of the backlobe. The transmission loss/reflector weight tradeoff (Table 5) thus provides the grid spacing and weight required to achieve the desired leakage level. The assumed strip thickness and width are probably the minimum which can be constructed. Thus the weight is also the minimum achievable with a stainless-steel grid. An aluminum grid with the same conductor thickness, width, and spacing would be 3 times lighter and would have nearly the same transmission and reflection loss as the stainless-steel grid considered. The reduction in LOFT antenna gain caused by the imperfectly reflecting grid is approximately equal to the reflection loss (Table 5).

Table 5

TRANSMISSION COEFFICIENT VS GRID SPACING
(STAINLESS STEEL, 3 mm WIDE, 6.35 microns THICK)

TRANSMISSION COEFFICIENT (dB)	STRIP SPACING (cm)	REFLECTOR WEIGHT* (kg)	REFLECTION LOSS (dB)
-10	10.9	22.0	0.62
-15	6.8	35.3	0.28
-20	4.4	54.6	0.14
-25	3.0	80.0	0.04
-30	2.0	120.0	0.02

*FOR 100- meter-diameter REFLECTOR

Section 4
RADIATION NEAR MAINLOBE

The far-field electrical characteristics for the LOFT antenna, including gain, mainlobe, first few sidelobes and cross-polarization calculated by CAL during the program, are discussed in this section. Patterns were computed by integration of reflector surface currents induced by the incident feed field. When the reflector surface was axisymmetric, the circumferential ϕ' integration was evaluated analytically, and the radial θ' integration was evaluated numerically using an available computer program modified by CAL for the LOFT antenna application (Figure 11). For cases in which the reflector surface is not axisymmetric, both ϕ' and θ' integrations were evaluated numerically using a CAL-developed computer program. The computer programs are described in Appendix B. The cost for obtaining patterns using the IBM 360/65 computer at CAL with the axisymmetric computer program is about one-fourth the cost of running the more general asymmetric reflector computer program.

The tradeoff study included effects on LOFT antenna performance due to:

- Trapezoidal tooth versus log-periodic dipole feed antennas.
- Reflector F/D ratio (0.3 to 0.5).
- Effect of conic reflector surfaces.
- Reflector surface distortions caused by temperature and torque effects.
- Feed blockage and scattering.
- Reflector grid.

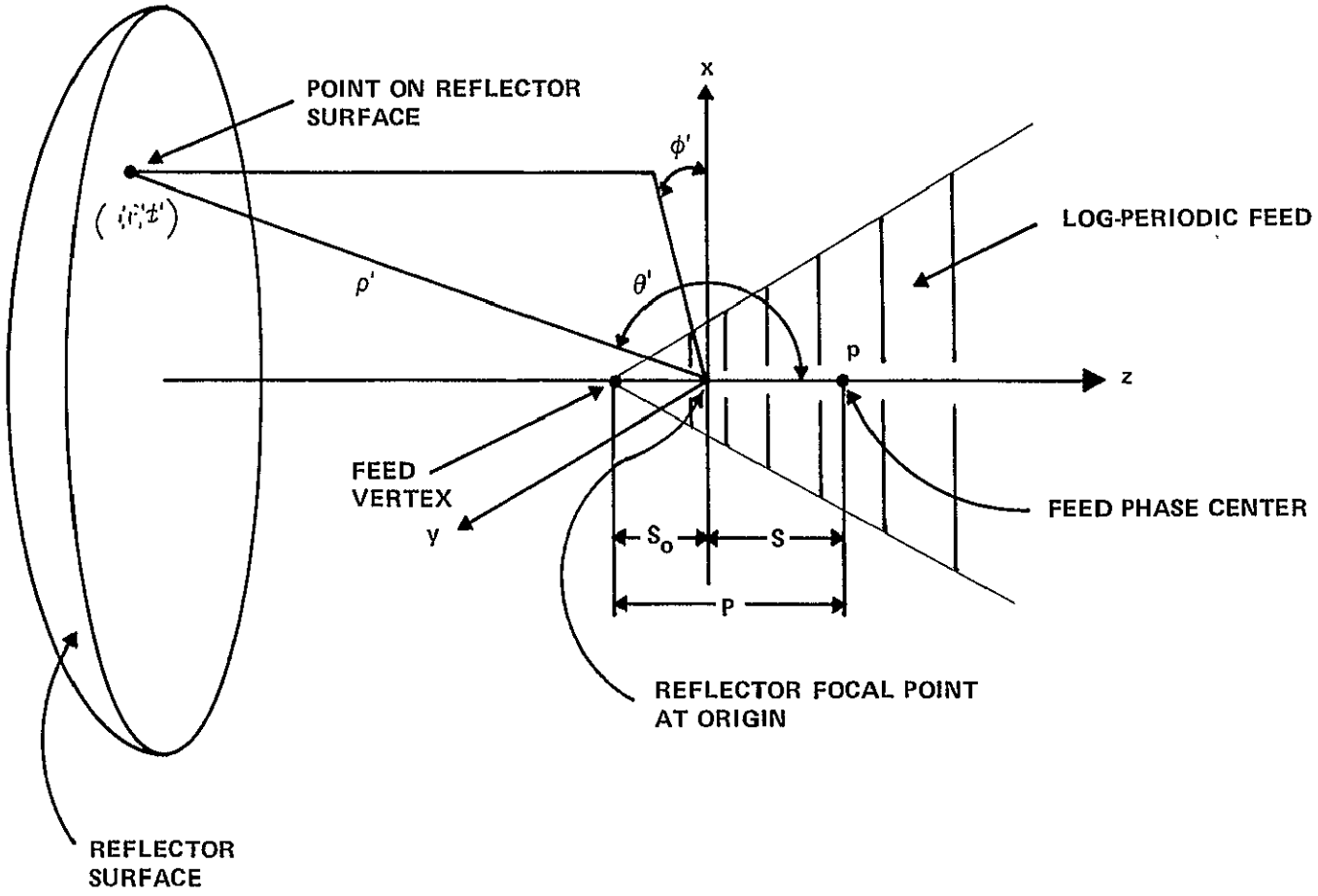

Figure 11 FEED–REFLECTOR GEOMETRY

The order of presentation is as follows. A description is first given of the feed patterns and approximation of the center region of the reflector by conics. Next, the effects of feed type, F/D ratio and conics are discussed and compared for both feed types. This comparison shows the advantage of using the trapezoidal tooth feed, so only this feed is used to analyze the effect of surface distortions caused by temperature and torque. Then, feed blockage and scattering are analyzed as a change in the reflector illumination function. Investigation of feed aperture blockage using dipole scattering is also included. Finally, the effect of an imperfectly reflecting grid surface is discussed.

4.1 FEEDS

Based on the feed investigation, Section 2, a log-periodic trapezoidal tooth array and a log-periodic dipole array were chosen for analysis of the LOFT antenna performance. The feed was placed near the focal point of the reflector as illustrated in Figure 11. The feed array is arranged along the reflector Z-axis, with elements in the X-direction. The reflector focal point is at the origin, and (ρ', θ', ϕ') are spherical coordinates of a point on the reflector surface. Point $\mathcal{P}$ is the phase center of the feed antenna. The distance, ρ, of the phase center away from the feed vertex is approximately proportional to wavelength. Therefore, the phase center cannot coincide with the origin (focal point) over the entire frequency range, unless the feed is moved for each change in operating frequency. Optimum performance over a wide frequency range with a fixed position feed is achieved, when the feed vertex is slightly closer to the reflector than the focal point [6].

Patterns and phase center displacements were found for the trapezoidal tooth [6,10] and log-periodic dipole [5] arrays and the optimum feed design for each was determined. A tradeoff had to be made between minimum phase center displacement and proper H-plane beamwidth. A small displacement could be obtained by using a short (along Z-axis) array, but then the H-plane beamwidth became too wide. The optimum feed patterns were accurately represented by the mathematical functions given in Appendix B. E- and H-plane patterns of the two

feeds are shown in Figure 12, along with the position of the reflector edge for F/D ratios of 0.3, 0.4, and 0.5. Feed phase center displacement S relative to the origin (Figure 11) in the E- and H-planes of the trapezoidal tooth feed were $S_E = (0.5\,\lambda - 0.8)$ meter and $S_H = (0.3\,\lambda - 0.8)$ meter, respectively. The 0.5-λ and 0.3-λ displacements can be easily met with many trapezoidal tooth designs [6], and the vertex displacement $S_0 = 0.8$ meter minimizes phase error at 150 MHz ($\lambda = 2$ meters). The E- and H-plane phase center displacements of the log-periodic dipole feed are nearly equal and the minimum obtainable for the optimum feed design was 0.72 wavelength [5]. Therefore, $S_E = S_H = (0.72\,\lambda - 2)$ meters was chosen to optimize performance of the log-periodic dipole feed over a 15- to 150-MHz band.

In the results which follow, cross coupling between orthogonal feed pairs is neglected. The feed polarization is assumed to be the same as a single dipole.

4.2 REFLECTOR SURFACE

For the LOFT application, all parts of the reflector should experience only tension caused by centrifugal force of the spinning structure. However, a parabolic surface cannot be maintained in tension in the central region of some parts of the reflector [27]. Therefore, the parabolic surface is approximated by conics over the inner portion of the reflector [28] as illustrated in Figure 13 for an F/D ratio of 0.5. A true parabolic surface is maintained for $0.5 \leq r/R \leq 1.0$. The conic surface for $0.4 < r/R < 0.5$ is tangent to the back stays and the parabolic surface at $r/R = 0.5$. Another conic surface for $0 \leq r/R < 0.4$ minimizes surface error relative to a true paraboloid. The error in meters shown in Figure 13 apply to a 100-meter-diameter reflector. Equations for the conic and parabolic surfaces in terms of ρ', θ', and F/D ratio were incorporated into the surface integral computer programs described in Appendix B.

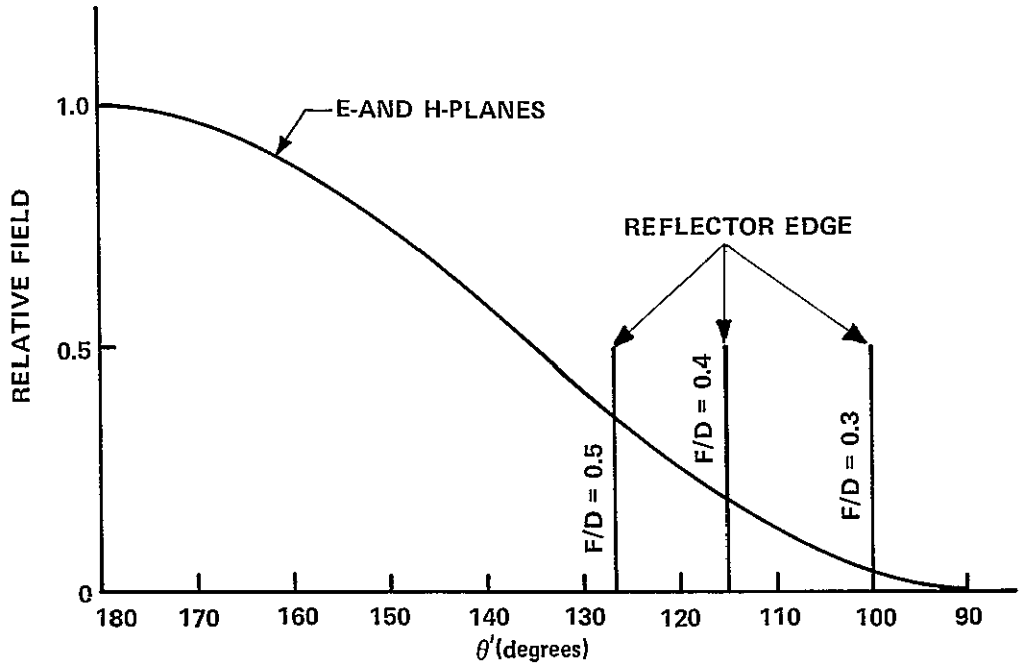

(A) TRAPEZOIDAL TOOTH

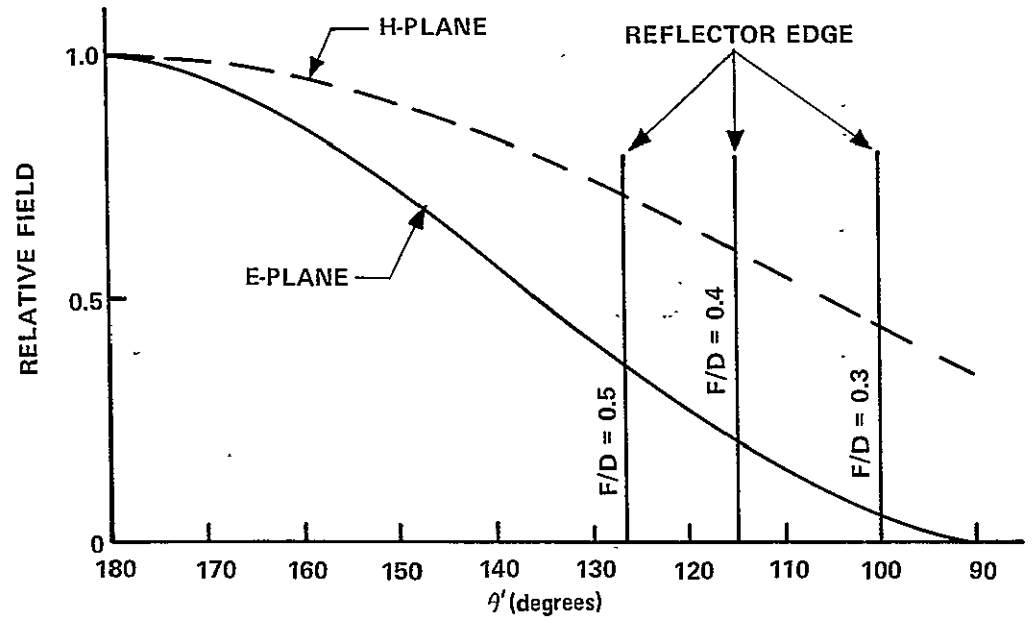

(B) LOG-PERIODIC DIPOLE

Figure 12 FEED PATTERNS

FOCAL LENGTH/DIAMETER (F/D) RATIO = 0.5

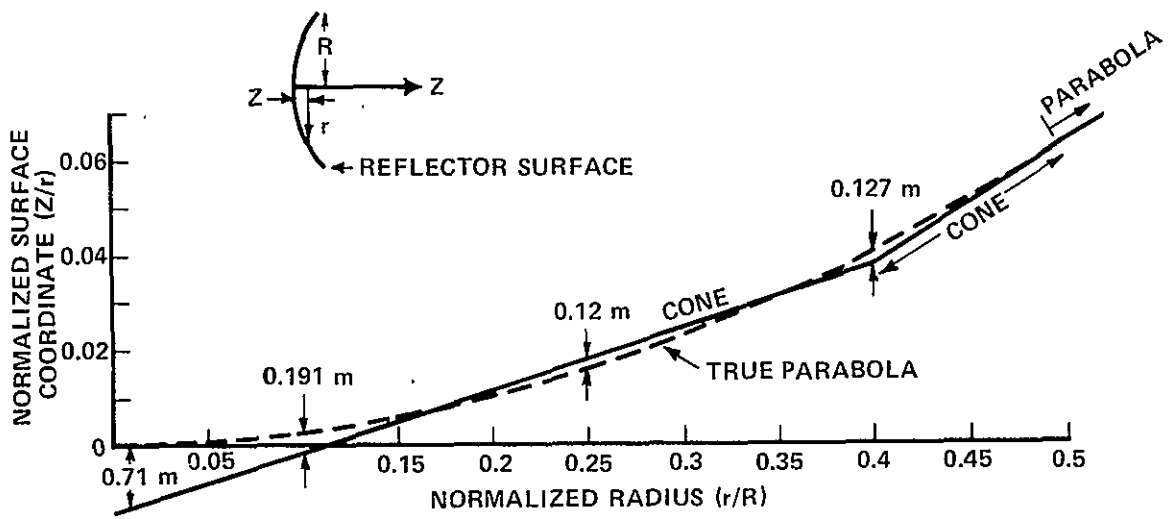

Figure 13 CONIC APPROXIMATION OF PARABOLIC SURFACE

4.3 EFFECT OF FEED, F/D RATIO, AND CONIC SURFACES

Far-field antenna patterns were computed for the following cases. First, a perfect paraboloid illuminated by a feed with no phase displacement error was analyzed. These patterns are representative of the best obtainable when there are no conic surfaces and the feed is moved to keep its phase center at the focal point. Then, the conic surfaces were introduced so the patterns are now applicable to the LOFT reflector and a movable feed. Finally, conic surfaces and feed phase displacement errors were introduced so the patterns are applicable to the LOFT reflector and fixed position feed. Patterns were computed for trapezoidal tooth and log-periodic dipole feeds, and reflector F/D ratios of 0.3, 0.4, and 0.5. The frequencies covered were 15, 30, 72 and 15 MHz, corresponding to reflector diameters of 5, 10, 24, and 50 wavelengths, respectively. The reflector was considered perfectly reflecting for these analyses.

The effects of conic surfaces and feed phase error as a function of frequency are illustrated in Figures 14 through 17. In each case, a trapezoidal tooth feed and F/D ratio of 0.5 were used. Only E-plane patterns are shown, because patterns in the 45° and H-planes were nearly the same. At 15 MHz, most pattern degradation is due to the large feed displacement ($S_E = 0.46\lambda$, $S_H = 0.26\lambda$), because the conic surface error relative to a paraboloid was small ($\pm 0.006\ \lambda$, Figure 13). At 150 MHz, most pattern degradation is due to surface error ($\pm 0.06\lambda$), because feed displacement was small ($S_E = 0.1\lambda$, $S_H = -0.1\lambda$).

The effect of reflector F/D ratio with a trapezoidal tooth feed is shown in Figures 18 (E-plane) and 19 (H-plane). The frequency was 30 MHz and both conic surfaces and feed phase were included. The same patterns with a log-periodic dipole feed are shown in Figures 20 and 21. The lowest sidelobe level far from mainlobe and the widest beamwidth occur at F/D = 0.3. Maximum gain occurs at F/D = 0.5 with the trapezoidal tooth feed. With the log-periodic dipole feed, gain is nearly the same and maximum at F/D = 0.4 and 0.5, but lower sidelobe level far from mainlobe occurs at F/D = 0.4. E- and H-plane

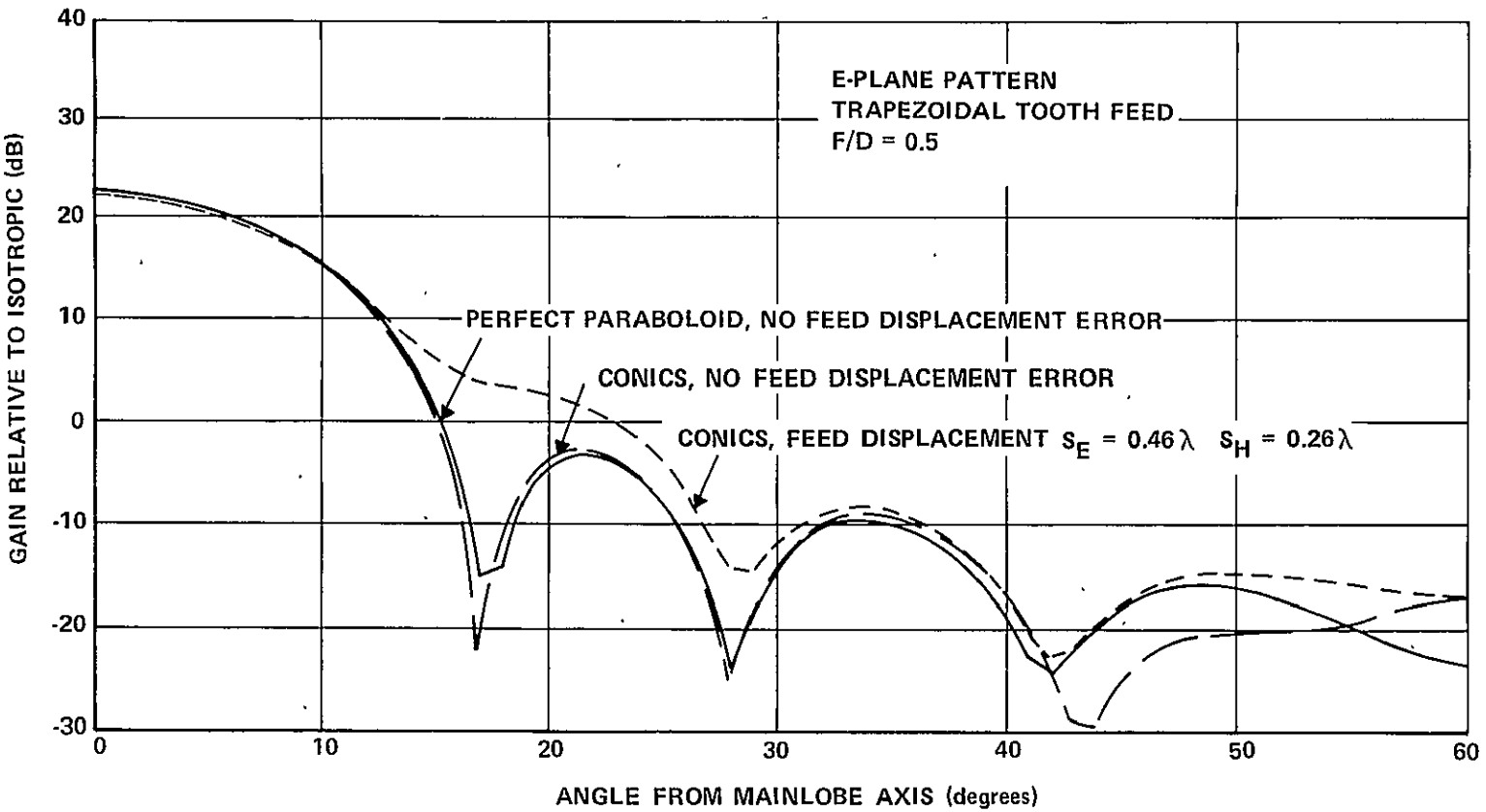

Figure 14 EFFECT OF CONIC SURFACES AND FEED PHASE: 15 MHz

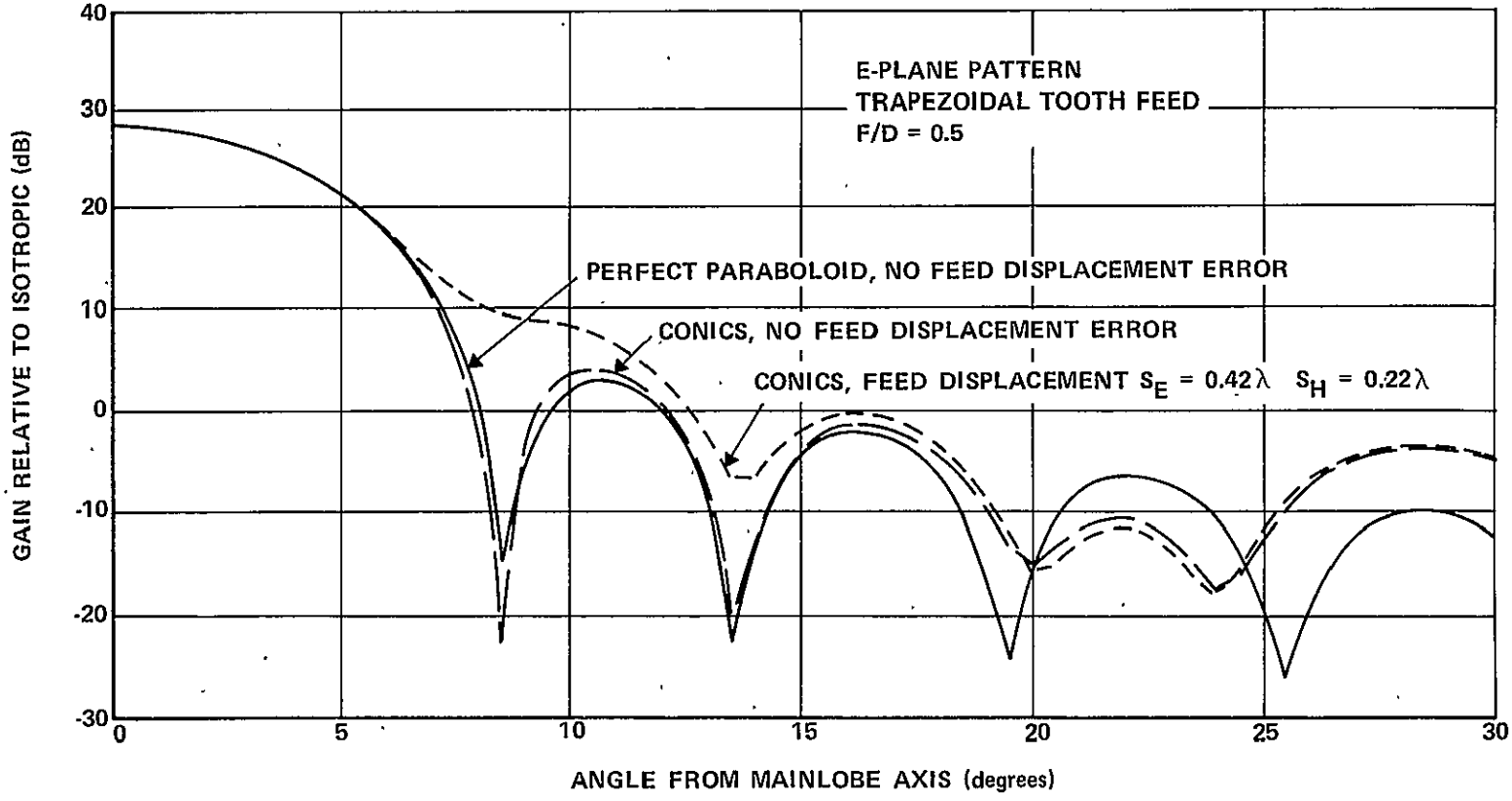

Figure 15 EFFECT OF CONIC SURFACES AND FEED PHASE: 30 MHz

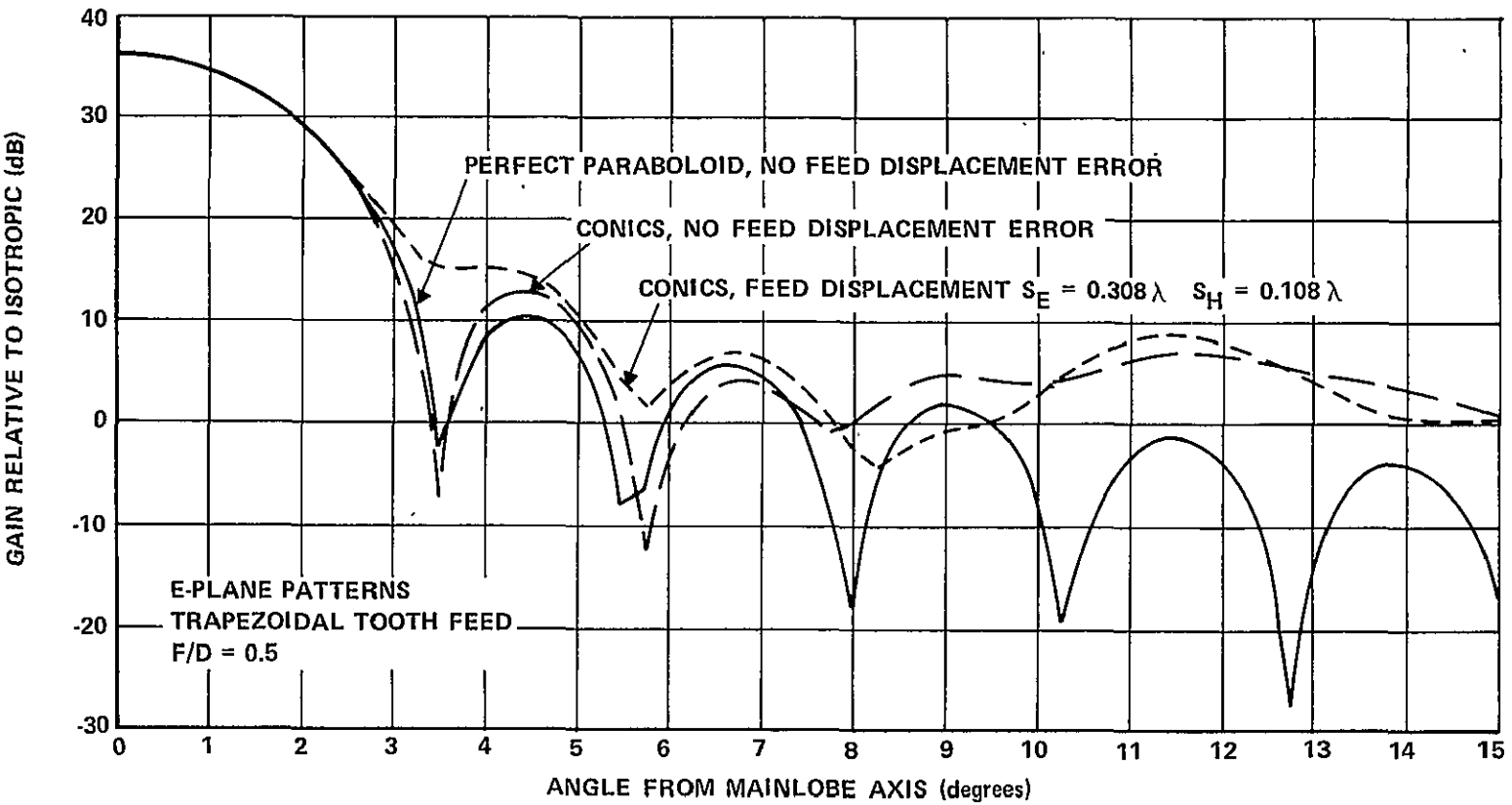

Figure 16 EFFECT OF CONIC SURFACES AND FEED PHASE: 72 MHz

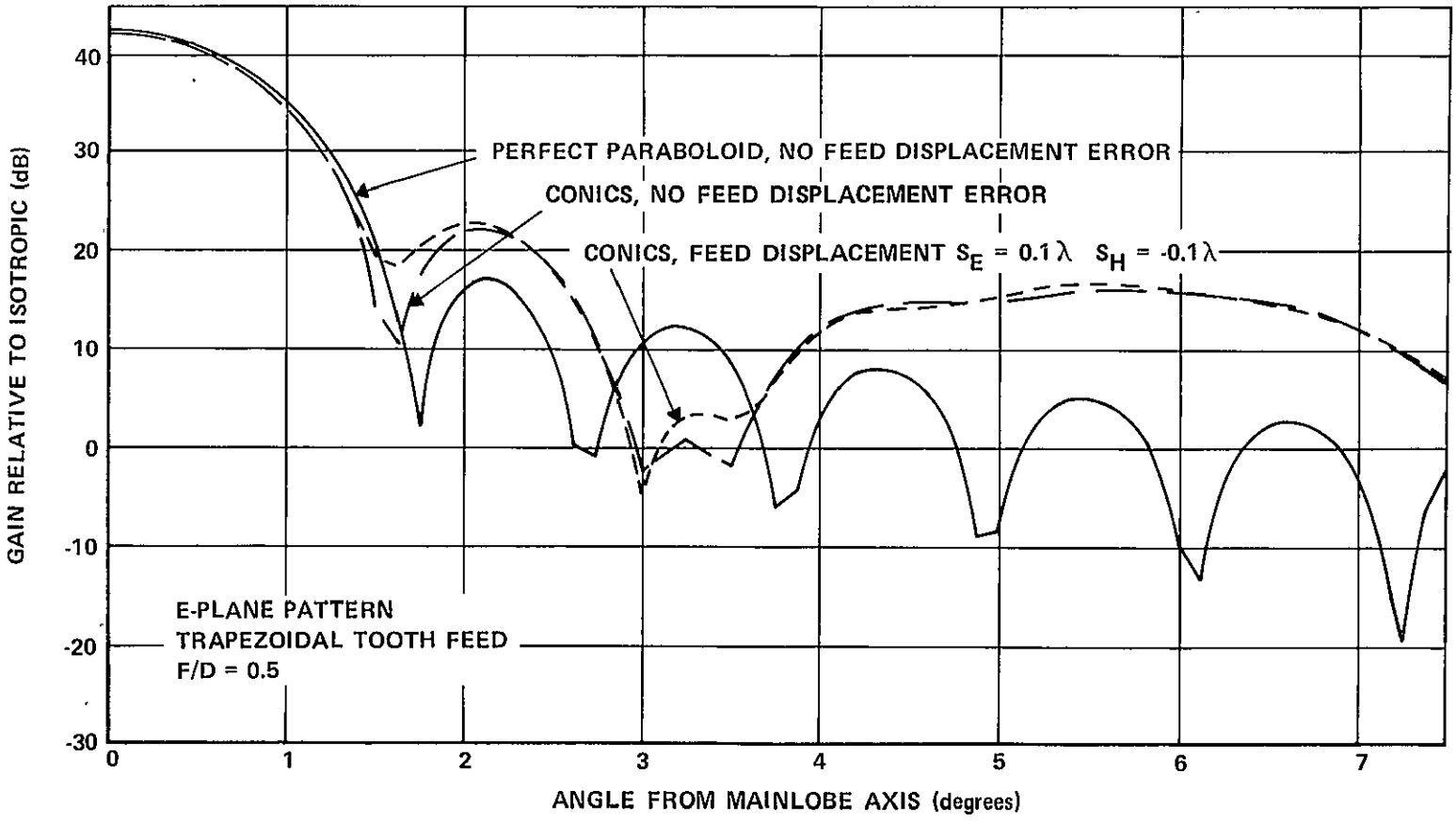

Figure 17 EFFECT OF CONIC SURFACES AND FEED PHASE: 150 MHz

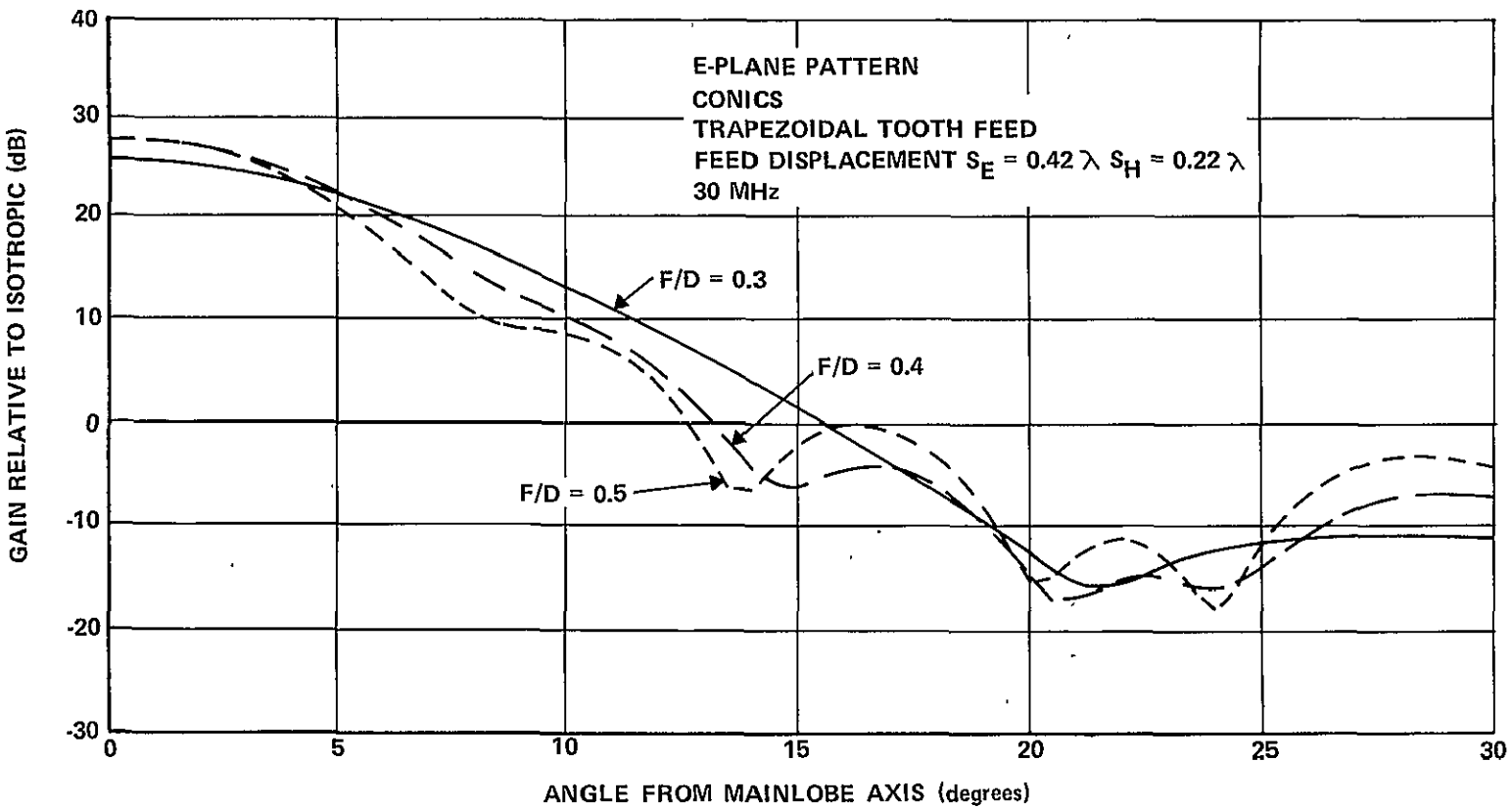

Figure 18 EFFECT OF F/D RATIO, TRAPEZOIDAL TOOTH FEED: E-PLANE

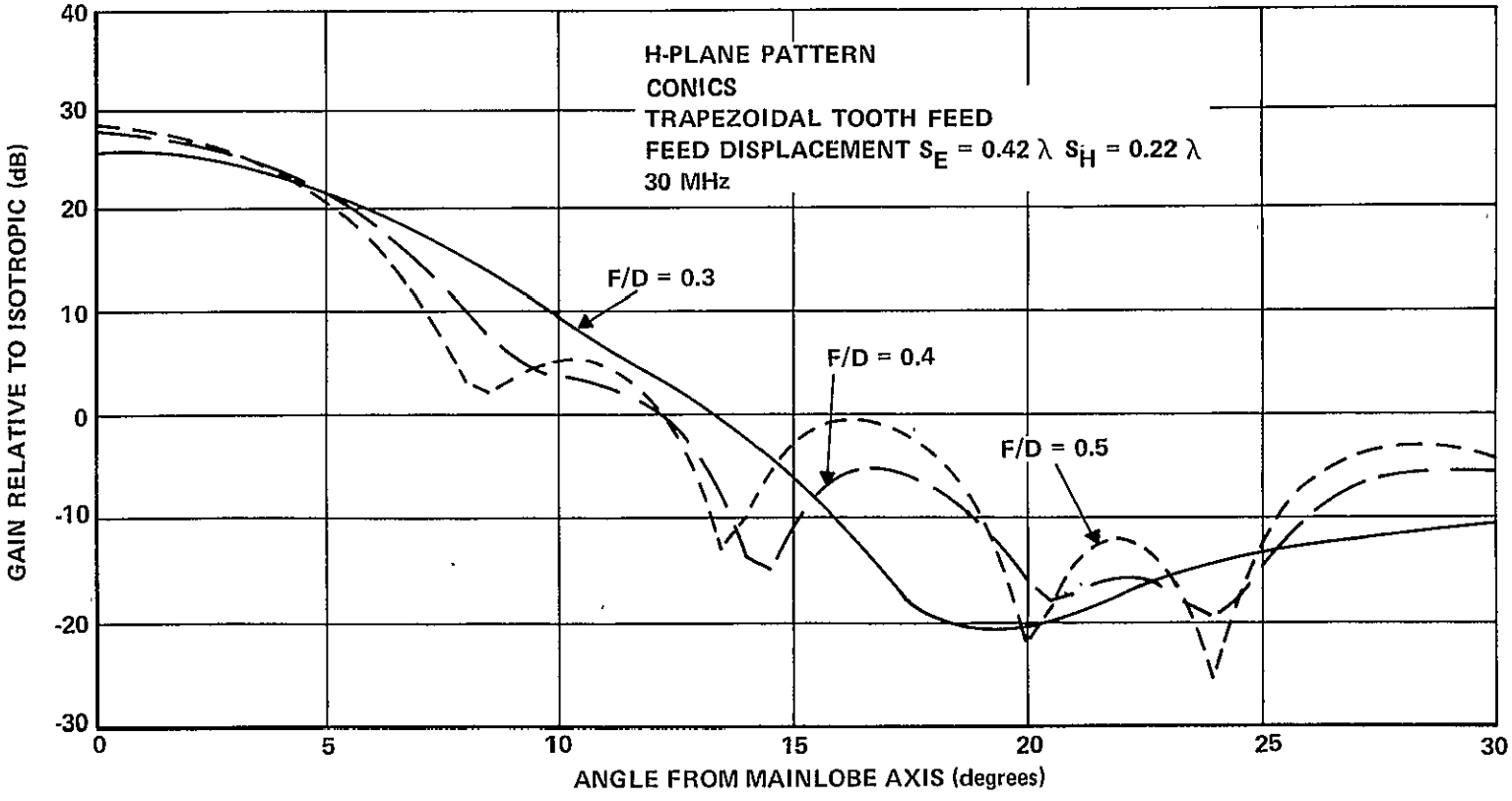

Figure 19 EFFECT OF F/D RATIO, TRAPEZOIDAL TOOTH FEED: H-PLANE

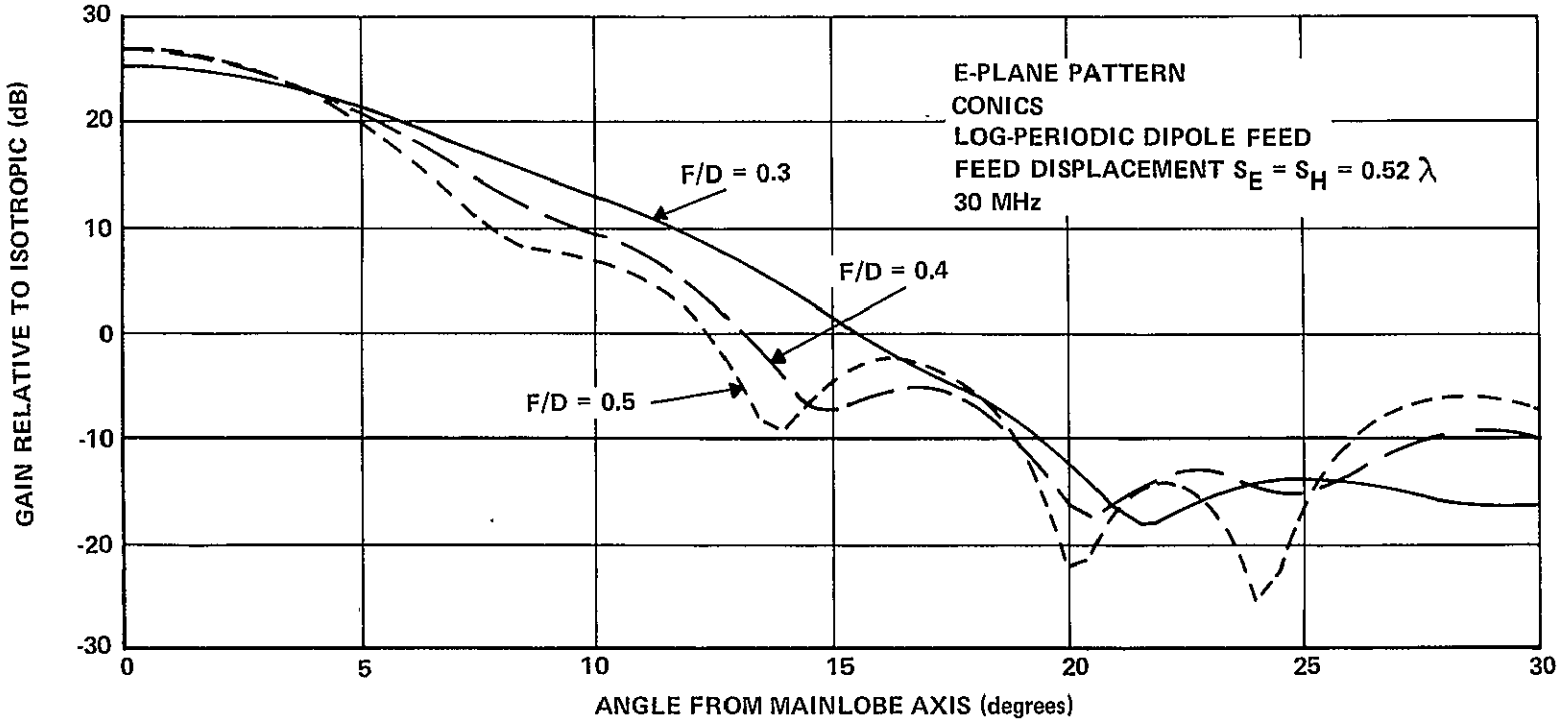

Figure 20 EFFECT OF F/D RATIO, LOG-PERIODIC DIPOLE FEED: E-PLANE

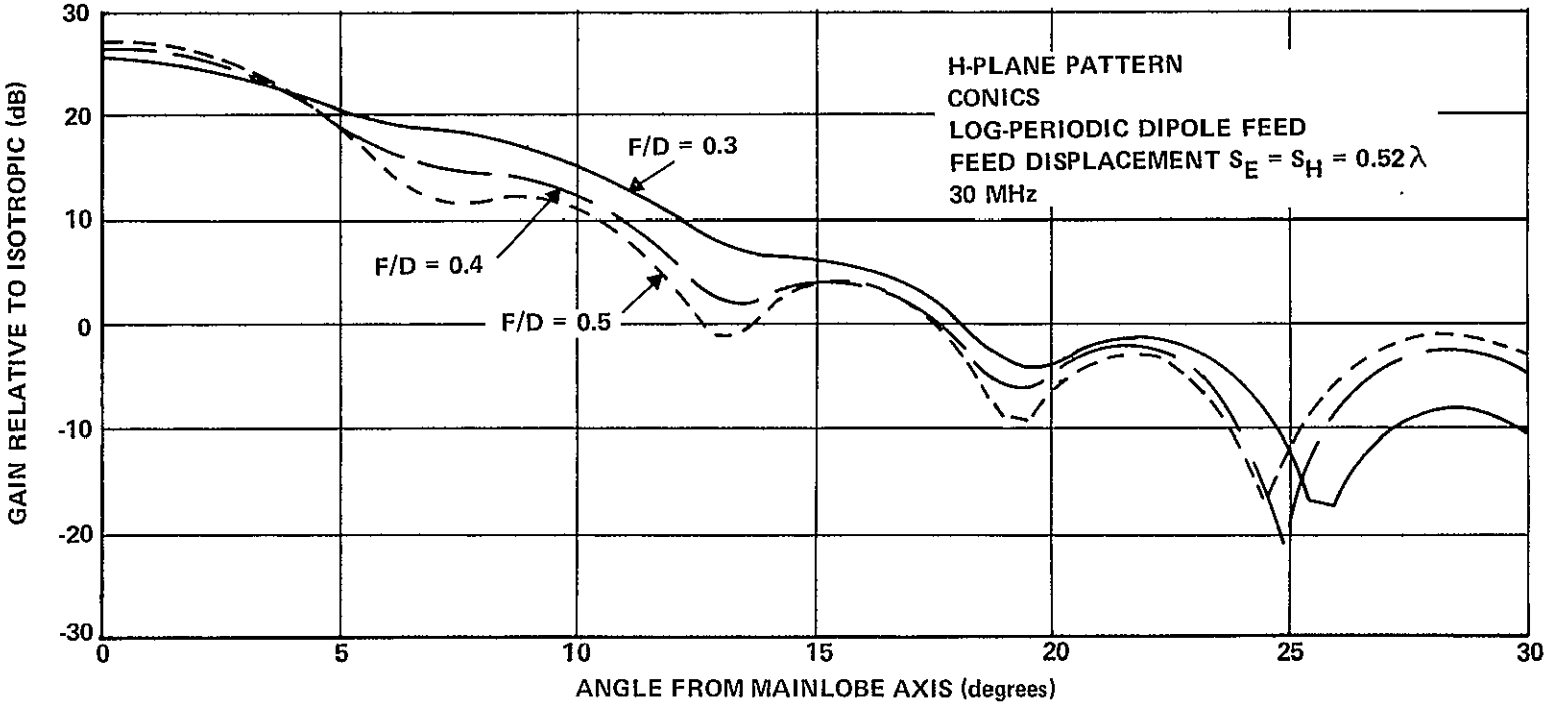

Figure 21 EFFECT OF F/D RATIO, LOG-PERIODIC DIPOLE FEED: H-PLANE

patterns are nearly the same, when a trapezoidal tooth feed is used; only null depths between sidelobes are different. Using the log-periodic dipole feed, H-plane patterns have high sidelobe level and narrow beamwidth, because there is little illumination taper in this plane (Figure 12B).

Typical patterns in the 45° plane are shown in Figure 22. Cross-polarization is maximum in this plane, having a null on-axis and a maximum at about one 3-dB beamwidth off-axis. There is no cross-polarization in the E- and H-planes, because of the assumed symmetry of reflector and feed.

A summary of all cases investigated is given in Tables 6, 7, 8 and 9 for frequencies of 15, 30, 72 and 150 MHz, respectively. Gain and beamwidth at the 3-dB and 20-dB points, sidelobe level relative to the mainlobe, and cross-polarization level relative to the mainlobe are given as functions of F/D ratio. Results for the trapezoidal tooth and log-periodic dipole feeds are also tabulated. Cross-polarization level relative to the mainlobe is tabulated only for the 45° plane pattern. The meaning of the notation in the first column on the left is:

"Paraboloid": Entire reflector is a perfect parabola. Also, there is no feed phase center displacement error.

"Conics": Inner portion of the reflector has conic surfaces as illustrated in Figure 13. No feed phase error is included.

"Conics, Phase": Conic reflector surfaces and feed phase center displacement error are both included.

The phase center displacements S_E and S_H in wavelenghs of both feeds at each frequency are given in the heading of each table.

The following trends and conclusions are apparent from the tabulated data:

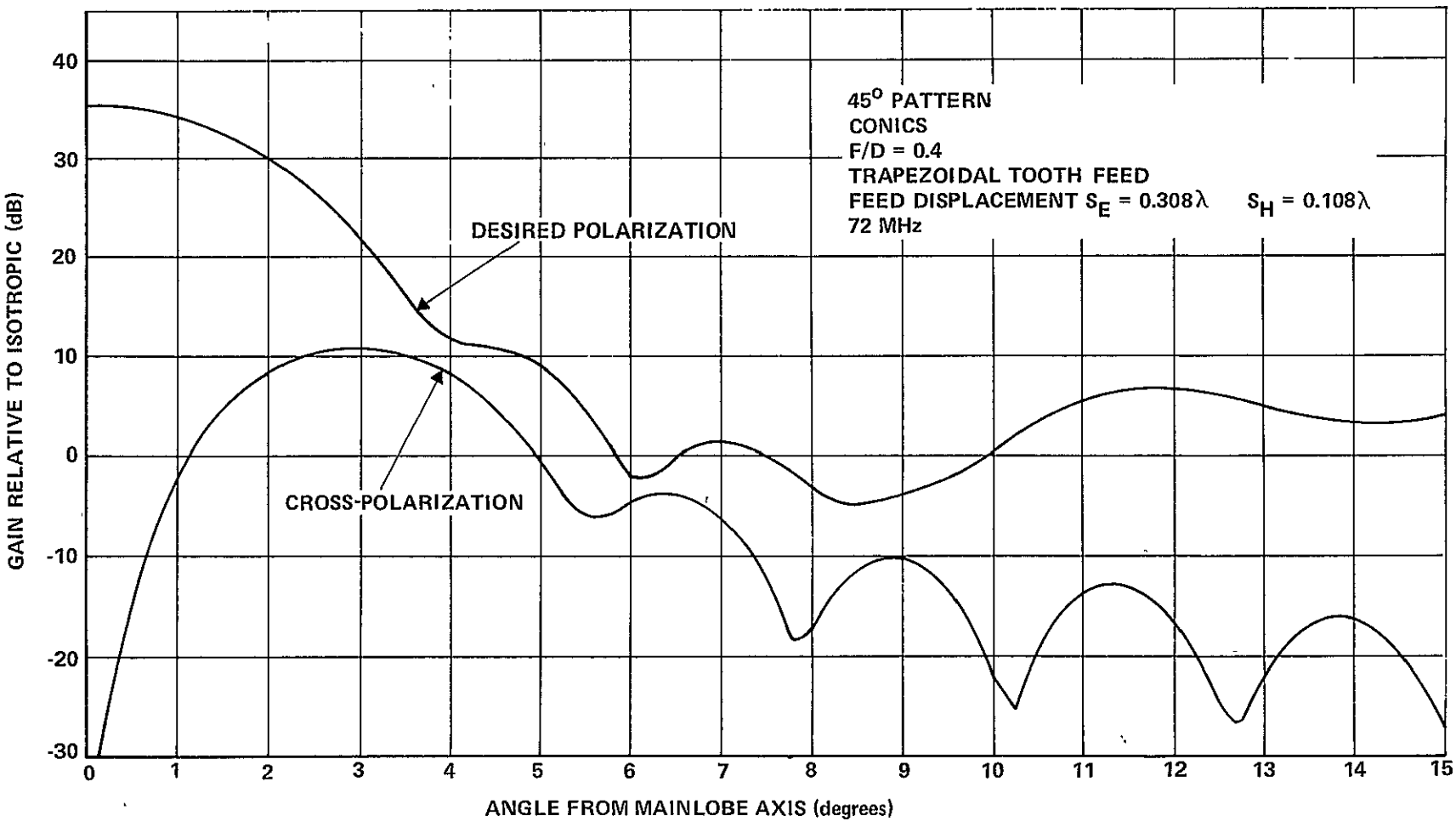

Figure 22 TYPICAL PATTERNS IN 45° PLANE

Table 6
ANTENNA PERFORMANCE SUMMARY: 15 MHz

TRAPEZOIDAL TOOTH (TT) FEED $S_E = 0.46\lambda$ $S_H = 0.26\lambda$

LOG-PERIODIC DIPOLE (LPD) FEED $S_E = S_H = 0.62\lambda$

F/D = 0.3	PATTERN	GAIN (dB)		BEAMWIDTH (degrees) (3 dB)		BEAMWIDTH (degrees) (20 dB)		SIDELOBE LEVEL (dB)		CROSS POLARIZATION* (dB)	
		TT	LPD	TT	LPD	TT	LPD	TT	LPD	TT	LPD
PARABOLOID	E	20.48	—	16.8	—	42.0	—	49.0	—	23	—
	45			16.9	—	41.5	—	42.0	—		
	H			17.0	—	42.4	—	41.0	—		
CONICS	E	20.40	21.67	16.9	16.3	42.0	40.0	43.5	45.5	23	20.5
	45			17.0	14.3	41.5	33.4	40.5	33.0		
	H			17.0	12.8	42.4	28.8	39.5	23.0		
CONICS, PHASE	E	19.70	18.92	17.5	16.8	54.3	56.4	46.0	39.0	23	18.5
	45			17.4	15.9	52.3	62.0	35.0	22.0		
	H			16.8	15.3	50.0	75.0	35.5	16.5		

F/D = 0.4

PARABOLOID	E	—	—	—	—	—	—	—	—	—	—
	45			—	—	—	—	—	—		
	H			—	—	—	—	—	—		
CONICS	E	22.10	21.92	14.1	14.3	32.8	33.4	31.5	34.0	24.5	23.5
	45			14.2	13.2	32.6	29.6	29.0	25.0		
	H			14.2	12.3	32.8	26.7	30.0	21.0		
CONICS, PHASE	E	21.62	20.65	14.5	14.3	46.0	47.0	32.9	32.0	24.2	22.5
	45			14.3	13.5	44.0	48.6	31.8	25.0		
	H			14.2	12.7	39.0	50.2	32.0	20.5		

F/D = 0.5

PARABOLOID	E	22.62	—	13.1	—	29.5	—	26.0	—	27.0	—
	45			13.2	—	29.5	—	25.0	—		
	H			13.3	—	29.6	—	25.0	—		
CONICS	E	22.50	21.56	13.0	13.4	29.2	30.4	25.5	27.0	27.0	26.5
	45			13.1	12.7	29.2	28.0	24.5	22.5		
	H			13.1	12.1	29.2	26.0	24.5	19.0		
CONICS, PHASE	E	22.22	20.91	13.2	13.3	41.0	41.0	20.3	20.0	26.7	25.0
	45			13.1	12.7	34.0	46.0	20.3	16.0		
	H			13.1	12.2	30.0	47.0	21.4	14.0		

*ASSUMING NO FEED CROSS-POLARIZATION

Table 7
ANTENNA PERFORMANCE SUMMARY: 30 MHz

TRAPEZOIDAL TOOTH (TT) FEED $S_E = 0.42\ \lambda$ $S_H = 0.22\ \lambda$

LOG-PERIODIC DIPOLE (LPD) FEED $S_E = S_H = 0.52\ \lambda$

		GAIN (dB)		BEAMWIDTH (degrees) (3 dB)		BEAMWIDTH (degrees) (20 dB)		SIDELOBE LEVEL (dB)		CROSS POLARIZATION* (dB)	
F/D = 0.3	PATTERN	TT	LPD	TT	LPD	TT	LPD	TT	LPD	TT	LPD
PARABOLOID	E	—	—	—	—	—	—	—	—	—	—
	45			—	—	—	—	—	—		
	H			—	—	—	—	—	—		
CONICS	E	26.48	27.67	8.5	8.18	20.6	19.6	36.0	39.5	23	20.5
	45			8.5	7.14	20.4	16.5	36.0	33.0		
	H			8.5	6.40	20.6	14.2	36.0	23.0		
CONICS, PHASE	E	25.82	25.39	9.1	8.50	27.0	27.2	37.0	39.0	23	18.5
	45			8.8	7.80	24.8	26.8	37.5	32.5		
	H			8.5	7.27	22.4	32.0	37.0	27.0		
F/D = 0.4											
PARABOLOID	E	28.14	—	7.12	—	16.6	—	32.0	—	24.5	—
	45			7.12	—	16.6	—	30.5	—		
	H			7.12	—	16.6	—	32.0	—		
CONICS	E	28.13	27.93	7.10	7.19	16.3	16.6	31.0	34	24.5	23.5
	45			7.10	6.60	16.2	14.7	30.0	25		
	H			7.10	6.14	16.3	13.2	31.0	20		
CONICS, PHASE	E	27.70	26.86	7.17	7.25	24.0	24.0	32.0	32	24.5	23.0
	45			7.10	6.74	20.0	23.2	32.5	27		
	H			7.06	6.32	17.0	23.5	32.5	23		
F/D = 0.5											
PARABOLOID	E	28.64	—	6.60	—	14.6	—	25.5	—	27.0	—
	45			6.62	—	14.6	—	25.5	—		
	H			6.62	—	14.7	—	25.5	—		
CONICS	E	28.50	27.56	6.55	6.72	14.8	15.0	24.5	26.5	27.0	26.5
	45			6.55	6.33	14.8	13.8	24.0	22.5		
	H			6.55	6.03	14.8	13.0	24.5	19.0		
CONICS, PHASE	E	28.27	27.02	6.64	6.72	20.0	20.0	20.0	20.0	27.1	26.0
	45			6.59	6.38	15.4	22.0	21.3	17.0		
	H			6.54	6.02	14.8	22.6	22.7	15.0		

*ASSUMING NO FEED CROSS-POLARIZATION

Table 8
ANTENNA PERFORMANCE SUMMARY: 72 MHz

TRAPEZOIDAL TOOTH (TT) FEED $S_E = 0.308\lambda$ $S_H = 0.108\lambda$

LOG-PERIODIC DIPOLE (LPD) FEED $S_E = S_H = 0.24\lambda$

F/D = 0 3	PATTERN	GAIN (dB)		BEAMWIDTH (degrees) (3 dB)		BEAMWIDTH (degrees) (20 dB)		SIDELOBE LEVEL (dB)		CROSS POLARIZATION* (dB)	
		TT	LPD	TT	LPD	TT	LPD	TT	LPD	TT	LPD
PARABOLOID	E	—	—	—	—	—	—	—	—	—	—
	45			—	—	—	—	—	—		
	H			—	—	—	—	—	—		
CONICS	E	33.98	35.16	3 52	3 39	8.4	8.1	29 0	32 5	23.0	20.0
	45			3.51	2.96	8.3	6 7	29 0	32.0		
	H			3.51	2.68	8.4	5 8	29 0	22.0		
CONICS, PHASE	E	33 63	34.65	3 70	3.42	10 3	9 0	28 5	32.0	23.0	20.0
	45			3.60	3.00	9.2	8 9	28.5	31.0		
	H			3 50	2.70	8 4	9.3	28.5	27 0		

F/D = 0 4

PARABOLOID	E	35.84	—	2 95	—	6.8	—	33.5	—	—	—
	45			—	—	—	—	—	—		
	H			—	—	—	—	—	—		
CONICS	E	35.64	35 42	2.95	2.98	6 7	6.78	29.0	30.5	24 5	23 5
	45			2 95	2 72	6 7	6.03	28.0	24 0		
	H			2 95	2 54	6 7	5.45	29 0	19 0		
CONICS, PHASE	E	35.42	35.17	3.02	2.99	8.4	7.20	28 3	25 0	24.7	23.0
	45			2 97	2.74	7.1	6 80	28.6	20 0		
	H			2.92	2,55	6.6	9.20	28.0	17.0		

F/D = 0.5

PARABOLOID	E	36.24	—	2.75	—	6.15	—	25.5	—	27.5	—
	45			2 75	—	6 15	—	25.0	—		
	H			2.75	—	6.15	—	25.5	—		
CONICS	E	36 02	35.05	2.70	2 78	6 0	6.15	23.0	25.0	27.5	26 5
	45			2.70	2.62	6.0	5 66	23 0	21 5		
	H			2.70	2.50	6.0	5 30	23.0	18.0		
CONICS, PHASE	E	35 90	—	2.75	—	6.8	—	20.4	—	27.2	—
	45			2.73	—	6 1	—	22.0	—		
	H			2.71	—	6 2	—	22.7	—		

*ASSUMING NO FEED CROSS-POLARIZATION

Table 9
ANTENNA PERFORMANCE SUMMARY: 150 MHz

TRAPEZOIDAL TOOTH (TT) FEED $S_E = 0.1\lambda$ $S_H = -0.1\lambda$

LOG-PERIODIC DIPOLE (LPD) FEED $S_E = S_H = -0.28\lambda$

F/D = 0.3	PATTERN	GAIN (dB)		BEAMWIDTH (degrees) (3 dB)		BEAMWIDTH (degrees) (20 dB)		SIDELOBE LEVEL (dB)		CROSS POLARIZATION* (dB)	
		TT	LPD	TT	LPD	TT	LPD	TT	LPD	TT	LPD
	E			1.73	—	4.20	—	46.0	—		
PARABOLOID	45	40.59	—	1.71	—	4.15	—	51.0	—	23.5	—
	H			1.71	—	4.17	—	45.0	—		
	E			1.65	1.60	3.80	3.72	24.5	28.0		
CONICS	45	39.91	41.20	1.65	1.39	3.75	3.12	24.5	25.5	23.0	20
	H			1.64	1.25	3.80	2.66	24.5	19.0		
	E			1.67	1.62	4.10	4.10	24.5	27.5		
CONICS, PHASE	45	39.81	40.57	1.66	1.43	3.80	4.15	24.5	27.0	23.0	20
	H			1.66	1.28	3.85	4.68	24.5	23.5		

F/D = 0.4

	E			—	—	—	—	—	—		
PARABOLOID	45	—	—	—	—	—	—	—	—	—	—
	H			—	—	—	—	—	—		
	E			1.38	1.40	3.10	3.13	23.0	25.0		
CONICS	45	41.62	41.45	1.38	1.29	3.10	2.79	22.5	20.5	24.5	23
	H			1.38	1.19	3.10	2.52	23.0	17.0		
	E			1.39	1.41	3.23	3.32	21.5	24.5		
CONICS, PHASE	45	41.56	41.18	1.38	1.30	3.07	3.10	22.8	20.0	24.4	23
	H			1.39	1.21	3.10	3.00	23.0	16.0		

F/D = 0.5

	E			1.32	—	2.90	—	25.5	—		
PARABOLOID	45	42.62	—	1.32	—	2.90	—	25.5	—	27.5	—
	H			1.32	—	2.90	—	25.5	—		
	E			1.27	1.31	2.76	2.85	20.0	21.0		
CONICS	45	42.02	41.06	1.27	1.24	2.76	2.60	20.5	18.5	27.0	26
	H			1.27	1.17	2.76	2.45	20.0	16.0		
	E			1.29	—	2.87	—	19.1	—		
CONICS, PHASE	45	41.98	—	1.28	—	2.77	—	19.7	—	26.9	—
	H			1.28	—	2.82	—	19.7	—		

*ASSUMING NO FEED CROSS-POLARIZATION

(1) The conic surfaces degrade performance more at high frequencies than at low frequencies.

(2) Feed phase center displacement degrades performance more at low frequencies than at high frequencies. This occurs because phase displacement was deliberately minimized at high frequency.

(3) At 15 and 30 MHz, some of the tabulated sidelobe levels are not much higher when feed phase error is included. This occurs because the first one or two sidelobes blend into the mainlobe. The deleterious effect of feed phase error will then show up as a much wider mainlobe beamwidth at the 20-dB points.

(4) Feed phase center displacement relative to the reflector focal point should be less than 0.4 wavelength. This can be accomplished with a fixed position, trapezoidal tooth antenna [6] but not with a fixed position, log-periodic dipole antenna [5].

(5) The optimum reflector F/D ratio using a trapezoidal tooth feed is 0.5, if maximum gain is desired. The worst case sidelobe level is 19 dB, when conic surfaces and feed phase center error are included. If F/D = 0.4 is used, gain is lower by 0.4 to 0.6 dB and the worst-case sidelobe level is 20 dB.

(6) The optimum reflector F/D ratio using a log-periodic dipole is 0.4. The worst-case sidelobe level is 17 dB and the gain is 0.7 to 1.6 dB lower than the gain obtainable with a trapezoidal tooth feed.

(7) Patterns using a trapezoidal tooth feed are essentially axisymmetric. E-plane patterns using a log-periodic dipole feed have 10 to 15 percent wider beamwidth than the H-plane patterns. Some radio astronomy applications require an axisymmetric mainlobe.

(8) Cross-polarization in the 45° plane is 1 to 2 dB worse using a log-periodic dipole feed as compared to using a trapezoidal tooth feed. It is emphasized that cross coupling in the feed has been neglected. A small F/D ratio also degrades the cross polarization.

It is concluded that the trapezoidal tooth feed antenna will provide better LOFT performance than a log-periodic dipole feed. The same conclusion obtains when each feed is moved to minimize phase center displacement error at a given operating frequency. The remainder of this report will concern itself only with the trapezoidal tooth feed. Feed measurements, however, are required to determine the cross-coupling obtainable with a trapezoidal tooth feed.

4.4 TEMPERATURE AND TORQUE EFFECTS

Surface distortions occur due to thermal and antenna steering (torque) forces. A temperature rise will lengthen all reflector members and tension stays, thereby deforming the surface from its shape at the design temperature. A steering torque normal to the reflector axis will exert unequal tension on the stays and deform the reflector from the axisymmetric shape it would otherwise have. The effect of these surface distortions on antenna performance will now be discussed. A perfectly reflecting surface is assumed.

Typical shapes of surface errors [29] due to temperature (solar radiation) and antenna steering torque are shown in Figure 23 as a function of normalized reflector radius for and F/D ratio of 0.443. Also shown is the

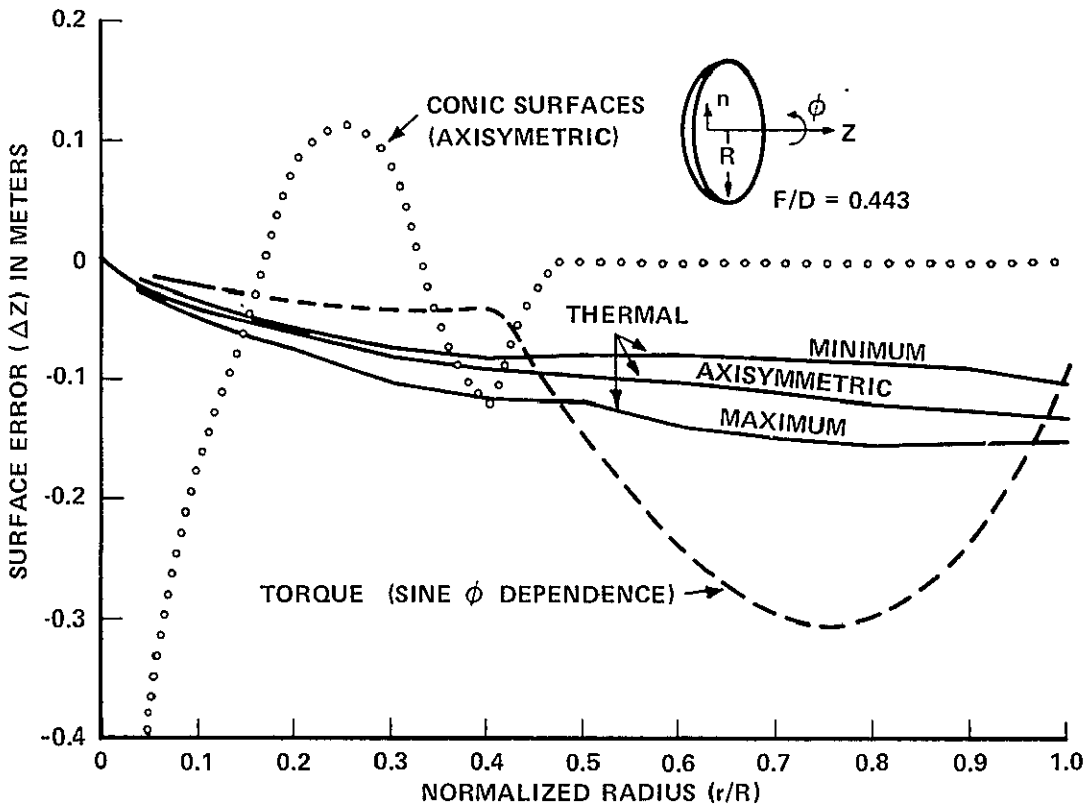

Figure 23 REFLECTOR SURFACE ERRORS

deviation of the conic surfaces for a 100-meter-diameter reflector relative to a parabola (this deviation is identically zero for normalized radius greater than 0.47, because conic surfaces are used only for smaller radii). Surface error due to temperature is mostly axisymmetric. The "minimum" and "maximum" curves indicate the total error, including circumferential variations (ϕ' direction). The exact ϕ' dependence given in Reference 29 was included in the far-field pattern computations. Surface error due to torque has sine ϕ' dependence: the curve in Figure 23 shows the error at $\phi' = 90°$.

The surface errors due to temperature and torque shown in Figure 23 were computed for a 50-meter-diameter reflector [29] rather than the 100-meter-diameter reflector considered in the CAL study. The surface error curves for a 100-meter reflector would be similar in shape but with a different maximum error [30]. The thermal surface error curve is for a worst case, where incident sunlight is parallel to one of the front tension stays. The torque surface error curve is for an applied torque of 3.71 newton-meters. During the CAL study, the surface errors due to thermal and torque effects (Figure 23) were scaled up by factors of 2 and 4 to parametrically investigate the effect of these errors on the reflector antenna patterns. The surface error due to torque would be present during reorientation of the antenna attitude. Far-field antenna patterns were computed using the asymmetric reflector computer program. (See Appendix B for a description of this computer program.)

All far-field patterns were computed using a trapezoidal tooth feed with the usual phase center displacement, conic surfaces, and for a reflector F/D ratio of 0.443. The calculations were performed for a frequency of 150 MHz, which provides the worst case reflector-surface-error-to-wavelength ratio. The cases covered follow.

Figure 24 H-plane, thermal surface error times 0, 1, 2, and 4*

*Indicates respectively: (0) no surface error (conic surfaces always present however), (1) surface error shown in Figure 23, (2) double the surface error shown in Figure 23, and (4) four times the surface error shown in Figure 23.

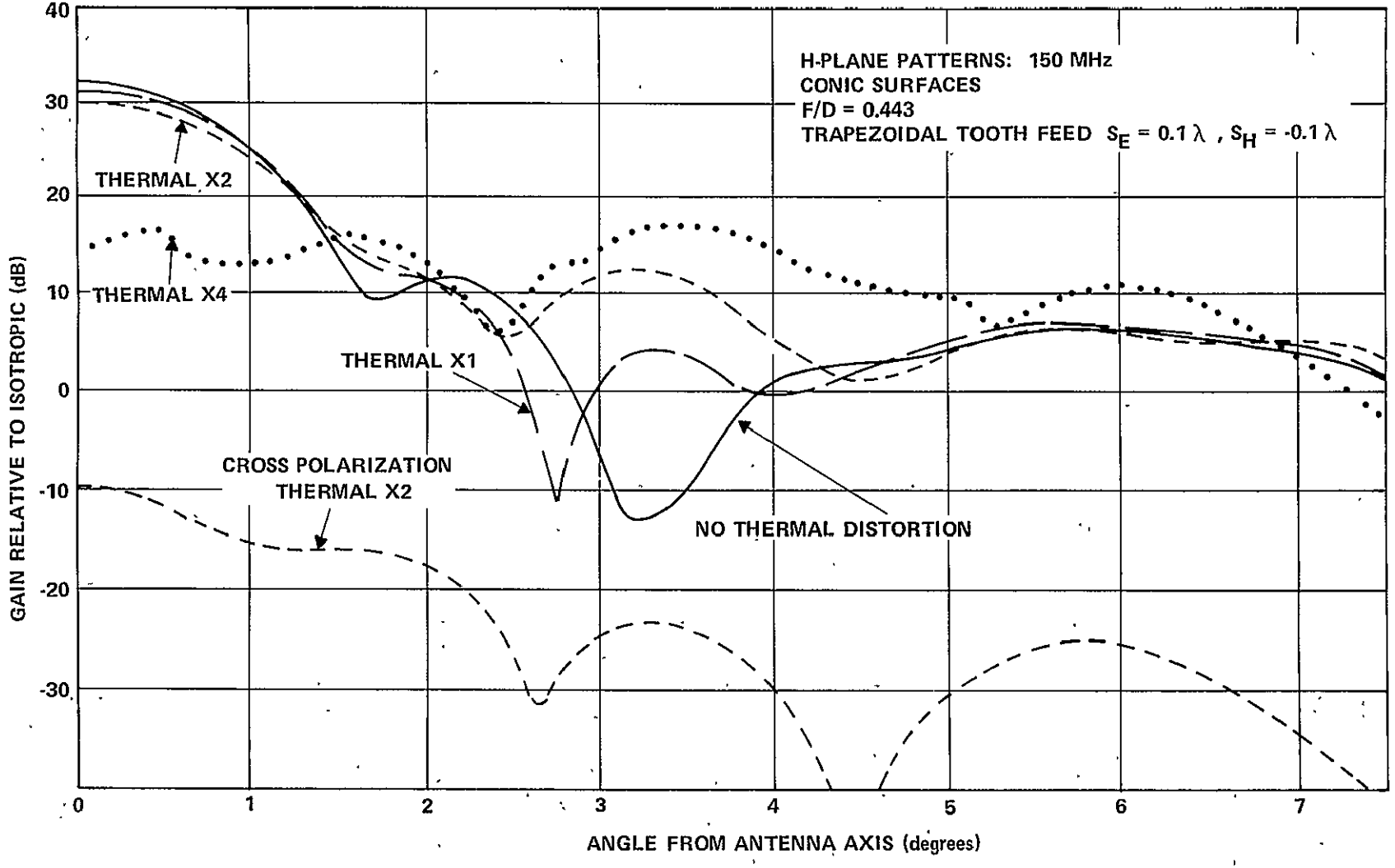

Figure 24 EFFECT OF THERMAL INDUCED SURFACE DISTORTIONS: 150 MHz

Figure 25 H-plane, torque surface error times 0, 1, 2 and 4

Figure 26 H-plane, both thermal and torque surface errors times 0, 1, and 2.

The mainlobe squints off-axis in the H-plane when torque is included due to the assumed sine ϕ' dependence of the surface error (Figure 23). This squint should remain in the plane of the applied torque and not follow the rotation of the LOFT antenna about its axis. Thus, if the torque plane is fixed in space, the squint will also be fixed in space.

E-plane patterns are not included, because they are not appreciably different from the H-plane patterns when torque is absent, and they do not pass through the mainlobe peak when torque is present. Cross-polarization is shown for the surface errors of Figure 23 doubled; it is zero when both thermal and torque surface distortions are zero, and increases as these distortions increase.

Gain, beam squint angle, beamwidth, sidelobe level, and cross-polarization level at 150 MHz as functions of surface distortions are given in Table 10. Gain applies to the mainlobe peak in the H-plane, which is greater than the gain on-axis when beam squint is present. E- and H-plane sidelobe and cross-polarization levels are relative to mainlobe peak level. E-plane beamwidths are not given when squint is present, because the E-plane pattern does not pass through the mainlobe peak.

4.5 FEED BLOCKAGE AND SCATTERING

The far-field computations presented so far have not included feed blockage and scattering. The feed produces a reflector surface current which radiates a field back toward the feed. This field incident on the feed is scattered by the feed and appears in the far field along with the field radiated by the reflector surface current. This scattered field will now be considered for a perfectly reflecting axisymmetric surface.

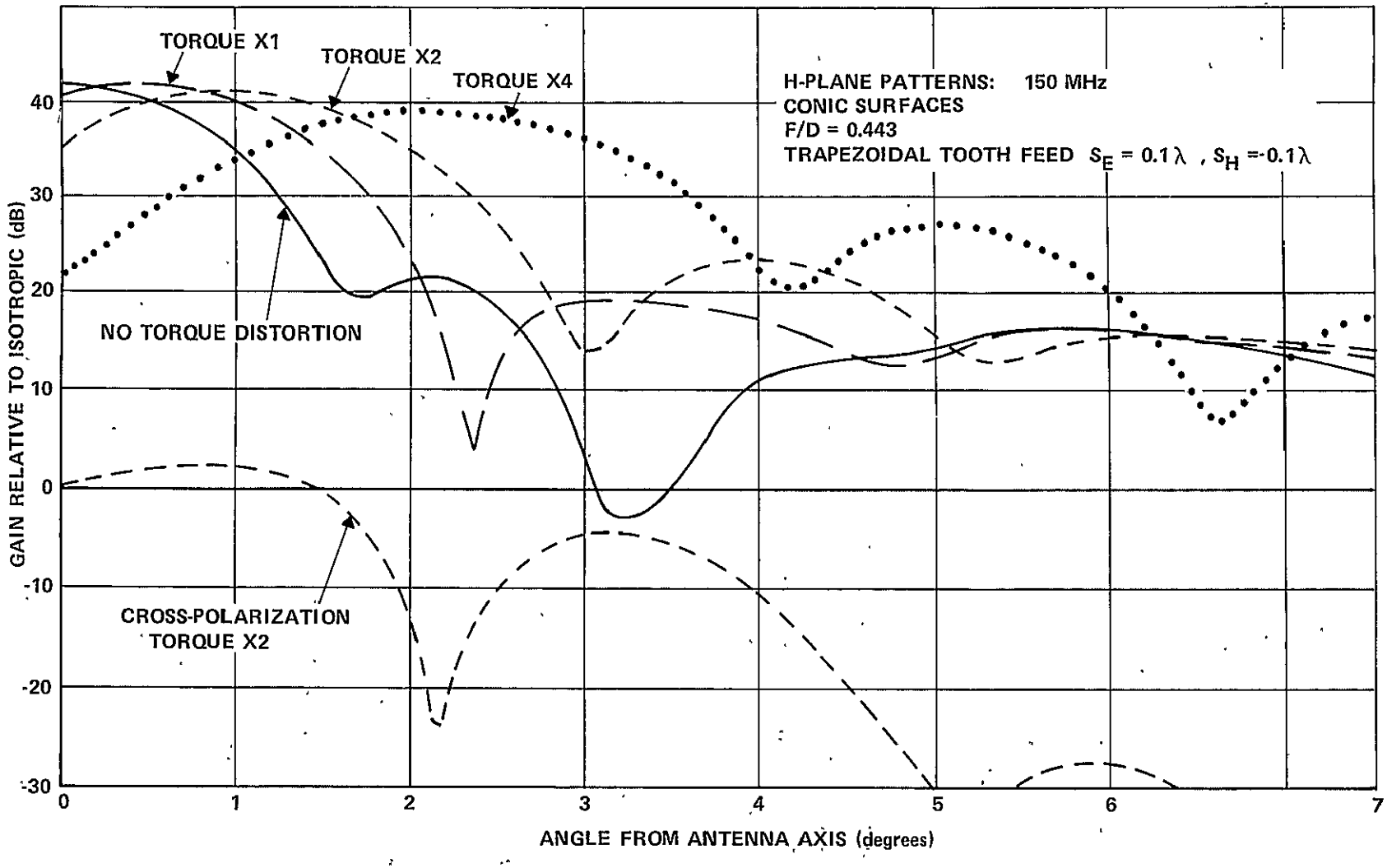

Figure 25 EFFECT OF TORQUE-INDUCED SURFACE DISTORTIONS: 150 MHz

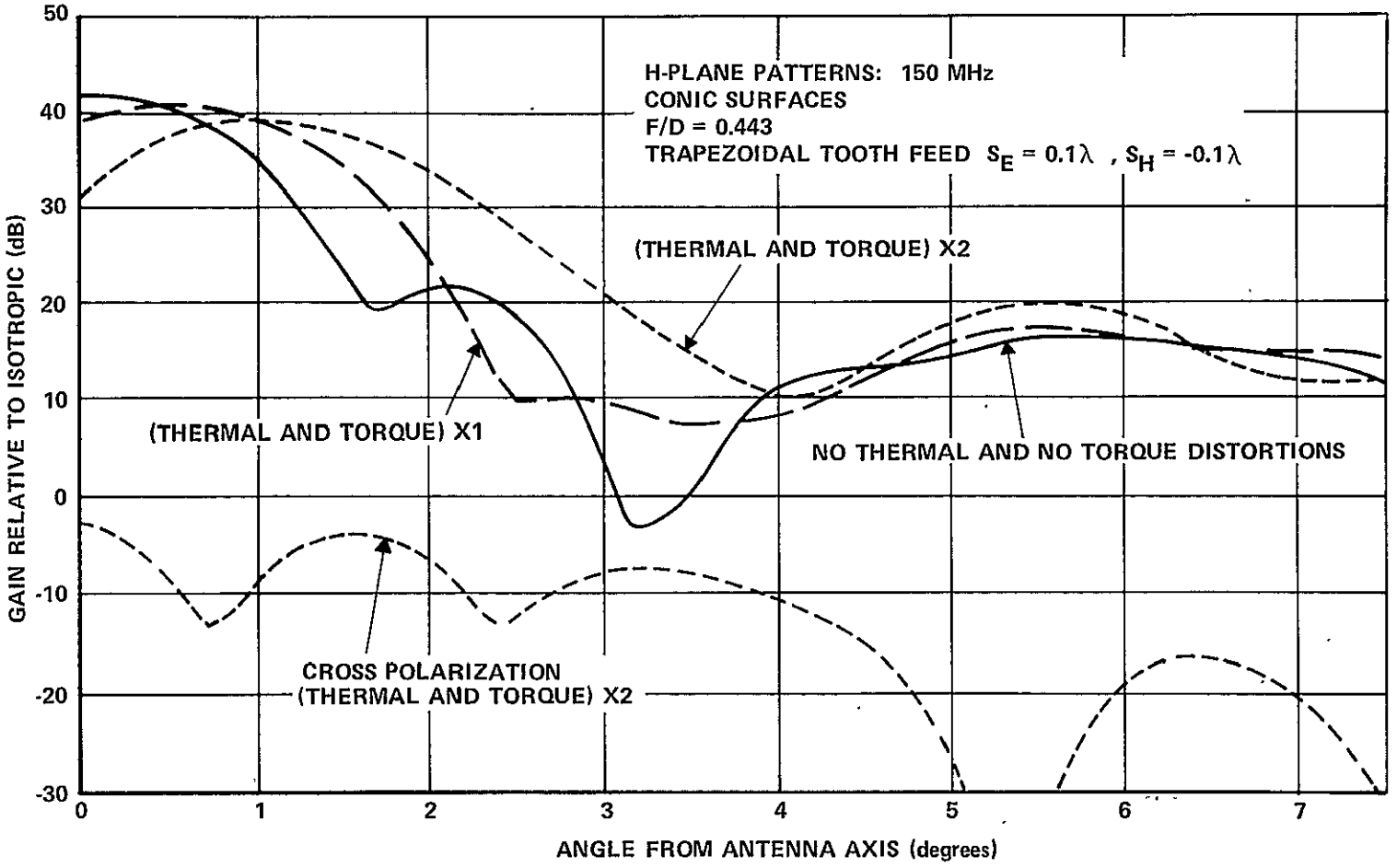

Figure 26 EFFECT OF THERMAL-AND TORQUE-INDUCED SURFACE DISTORTIONS: 150 MHz

Table 10

EFFECT OF SURFACE DISTORTIONS CAUSED BY TEMPERATURE AND TORQUE

CONIC AND PARABOLIC SURFACES
F/D = 0.443
TRAPEZOIDAL TOOTH FEED WITH PHASE CENTER DISPLACEMENTS $S_E = 0.1\lambda$, $S_H = -0.1\lambda$
150 MHz

CASE	GAIN (dB)	SQUINT ANGLE (degrees)	3-dB BEAMWIDTH (degrees)		SIDELOBE LEVEL (dB)		CROSS-POLARIZATION** (dB)	
			E	H	E	H	E	H
NO THERMAL OR TORQUE SURFACE ERROR	41.9	0	1.33	1.33	21.4	20.4	∞	∞
THERMAL SURFACE ERROR*	41.1	0	1.39	1.39	22.0	19.3	45.4	49.4
THERMAL SURFACE ERROR DOUBLED	39.9	0	1.48	1.48	21.0	17.3	35.2	39.5
THERMAL SURFACE ERROR QUADRUPLED	26.3	0	BEAM SPLIT		0.0	- 0.8	15.4	17.8
TORQUE SURFACE ERROR*	41.6	0.5	—	1.42	20.7	22.5	29.7	43.4
TORQUE SURFACE ERROR DOUBLED	40.9	1.0	—	1.53	18.3	17.5	25.2	38.4
TORQUE SURFACE ERROR QUADRUPLED	38.6	2.1	—	2.02	14.3	12.1	26.7	32.6
THERMAL AND TORQUE SURFACE ERRORS	40.9	0.5	—	1.44	22.3	23.8	28.5	46.3
BOTH THERMAL AND TORQUE SURFACE ERRORS DOUBLED	38.9	1.0	—	1.46	15.1	19.0	24.2	41.5

* SURFACE ERRORS DUE TO TEMPERATURE AND TORQUE GIVEN IN FIGURE 23

**ASSUMING NO FEED-CROSS-POLARIZATION

Feed scattering can be treated as an aperture blockage effect (Figure 27). The spherical wave radiated by the feed is columnated (approximately) into a plane wave by the reflector. The part of the plane wave intercepted by the feed is scattered in all directions, so as far as the far-field mainlobe and first few sidelobes are concerned, the reflector aperture illumination is zero (approximately) in the intercepted region. The equivalent blockage diameter of a log-periodic feed is approximately equal to its longest element length [6] or 10 meters for the LOFT antenna (one-half wavelengths at 15 MHz). Thus, the limits of integration in the axisymmetric reflector computer program were set to correspond to 10- and 100-meter diameters rather than 0 and 100 meters.

Far-field pattern computations with and without feed blockage are summarized in Table 11. A trapezoidal tooth feed with the usual phase center displacement, conic surfaces, and an F/D ratio of either 0.4 or 0.5 were assumed. Pattern shapes did not change appreciably when feed blockage was included; sidelobe peaks and null depths in most cases changed less than 2 dB. Beamwidths were only 0.5 to 1.0 percent wider with feed blockage, thus they are essentially the same as the beamwidths given in Tables 2 through 5. From Table 11, it is seen that feed blockage reduces gain 0.1 dB or less and increases sidelobes only slightly in most cases. Feed blockage caused more degradation with an F/D ratio of 0.4 as compared to 0.5. The reason that feed blockage caused so little far-field pattern degradation is that the patterns have already deteriorated owing to conic surface and feed phase errors. In fact, performance improved slightly at 150 MHz, because the feed blocks the reflector where conic surface error is large (Figure 23, $0 \leq r/R < 0.1$). If a perfect paraboloid with an F/D ratio of 0.4 and a trapezoidal tooth feed with no phase error were used, sidelobe level would increase from 34 dB without feed blockage to 26 dB with feed blockage [31].

An analysis of aperture blockage, approximating the feed as a dipole scatterer, is given in Appendix C. It is shown that direct radiation from the

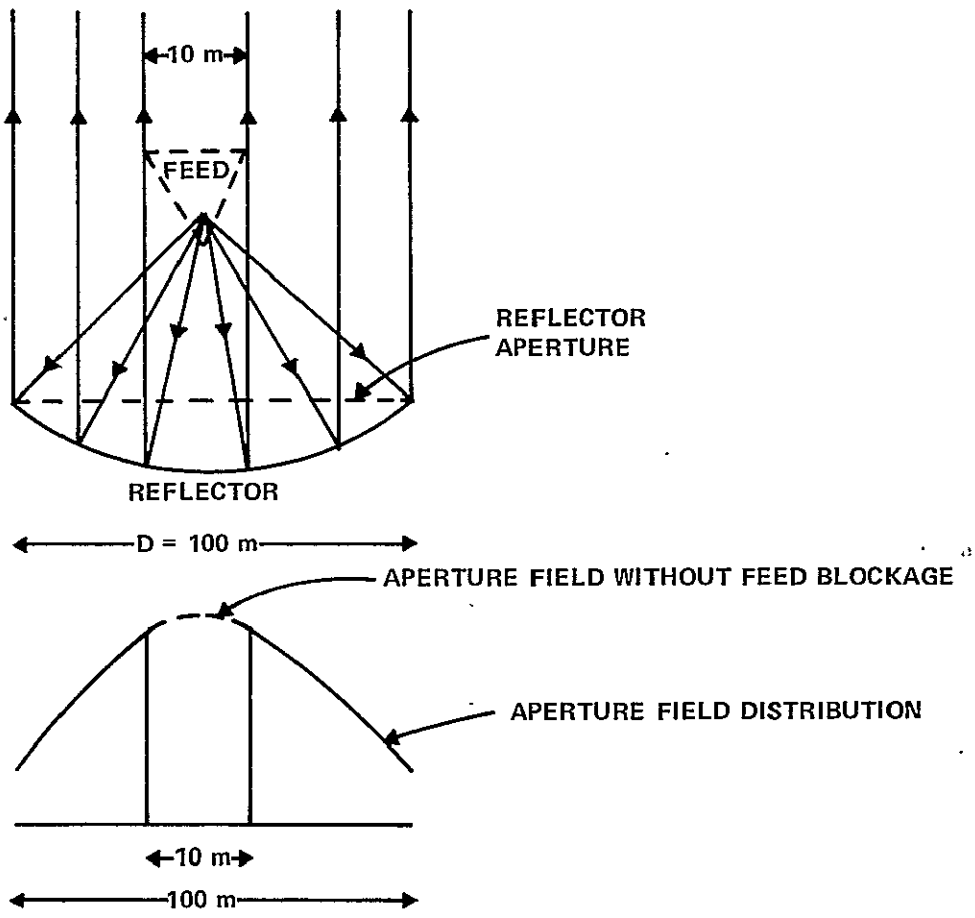

Figure 27 APERTURE BLOCKAGE BY FEED

Table 11
EFFECT OF FEED BLOCKAGE

CONIC AND PARABOLIC SURFACES
F/D = 0.4 OR 0.5
TRAPEZOIDAL TOOTH FEED WITH PHASE CENTER DISPLACEMENTS
$S_E = 0.5\lambda$ -0.8 AND $S_H = 0.3\lambda$ -0.8 METERS
15, 30, 72, AND 150 MHz

	FREQUENCY (MHz)	PATTERN	GAIN (dB) NO BLOCKAGE	GAIN (dB) WITH BLOCKAGE	SIDELOBE LEVEL (dB) NO BLOCKAGE	SIDELOBE LEVEL (dB) WITH BLOCKAGE	CROSS-POLARIZATION* IN 45° PLANE (dB) NO BLOCKAGE	CROSS-POLARIZATION* IN 45° PLANE (dB) WITH BLOCKAGE
F/D = 0.4	15	E	21.62	21.53	32.9	27.7	24.2	23 1
		45			31.8	27.4		
		H			32 0	28.2		
	30	E	27.70	27 61	32.0	31.8	24.5	24.5
		45			32.5	31.4		
		H			32.5	31.3		
	72	E	35.42	35.32	28.3	30.3	24.7	24.6
		45			28.6	31.1		
		H			28.0	24.3		
	150	E	41 56	41.63	21.5	20.8	24.4	24.5
		45			22.8	22.8		
		H			23 0	23.8		
F/D = 0.5	15	E	22 22	22.18	20.3	19.0	26.7	26.6
		45			20.3	19.8		
		H			21.4	20.6		
	30	E	28.27	28.22	20.0	18 7	27.1	27.0
		45			21.3	20.2		
		H			22.7	21.3		
	72	E	35.90	35.85	20.4	19 1	27.2	27.1
		45			22.0	20.5		
		H			22.7	21 4		
	150	E	41.98	42.06	19.1	19 2	26 9	27.0
		45			19.7	20 2		
		H			19.7	20.5		

*ASSUMING NO FEED-CROSS-POLARIZATION

feed antenna is expected to be larger than the field scattered from the feed. Thus, calculated radiation patterns for the LOFT antenna, which include direct feed radiation, are essentially accurate, even though the exact scattering pattern of the feed is not included.

4.6 REFLECTOR GRID

The effect of the reflector grid was analyzed by multiplying the surface current distribution of a perfect reflector by the grid reflection coefficient, equations (1) and (3), Section 3. These equations apply for a rectangular mesh reflector consisting of radial and circumferential strip conductors connected together at the junctions and an arbitrary feed polarization. The resultant current distribution was incorporated into the axisymmetric reflector computer program. The results of Section 3 indicate that the following guidelines should be used in the selection of a grid.

- It is not important that the orthogonal conductors are connected at the junctions, because the angle of incidence of the feed field onto the reflector is relatively small (less than 40° for any reflector whose F/D ratio is 0.3 or greater).

- A square mesh should be used rather than a rectangular mesh to keep the polarization of the reflected field nearly the same as that of the incident field.

- Conductor thickness and conductivity need only be large enough so that the term involving strip impedance, Z, is small relative to other terms. As shown in Section 3, stainless-steel conductors only 6.35 microns thick will suffice and aluminum conductors could be even thinner.

- A uniform-size mesh should be used throughout the reflector surface to minimize phase error due to the grid.

- The grid must have continuity in orthogonal directions. A weave with poor contact between adjacent conductors is unsuitable.

- The grid has most effect on radiation patterns at the highest operating frequency.

Far field patterns and gain were computed at 150 MHz for a uniform square mesh grid and the following parameters.

Reflector diameter	100 meters
F/D ratio	0.4
Conic and parabolic surfaces	
Trapezoidal tooth feed with usual phase center displacement ($S_E = 0.1\lambda$, $S_H = -0.1\lambda$ at 150 MHz)	
Frequency	150 MHz (worst case for grid)
Material conductivity	1.43×10^6 mho/meter (stainless steel)
Conductor thickness	12.7 microns
Conductor width	0.254 cm
Conductor spacings	2.54, 12.7 and 22.9 cm

Although an F/D ratio of 0.5 would probably be used in practice to achieve maximum gain, a ratio of 0.4 was chosen for this example, because the sidelobe level was lower and any change in sidelobe level due to the reflector grid would be more apparent.

The gain of the antenna for the grids investigated is given in Table 12. Also, the loss of gain due to grid leakage and dissipation is compared with the normal incidence reflection loss.

The loss of gain estimated from normal incidence reflection loss is slightly pessimistic, because the grid's reflection coefficient increases at non-normal incidence angles.

The pattern shapes for each grid were almost identical to the pattern computed for a perfect reflector. The mainlobe shape was unchanged; sidelobe peak level relative to the mainlobe changed less than 0.3 dB; and null depths changed only a few dB. The reason for so little change in pattern shape, even for the 9-inch spaced grid, is that the additional reflector phase error due to the grid was less than 10°.

A grid with nonuniform grid spacing causes more phase error than a uniformally spaced grid. Antenna patterns were computed for the variable grid spacing shown in Figure 21. Conductor thickness and width were held constant at 12.7 microns and 0.254 cm, respectively. Spacing between circumferential conductors was held constant at 22.9 cm. Spacing between radial conductors was varied as shown in Figure 28. The performance of this reflector grid relative to a perfectly reflecting grid is shown in Table 13.

As seen from the tabulated sidelobe levels, pattern shapes are no longer the same; in particular, the first E-plane sidelobe is 3.4 dB higher when the nonuniformally spaced grid is used. If a nonuniform grid is used, the spacing should not exceed 10 cm, in which case, phase error due to the grid will be small. Nonuniform grids with larger than 10-cm spacing should be evaluated with the surface integral computer program.

Table 12

EFFECT OF CONDUCTING GRID ON GAIN

GRID SPACING d (cm)	GAIN (dB)	GAIN LOSS (dB)	NORMAL INCIDENCE REFLECTION LOSS (dB)
PERFECT REFLECTOR	41.56	0	0
d = 2.54	41.55	0.01	0.035
d = 12.7	40.76	0.80	0.87
d = 22.9	38.90	2.66	3.25

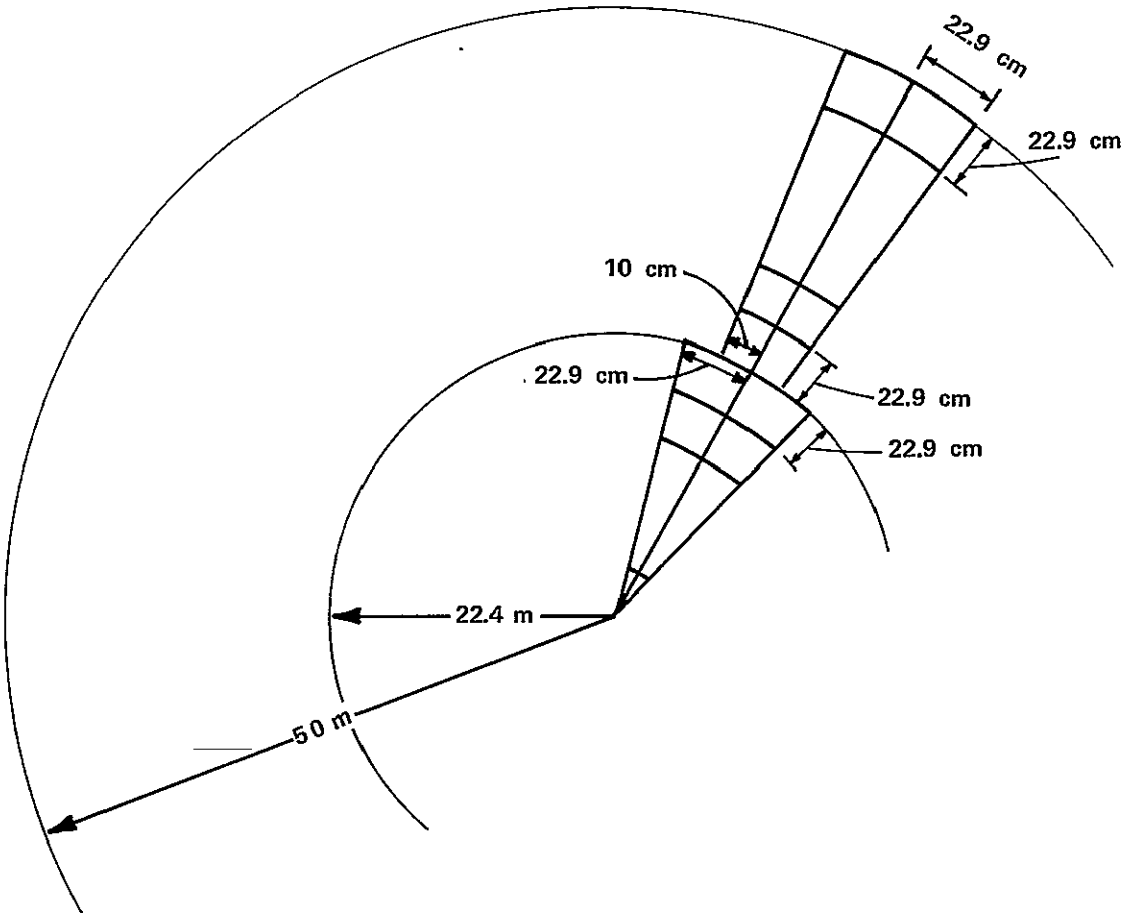

Figure 28 REFLECTOR GRID WITH NONUNIFORM SPACING

Table 13

EFFECT OF VARIABLE GRID SPACING

PARAMETER			PERFECT REFLECTOR (dB)	REFLECTOR SHOWN IN FIGURE 21 (dB)
GAIN			41.6	39.5
SIDELOBE LEVEL RELATIVE TO MAINLOBE	E-PLANE	1st LOBE	21.5	18.1
		2nd LOBE	25.8	26.3
	45° PLANE	1st LOBE	22.8	22.7
		2nd LOBE	25.8	26.2
	H-PLANE	1st LOBE	23.0	23.3
		2nd LOBE	25.5	25.0
CROSS-POLARIZATION IN 45° PLANE			24.4	26.2

Section 5
RADIATION FAR FROM MAINLOBE

Far from the mainlobe, field computation using a surface integral theory is unreliable, because the surface current distribution, due mainly to reflector edge effects, is not known with sufficient accuracy. Therefore, geometric diffraction theory (GDT) was used to calculate far-out sidelobe level. GDT considers fields only at the rim of the reflector and no integration is involved. A derivation of the GDT equations is given in Appendix D.

The surface integrals considered only well-defined surface distortions such as thermal and torque perturbations and the conics. There is, in addition, a billowing of the surface between reflector support members. Billowing is treated as a random surface error and the sidelobe level was computed using Equation 8, Reference 32.

Radiation in the shadow region was computed with GDT and from direct feed radiation which leaks through the grid. Direct feed radiation in the illuminated region is also considered. GDT does not accurately provide the backlobe level (180° away from mainlobe), because this direction is a geometric caustic. Instead, the backlobe was computed by integration of the feed field over a complete spherical surface except the area occupied by the reflector [33]. This theory considered only uniform reflector illumination and thus was modified by CAL to include the pattern of a trapezoidal tooth feed.

Radiation far from the mainlobe arising from edge diffraction, random surface errors, direct feed radiation, and reflector grid leakage are discussed in this section. No attempt is made to combine the radiation from all these mechanisms and to compute a resultant far-field pattern because the phase of the various contributions is not known with sufficient accuracy. Instead, the sidelobe level computed for each mechanism is separately described. This

method indicates clearly which is the dominant mechanism and the design changes necessary to improve performance. For example, if direct feed radiation dominates over all other causes of far-out sidelobe level, there is no point in trying to reduce far-out sidelobe level by improving reflector surface tolerance, or decreasing reflector F/D ratio. The average sidelobe power level of the composite pattern is the sum of the sidelobe power levels from all causes.

The subject of radiation far from the mainlobe is presented in the following manner. First, the parameters of the antenna analyzed are given. Then, GDT is compared with surface integral theory. Finally, patterns covering a 360° sector, showing separately the contributions of the various radiation mechanisms, are presented.

5.1 ANTENNA PARAMETERS

Calculations were performed for a reflector with conic surfaces and an F/D ratio of 0.4 or 0.5. A trapezoidal tooth feed with the previously used phase center displacements ($S_E = 0.5\lambda - 0.8$, $S_H = 0.3\lambda - 0.8$) was assumed. The conic surfaces and feed phase do not effect any of the results except those determined from the surface integral computer program. The feed patterns used are shown in Figure 29 and are representative of typical measured patterns of a trapezoidal tooth feed [6] having a worst-case front/back ratio of 10 dB. The computed gain of the feed based on these patterns is 9.6 dB. Thus, the backlobe gain of the feed (in the direction of the LOFT antenna mainlobe) is 0.4 dB.

Random surface errors representing reflector panel billowing of 0.03- and 0.1-meter RMS were assumed. These RMS errors correspond to peak-to-peak errors about three times larger. The correlation interval of the random surface error was set equal to an assumed reflector panel size of 1 meter.

A uniform, square mesh, reflector grid having 8.6-dB transmission loss at 150 MHz was assumed. The grid had 3-millimeter-wide conductors spaced

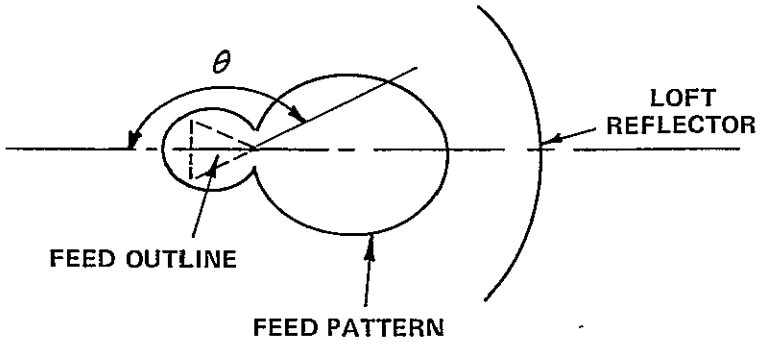

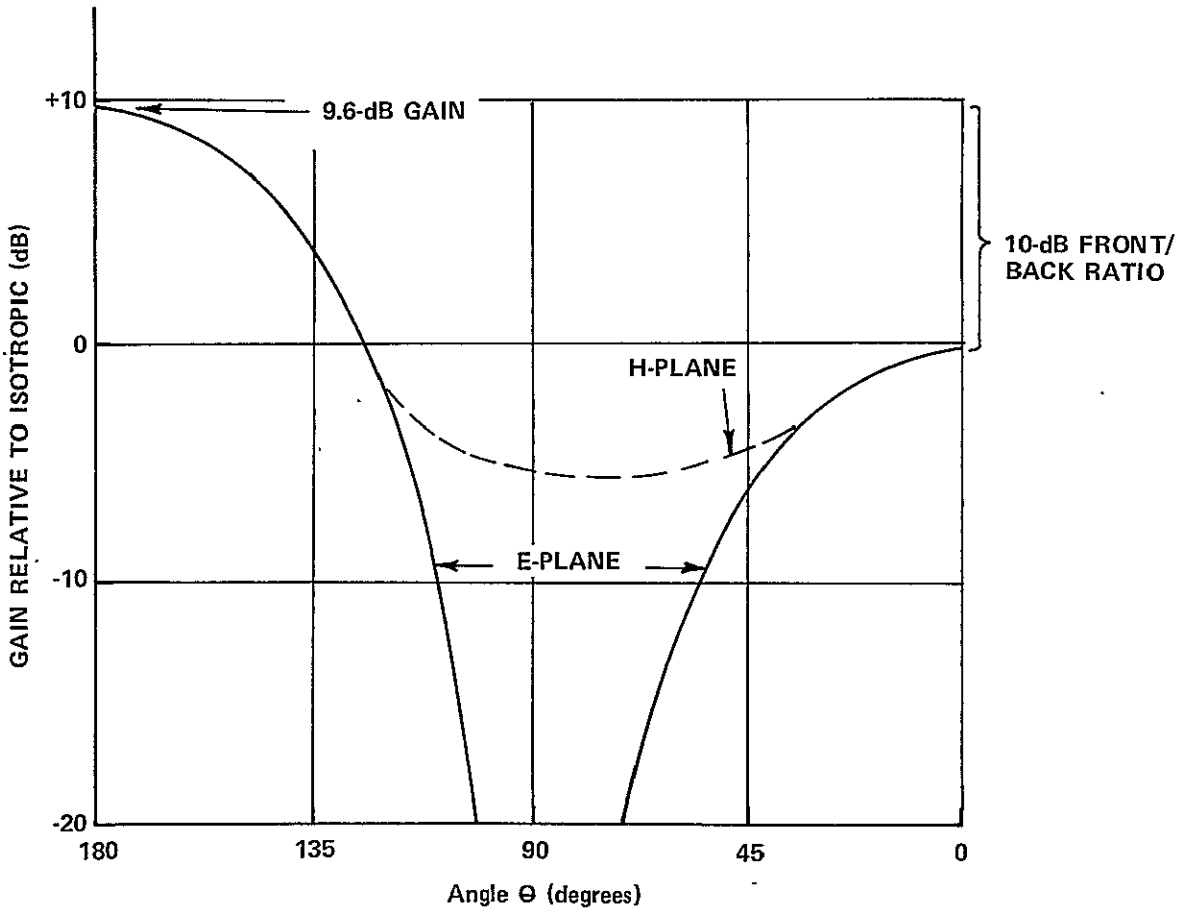

Figure 29 ASSUMED TRAPEZOIDAL TOOTH FEED PATTERNS

12 centimeters apart. This grid had transmission losses of 14.5, 22.0 and 28.0 dB at 72, 30 and 15 MHz, respectively. Its normal incidence reflection loss varied from 0.02 dB at 15 MHz to 0.60 dB at 150 MHz.

5.2 COMPARISON OF SURFACE INTEGRAL AND GDT

GDT relies heavily on geometric optic concepts. It was considered useful to compare the results obtained using GDT with those obtained using surface integral theory. The two theories gave results which agreed to within 3 dB on sidelobe level for an F/D ratio of 0.4 and within 1-1/2 dB for an F/D ratio of 0.5 when the reflector was a perfect paraboloid and feed phase error was zero. Equally good agreement occurred with a log-periodic dipole feed which gave a very nonuniform edge illumination. Therefore, confidence was established that GDT gave the proper sidelobe level, provided reflector surface error and feed phase error are small.

GDT and surface integral theory at 72 MHz are compared in Figure 30. The solid curves are for an F/D ratio of 0.4, and the dashed curves are for an F/D ratio of 0.5. Only H-plane patterns are shown, because GDT predicts the highest sidelobe level in this plane (3 dB higher than E-plane sidelobes). Conic surfaces and feed phase are included in the surface integral calculation. Direct feed radiation is also shown in Figure 30. The sidelobe patterns determined from GDT actually have many peaks and nulls; the curves shown are envelopes of sidelobe peaks. GDT predicts a 4- to 6-dB higher sidelobe level for an F/D ratio of 0.5 than for an F/D of 0.4, the reason being stronger reflector edge illumination.

The overall sidelobe level based on surface integral theory is the same for both F/D ratios and higher than GDT sidelobe level for either F/D ratio, especially near the mainlobe. The discrepancy results from feed phase and surface errors which increase sidelobe level as computed by surface integral theory, whereas GDT cannot account for either error. Direct feed radiation is stronger than sidelobe radiation computed from either surface integral or GDT at angles far from the mainlobe.

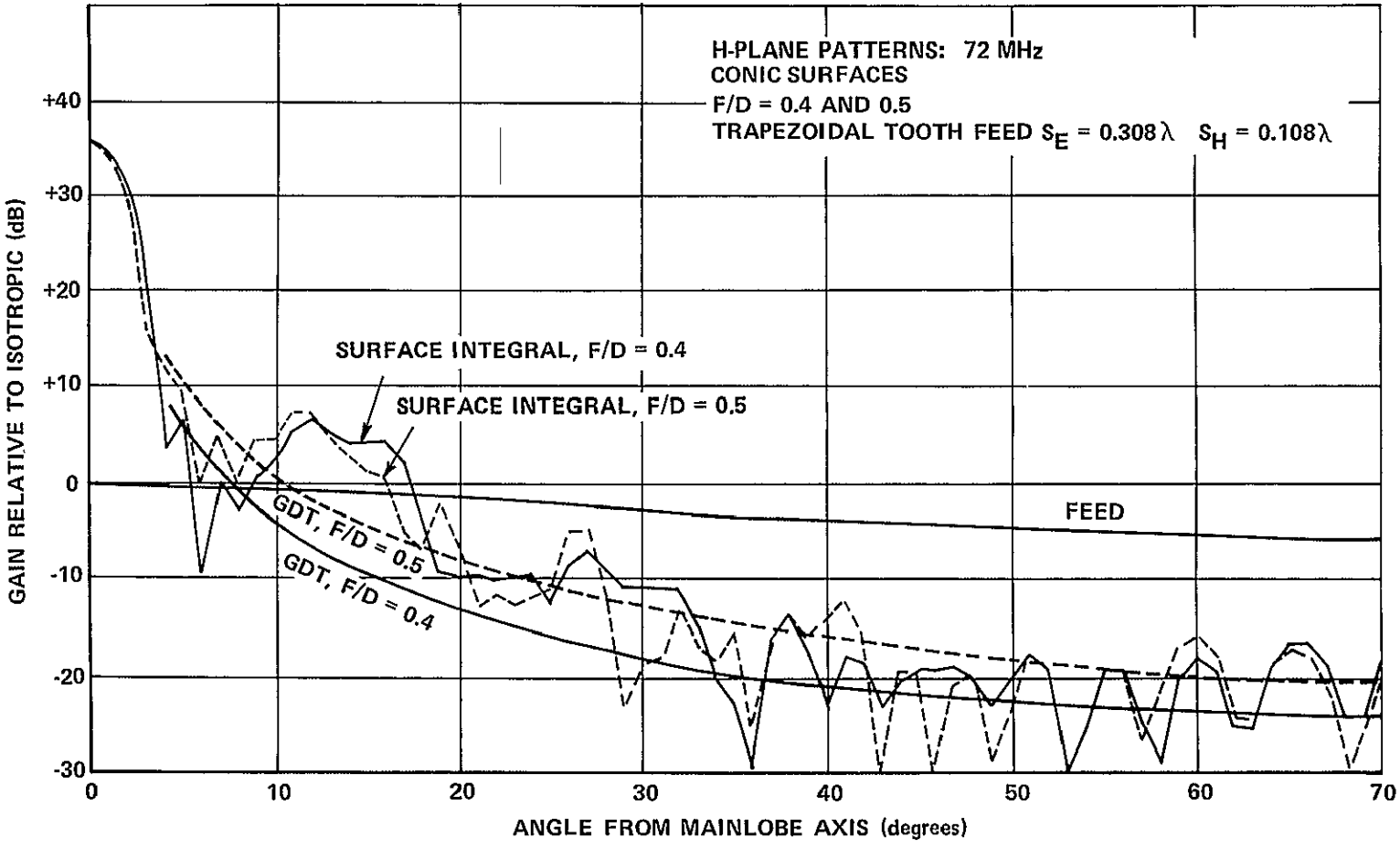

Figure 30 SURFACE INTEGRAL THEORY VS GDT, 72 MHz

Similar patterns at 150 MHz are shown in Figure 31. The trends are the same as at 72 MHz (Figure 30). The increased discrepancy in computed sidelobe level between surface integral and edge diffraction theories at 150 MHz as compared to 72 MHz is caused by the larger surface error in wavelengths at the higher frequency.

5.3 RADIATION PATTERNS

Computed H-plane patterns at 15, 30, 72 and 150 MHz are shown in Figures 32, 33, 34, and 35 for an F/D ratio of 0.5. Only half the pattern is shown, because it is symmetric about the antenna axis. The GDT solution is invalid at the shadow boundary and over an angular sector each side of this boundary. The actual edge diffraction radiation would follow approximately a straight-line approximation between the minima of the GDT envelope on each side of the shadow boundary, as indicated by the "actual edge diffraction" dashed curve in the figures. The abrupt drop in feed radiation at the shadow boundary equals the reflector grid transmission loss at each frequency.

At 15 MHz, the agreement between surface integral theory and GDT is excellent, but agreement becomes progressively worse as frequency increases, because the conic surfaces increase sidelobe level as computed by surface integral theory.

Random surface error contributes significantly to sidelobe level only at the higher frequencies. Reflector panel billowing should be kept below 0.03-meter RMS (0.1-meter peak-to-peak) to keep sidelobe level for frequencies up to 150 MHz below the sidelobe level due to other causes.

The reflector grid used in this example gave feed leakage radiation in the shadow region 40 dB below the mainlobe independent of frequency. At frequencies above 72 MHz, feed leakage is larger than edge diffraction in the shadow region and at 15 MHz, and edge diffraction forms the larger contribution. The behavior of other grid designs can be easily determined from the feed

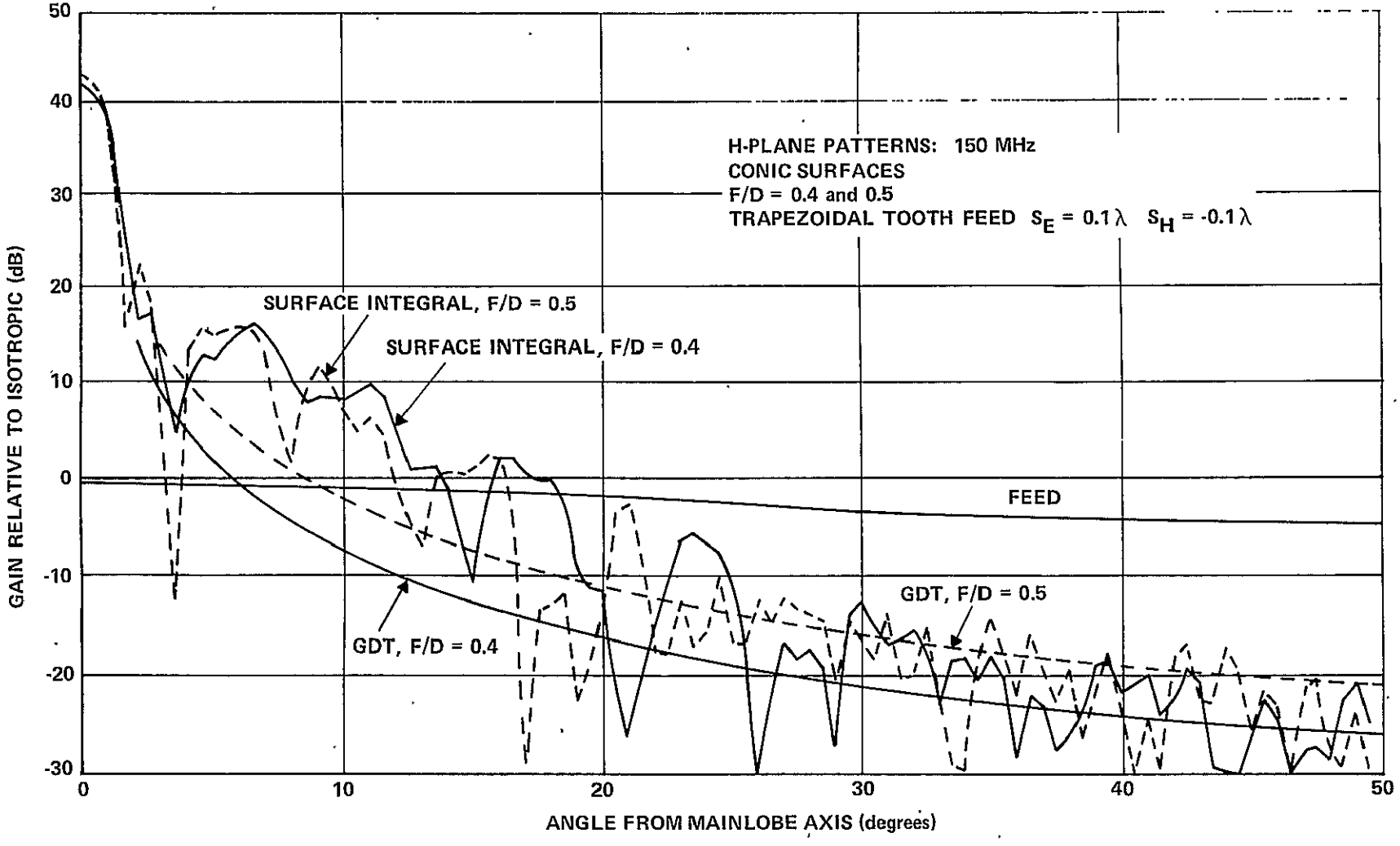

Figure 31 SURFACE INTEGRAL THEORY VS GDT, 150 MHz

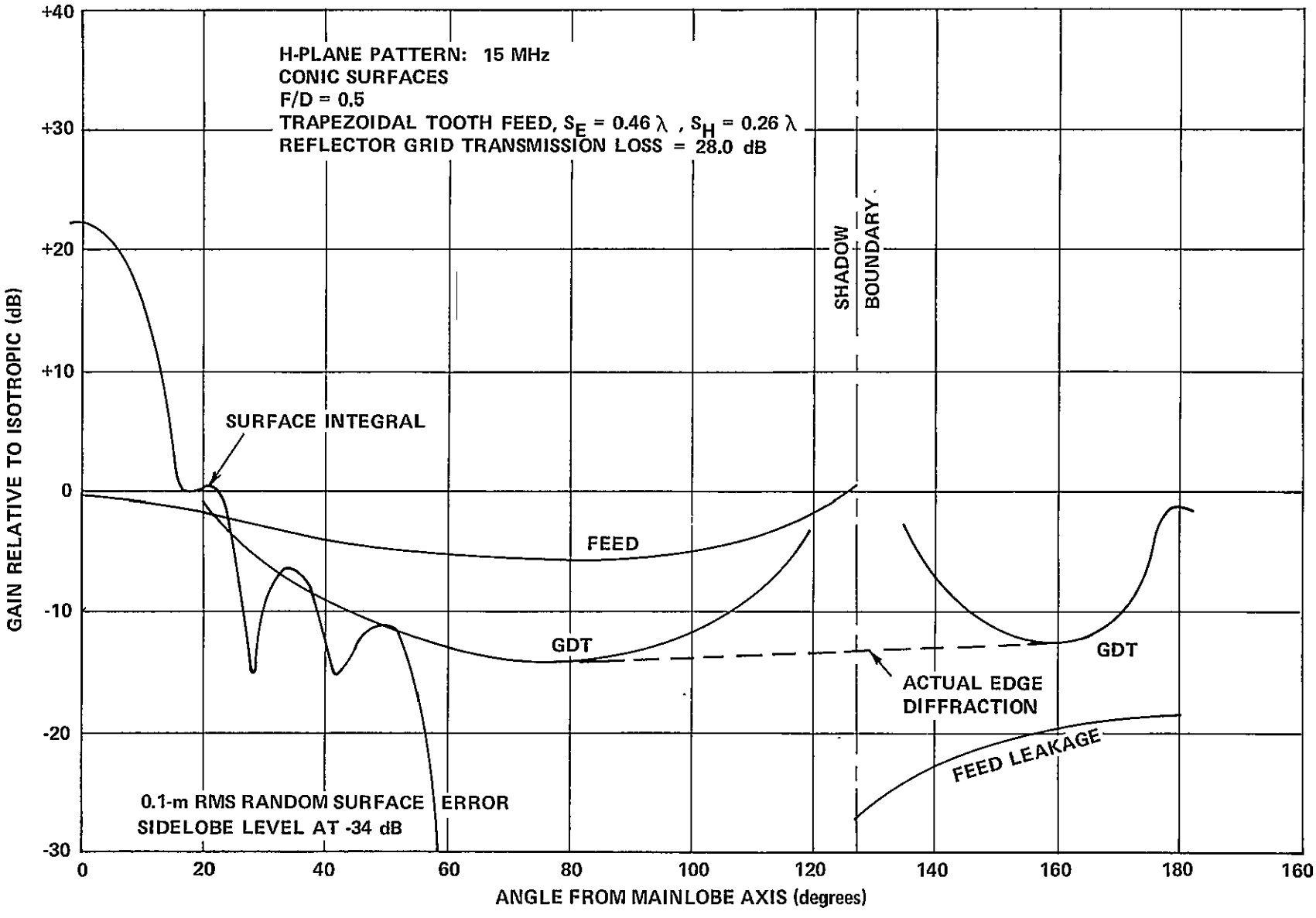

Figure 32 360^{o} H-PLANE PATTERNS: 15 MHz

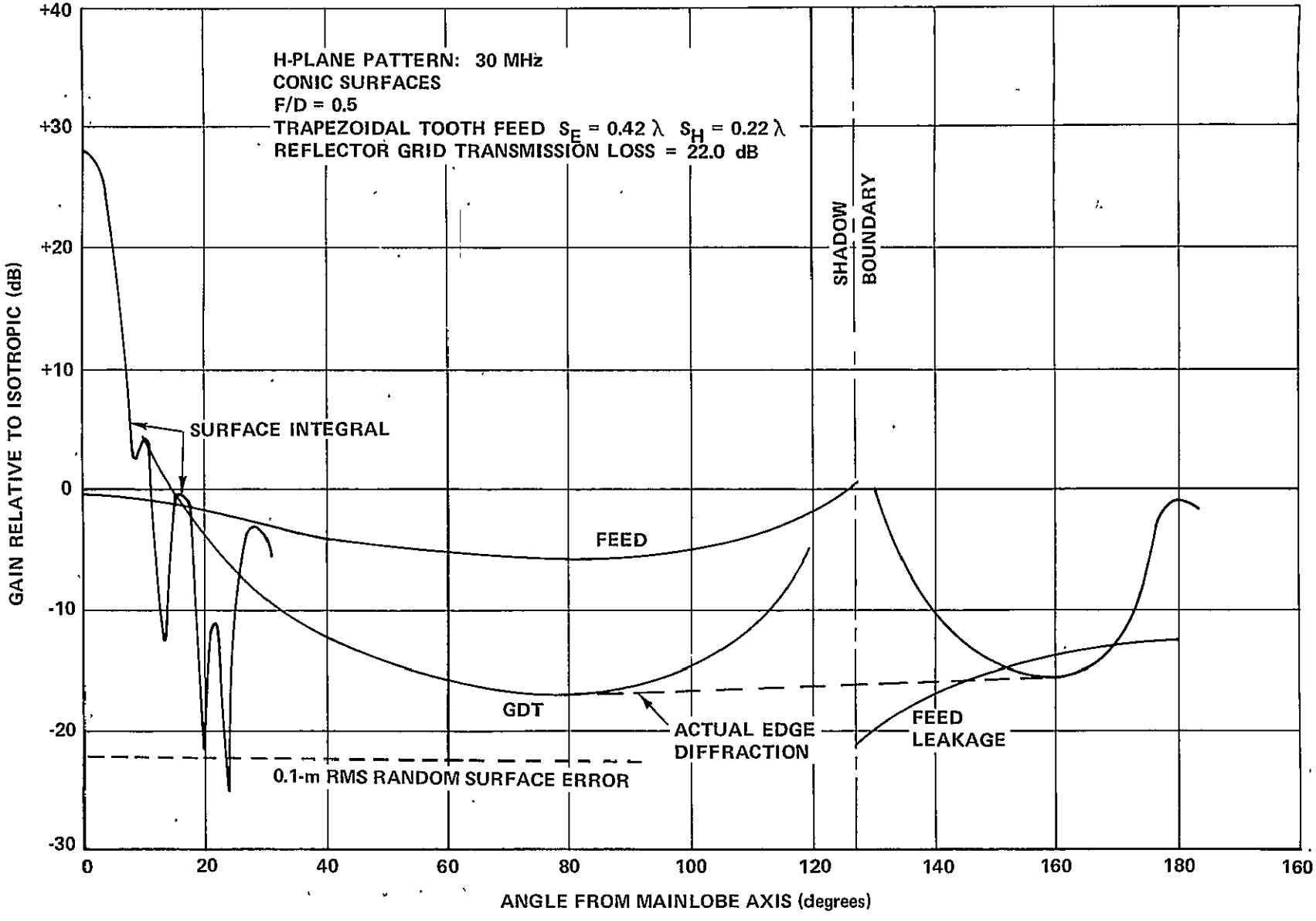

Figure 33 360^{o} H-PLANE PATTERNS: 30 MHz

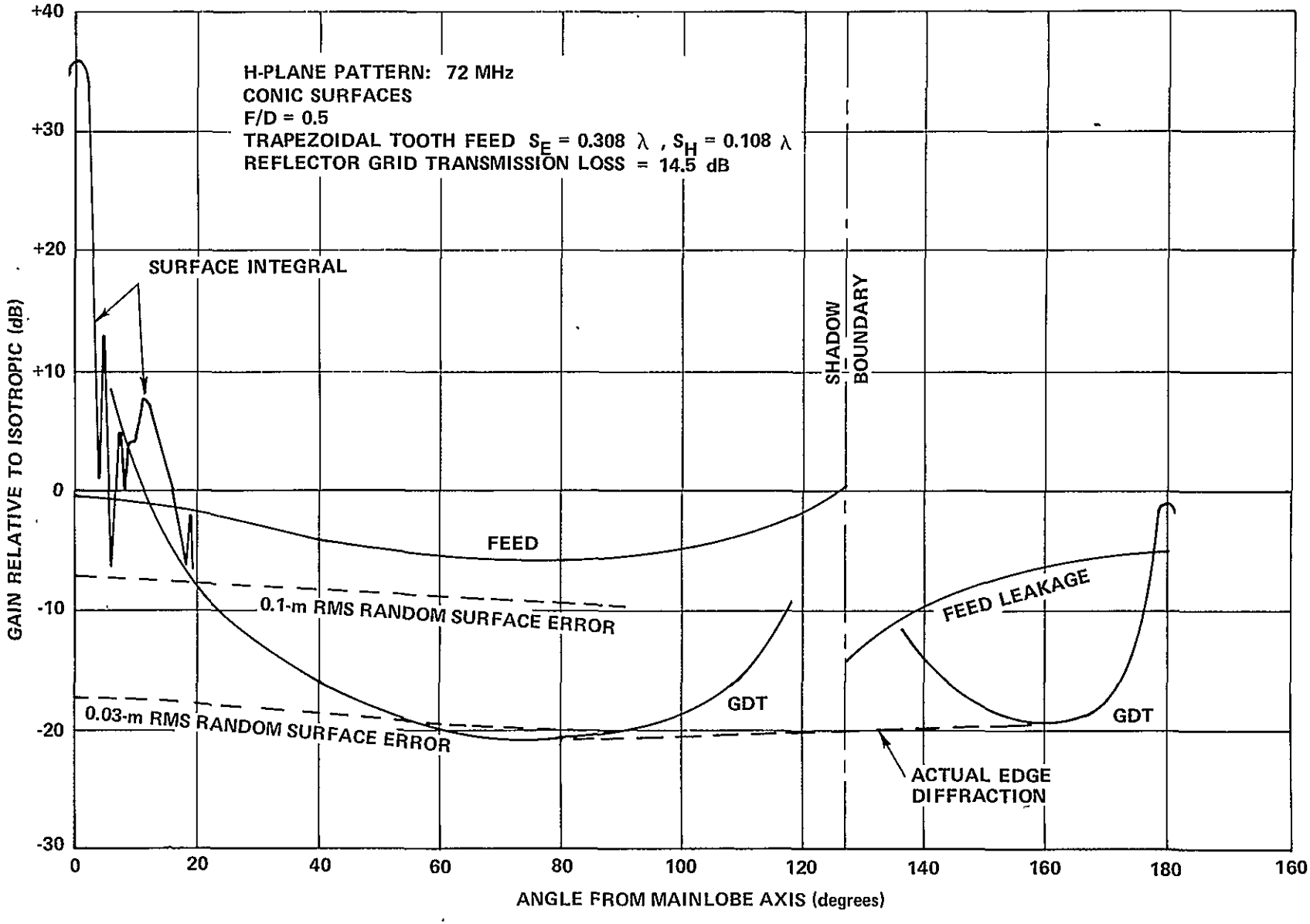

Figure 34 360° H-PLANE PATTERNS: 72 MHz

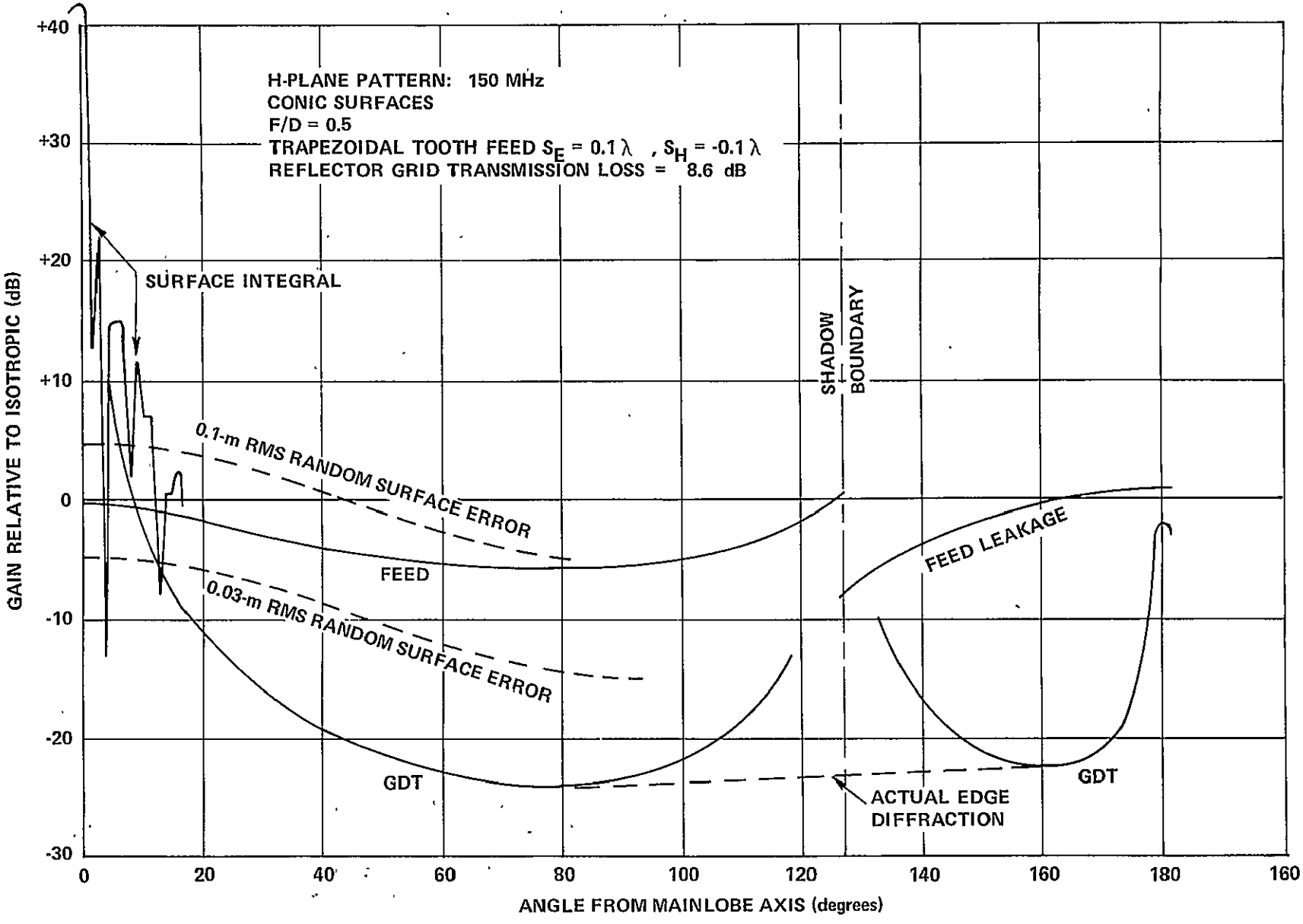

Figure 35 360° H-PLANE PATTERNS: 150 MHz

leakage curves shown. If a grid has a transmission loss of T dB at 150 MHz, then the feed leakage curves are lowered at each frequency by (T-8.6 dB).* Grid parameters for a given transmission loss at 150 MHz can be found in Section 3.

The backlobe gain relative to isotropic is -1.0 dB independent of frequency. This gain is constant, because it is a function of feed fields only, which are essentially independent of frequency.

The effect of F/D ratio on 72 MHz, H-plane patterns is shown in Figure 36. The straight-line extrapolation of GDT, previously discussed, is shown. Surface integral results were already presented in Figure 30 and are, therefore, not repeated. Feed radiation and sidelobe level due to random surface errors are the same for both F/D ratios.

GDT predicts a lower sidelobe level in both illuminated and shadow regions, if an F/D ratio of 0.4 is used in place of 0.5. The backlobe is also lower when F/D = 0.4, because the edge illumination is lower. However, Figures 30 and 31 illustrate that near sidelobe levels based on surface integral theory are the same for both F/D ratios. In any event, direct feed radiation dominates in the illuminated region. Therefore, using an F/D ratio of 0.4, rather than 0.5, reduces sidelobe level only in the shadow region, but feed leakage through the reflector grid must be reduced to the edge diffraction level for the reduced sidelobe level to be realized.

E- and H-plane patterns at 72 MHz are compared in Figure 37 for an F/D ratio of 0.5. Again, surface integral results are omitted and straight-line extrapolations of the GDT results are shown. Sidelobe level due to random

*This simple rule is accurate for transmission losses greater than 10 dB. Equation (4), Section 3 gives the exact transmission loss.

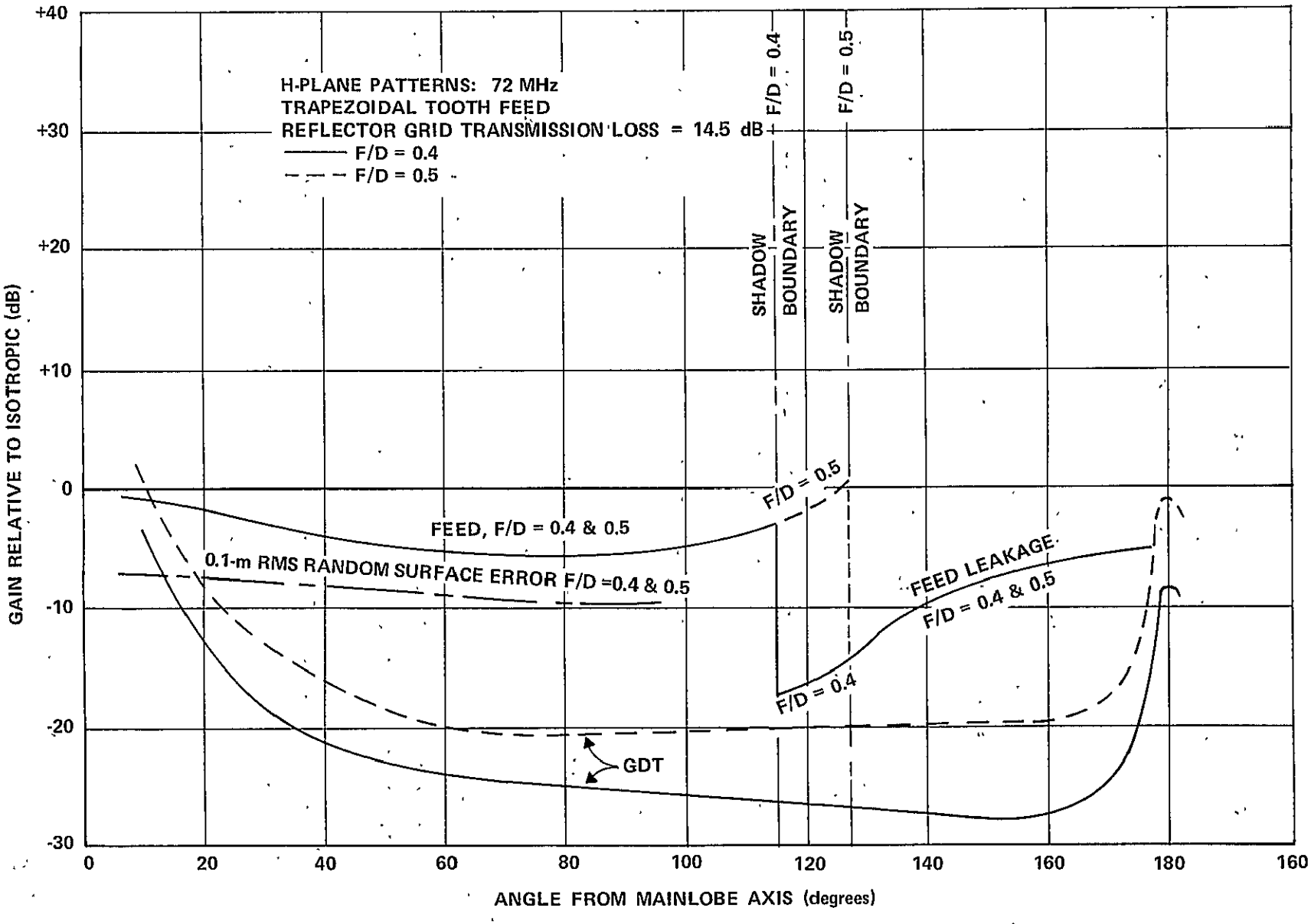

Figure 36 360° H-PLANE PATTERNS: EFFECT OF F/D RATIO

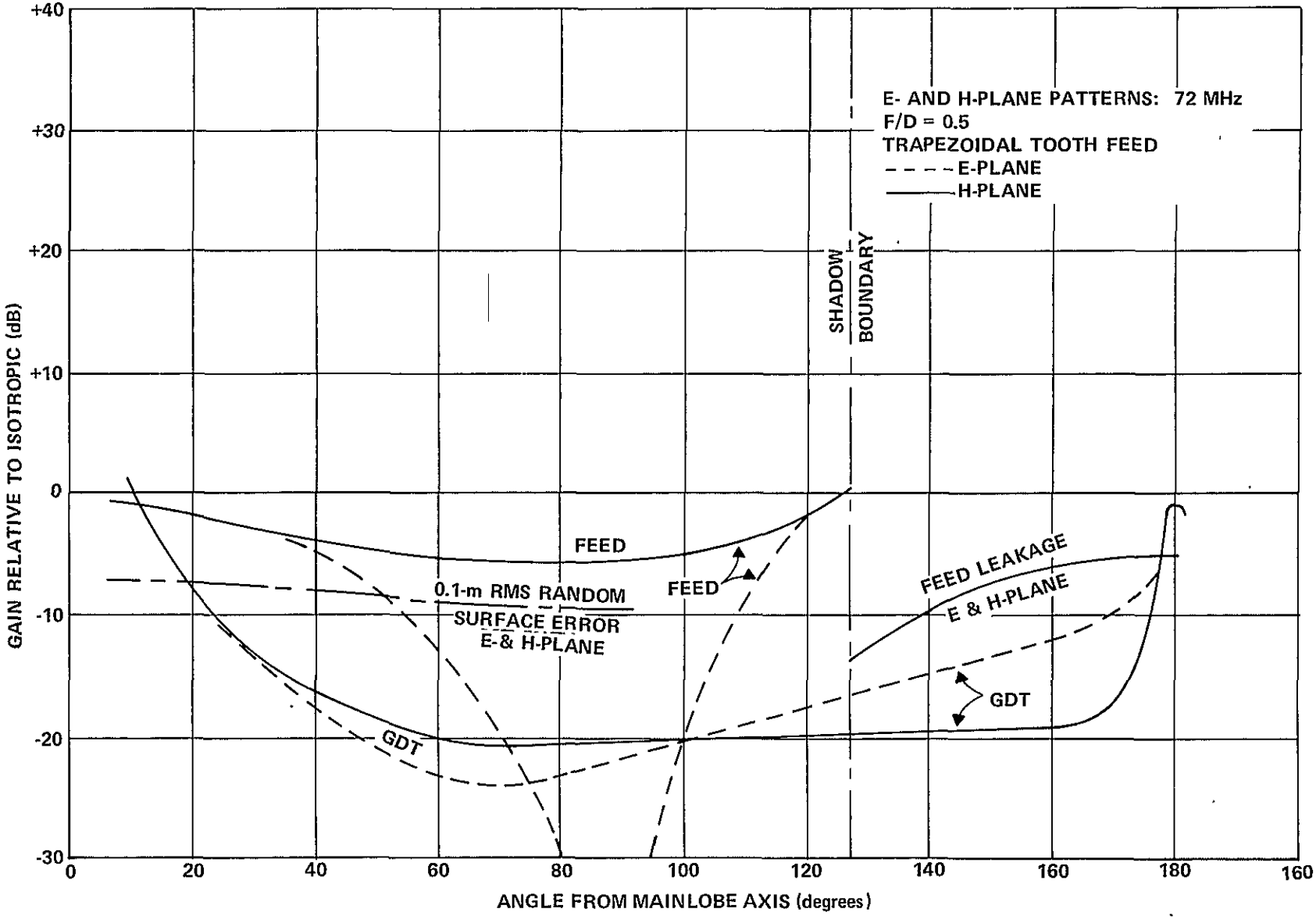

Figure 37 360° E- AND H-PLANE PATTERNS: 72 MHz

surface errors is the same in both planes. H-plane edge diffraction is higher than E-plane diffraction in the illuminated region and lower in the shadow region, but feed radiation is still dominant.

At other frequencies, the edge diffraction pattern shapes are identical to the 72-MHz pattern shapes, except that the backlobe level relative to isotropic remains fixed. The relative level between patterns for different F/D ratios, and the relative level between E- and H-plane patterns remain the same as shown at 72 MHz. The absolute level (gain relative to isotropic) of the edge diffraction patterns changes with frequency as shown in Figures 32 through 35.

Section 6
CONCLUSIONS AND RECOMMENDATIONS

Conclusions of the CAL study of RF parameters for the 15- to 150-MHz, 100-meter-diameter LOFT antenna are given in this section in the following order:

- Feed investigation
- Reflector grids
- Radiation at and near mainlobe
- Radiation far from mainlobe

Areas where further studies are recommended are also discussed. The parameters and expected performance of an optimum-design LOFT antenna are described.

6.1 FEED INVESTIGATION

A trapezoidal tooth or triangular tooth log-periodic antenna is the recommended feed. This antenna provides an axisymmetric pattern with proper beamwidth to illuminate a parabolic reflector whose F/D ratio is between 0.4 and 0.5. Phase error due to the feed is small enough that the feed need not be moved when operating frequency is changed. Orthogonal linear polarization can be provided by arrangement of four tooth structures in pyramid fashion. An experimental program establishing the optimum feed design is needed and recommended.

A log-periodic dipole array is not recommended at present, because of its unequal E- and H-plane beamwidths and large phase error. However, if the pyramid-arranged tooth structures exhibit excess cross-polarization, as determined during a recommended measurements program, the log-periodic dipole array should be reconsidered.

A conical spiral feed is not recommended, because dual-sense circular-polarized versions have not been successful to date.

A multiturn cyclindrical helix is not recommended, because its bandwidth is too narrow and it would be difficult to deploy in the LOFT application (16 arms and 45° incremental phasing are required).

The conical transmission line feed results in a far-field pattern having low gain, high sidelobes, and large cross-polarization. Therefore, this feed is not recommended, even though it is much easier to deploy than the other feeds surveyed. However, eight of the front tension stays could be conductors without causing significant far-field pattern deterioration when any of the log-periodic feeds are used. The conducting stays could then be used as a backup conical transmission line feed.

6.2 REFLECTOR GRIDS

Grids consisting of orthogonal strip conductors have been analyzed. Grids with conductor spacing up to 50 times larger than conductor width have sufficiently high reflectivity and low transmissivity. For proper operation at frequencies up to 150 MHz, conductor spacing should be less than 15 centimeters. The effect of finite conductivity is small, if the conductor width exceeds 3 millimeters and the conductor thickness exceeds 6 microns, even when the material is stainless steel. A square mesh should be used to keep reflected and incident polarizations nearly the same. A uniform-size mesh should be used throughout the reflector surface to minimize phase error due to the grid. However, a nonuniform mesh whose maximum conductor spacing is less than 10 centimeters has sufficiently small phase error.

A weaved grid should not be used unless good electrical contact at the junctions of adjacent conductors can be guaranteed. The reflectivity of weave designs, which rely only on mechanical contact at the junctions, should

be measured. Grids which have continuous conductors in orthogonal directions, or rectangular weaves which are welded or soldered at the junctions can be analyzed theoretically, thereby eliminating the necessity of measurements. Measurements, however, should be performed to check the result of such analyses.

The material for a 100-meter-diameter stainless steel grid will weigh at least 20 kilograms. If leakage radiation at all frequencies up to 150 MHz must be reduced to the level of the edge diffracted fields everywhere in the shadow region, the required stainless steel grid will weigh approximately 100 kilograms. An aluminum grid weighs about three times less than a stainless-steel grid.

6.3 RADIATION AT AND NEAR MAINLOBE

Computations of far-field patterns at and near the mainlobe established the superiority of the trapezpidal tooth feed (0.7- to 1.6-dB higher gain, 2-dB lower sidelobe level) over the log-periodic dipole feed. The optimum F/D ratio is between 0.4 and 0.5; a 2-dB lower sidelobe level and a 0.5-dB lower gain occur with an F/D ratio of 0.4 as compared to 0.5.

Feed phase center displacement has maximum effect on far-field patterns at low frequencies. At 15 MHz, feed phase center error reduced gain by 0.3 dB and increased sidelobe level by 4 dB relative to the far-field patterns obtained with no phase center error (trapezoidal tooth feed and F/D = 0.5). Feed phase center displacement relative to the reflector focal point must be less than 0.4 wavelength to maintain far-field pattern deterioration within these limits.

Conic-reflector surface error has maximum effect on far-field patterns at high frequencies. At 150 MHz, conic surfaces reduced gain by 0.6 dB and increased sidelobe level by 6 dB as compared to far-field patterns obtained with a perfect paraboloid (trapezoidal tooth feed and F/D = 0.5).

Conic approximations to a perfect paraboloid other than the ones used in this report should be investigated. The CAL surface integral computer programs can handle reflector surfaces with arbitrary shape.

The effect on far-field patterns of reflector surface distortions caused by temperature and torque has been investigated. Assuming surface errors twice as large as those computed for a 50-meter-diameter LOFT and a frequency of 150 MHz, thermal surface error reduced gain by 2 dB and increased sidelobes by 3 dB, torque surface error reduced gain by 1 dB and increased sidelobes by 3 dB and a combination of both thermal and torque surface errors reduced gain by 3 dB and increased sidelobes by 6 dB. A 1° mainlobe squint occurred when torque was present. Thus, the LOFT antenna is still usable for the doubled surface errors. At lower frequencies, gain reduction and sidelobe increase would be less severe. Temperature and torque errors of the same magnitude as computed for a 50-meter-diameter LOFT cause small far-field pattern deterioration. Surface distortions caused by temperature and torque should be computed for a 100-meter-diameter LOFT reflector and the resultant far-field patterns determined with the CAL computer programs.

Feed blockage and scattering has only a minor effect on sidelobe level, because the sidelobe level is already high due to reflector surface distortions, feed phase center displacement, and direct feed radiation. The computed gain reduction caused by feed blockage is only 0.1 dB.

6.4 RADIATION FAR FROM MAINLOBE

Radiation far from the mainlobe is caused by random surface errors, edge diffraction, direct feed radiation, and leakage of feed fields through the reflector grid. In the illuminated region, direct feed radiation dominates over the other radiation mechanisms, provided random reflector surface error is less than 0.03-meter RMS (0.1-meter peak-to-peak). Edge diffraction becomes more significant at lower frequencies, but it is still less than direct feed radiation even at 15 MHz.

In the shadow region, feed leakage through the reflector grid is stronger than edge diffraction (the only other shadow region radiation mechanism) at the higher frequencies, unless reflector grid spacing is made very small (approximately 3 centimeters). A spacing of 12 centimeters will attenuate leakage radiation to a level 40 dB below mainlobe level and reduce mainlobe gain by 0.02 dB (at 15 MHz) to 0.6 dB (at 150 MHz). Shadow region edge diffraction is 25 dB (at 15 MHz) to 65 dB (at 150 MHz) below mainlobe level, except at the backlobe (180° away from mainlobe). The backlobe level is about -1 dB relative to isotropic level.

As a rough rule of thumb, sidelobe level far from the mainlobe is -5 dB relative to isotropic, provided surface errors are not extremely large.

6.5 OPTIMUM LOFT ANTENNA

Based on the CAL electrical performance tradeoff study, a LOFT antenna with the following parameters is recommended.

Feed Type	Trapezoidal tooth (must have polarization diversity capability)
Feed Position	Fixed; apex 0.8 meter closer to reflector than the focal point
Reflector Diameter	100 meters
Reflector F/D Ratio	0.5
Conic Surfaces	See Figure 13
Reflector Surface Random Error	0.03-meter RMS maximum
Reflector Grid	Uniform square mesh
Grid Conductor Material	Stainless steel is satisfactory
Grid Conductor Thickness	At least 6 microns

Grid Conductor Width	3 millimeters
Grid Conductor Spacing	12 centimeters
Reflector Grid Weight	20 kilograms (stainless steel)

The expected performance of this optimum antenna is summarized below:

Gain (including feed phase and conic surface errors and reflector grid) relative to isotropic	22.2 to 41.4 dB (15 to 150 MHz)
Gain loss due to feed phase error	0.3 dB maximum
Gain loss due to conic surfaces	0.6 dB maximum
Gain loss due to reflector grid	0.6 dB maximum
3-dB Beamwidth	13.2° to 1.29° (15 to 150 MHz)
Sidelobe level (including feed phase and conic surface errors)	19-dB worst case
Sidelobe level if there were no feed phase error and no conic surfaces	25-dB worst case
Sidelobe level far from mainlobe	-5 dB relative to isotropic
Cross-polarization level (with practical trapezoidal tooth feed)	10 to 15 dB

It should be noted that gain losses should not be added to compute gain obtainable with a LOFT antenna consisting of a perfect paraboloid, perfectly reflecting grid, and zero feed phase, because the maximum losses shown do not occur at the same frequency. A "perfect" LOFT antenna would have 22.6-dB gain at 15 MHz and 42.6-dB at 150 MHz and a 25-dB sidelobe level. The recommended reflector grid has negligible effect (0.3 dB) on sidelobe level.

The sidelobe level far from the mainlobe applies to both illuminated and shadow regions. The sidelobe level in the shadow region can be reduced to -13 dB relative to isotropic by using an F/D ratio of 0.4 and a finer mesh grid (3-cm conductor spacing).

The large estimated cross-polarization is due to the expected large cross-coupling between orthogonal trapezoidal tooth feed pairs. Orthogonal log-periodic dipole arrays have about 25-dB cross-coupling, but this feed results in lower LOFT antenna gain, higher sidelobes, and unequal E- and H-plane beamwidths.

Appendix A

CONICAL TRANSMISSION LINE FEED

A.1 FEED EQUATIONS

The field of a multiconductor conical transmission line has been derived [19]. Assuming small strip widths, field equations (19) through (22) in Reference 19 reduce to:

$$E_\theta = \frac{60\,V e^{-iKR}}{RZ} \sum_{n=0}^{N-1} e^{i\frac{2n\pi}{N}} f_n(\theta, \phi)$$

$$E_\phi = \frac{60\,V e^{-iKR}}{RZ} \sum_{n=0}^{N-1} e^{i\frac{2n\pi}{N}} g(\theta, \phi) ,$$

where

$$f_n(\theta, \phi) = \frac{\left[A \cos\phi + B \sin\phi\right] \sec^2\frac{\theta}{2}}{2(A^2+B^2)}$$

$$g(\theta, \phi) = \frac{\left[B \cos\phi - A \sin\phi\right] \tan\frac{\theta}{2}}{\left[A^2+B^2\right] \sin\theta}$$

$$A = \cos\phi \tan\frac{\theta}{2} + \sin\frac{2n\pi}{N} \tan\frac{\theta_o}{2}$$

$$B = \sin\phi \tan\frac{\theta}{2} - \cos\frac{2n\pi}{N} \tan\frac{\theta_o}{2}$$

$$K = \frac{2\pi}{\lambda}$$

R, θ, ϕ = spherical coordinates of observation point (Figure 5, Section 2.3)

θ_o = half angle of conic surface

V = magnitude of generator voltage (Figure 5, Section 2.3)

Z = impedance presented to each generator.

Impedance Z for the 6- and 8-conductor lines is given in Reference 19, equations (15) and (16).

6-conductor $Z = 60 \ln \frac{3.464}{\alpha}$

8-conductor $Z = 60\left[\ln \frac{2}{\alpha} + 1.25\right]$

where α is strip width in radians (Figure 5).

The front/back ratio of the transmission line feed can be found by evaluating the above field equations at $\theta = 0°$ and $\theta = 180°$.

$$\frac{E(0°)}{E(180°)} = \cot^2 \frac{\theta_o}{2}$$

Thus, the front/back ratio is independent of ϕ (field is circularly polarized), strip width and number of conductors, and is only a function of cone half-angle.

Example

Figure 38 shows the E_θ and E_ϕ fields for a 6-conductor line with $\theta_o = 58°$ as a function of θ in the $\phi = 90°$ plane. The $\phi = 90°$ plane bisects the n = 0 and n = 3 conductors. Figure A-2 shows the E_θ and E_ϕ fields in the $\phi = 60°$ plane which cuts midway between the n = 0 and n = 5 conductors. All fields are normalized by the same constant. Except for the 180° phase reversal of E_θ at $\theta = \theta_o = 58°$, the field phase is constant as a function of θ in these two ϕ planes. The components E_θ and E_ϕ are in phase quadrature in these two planes, which is required for circular polarization. The magnitude of E_θ becomes very large as a conductor is approached (Figure 38), and zero at the reflector rim midway between conductors (Figure 39). The E_ϕ component is nearly uniform over the entire reflector surface.

A.2 DISCUSSION OF FEED FIELDS

The magnitudes of E_θ and E_ϕ become very different as the reflector rim is approached. Therefore, the aperture radiation (far-field pattern of the parabolic antenna) is not circularly polarized for angles off the peak of the mainlobe.

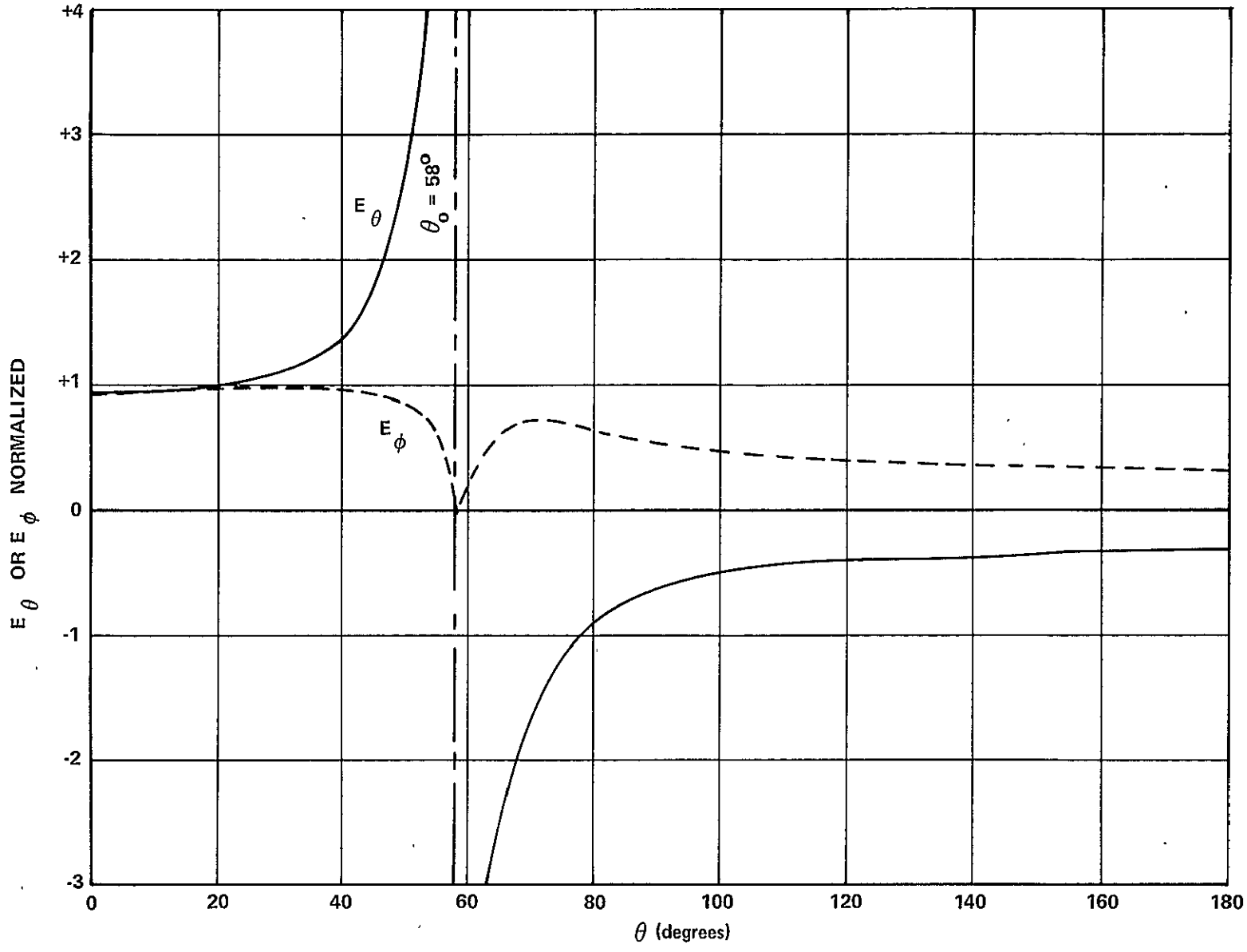

Figure 38 E_θ AND E_ϕ VS θ , ϕ = 90° PLANE

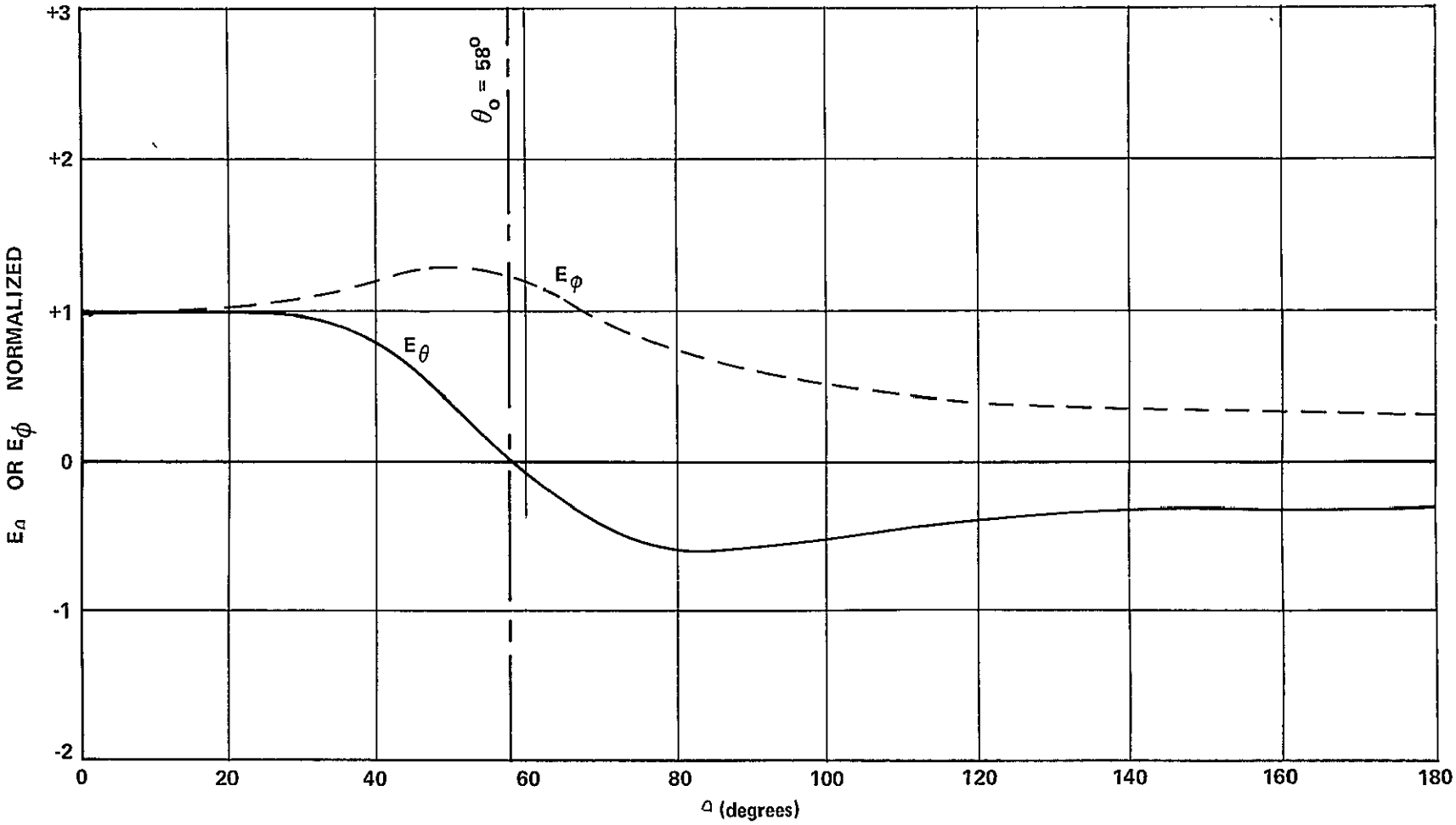

Figure 39 E_θ AND E_ϕ VS θ, $\phi = 60^o$ PLANE

The transmission line fields are substantial outside the angle subtended by the feed and reflector. In fact, half the power radiated by the feed is within the conic (and illuminating the reflector) and half is outside the conic independent of the conductor widths and the number of conductors [20]. As mentioned previously, antenna patterns deteriorate, if the reflector subtends an angle larger than the conic angle, because of the phase reversal of E_θ . Therefore, half the feed power is lost as spillover. Hughes Aircraft Company investigated the possibility of using auxiliary reflectors to collimate some of this spillover field but abandoned the study as impractical for broadband antennas [20,21]. A collimating lens within the cone did concentrate slightly more than half the feed power onto the reflector. Although the lens is practical for microwave antennas, it is not practical for the LOFT antenna because of its large size and weight. Even with the lens, the spillover and cross-polarization losses were so large that the parabolic antenna gain was 31 percent of the gain of a uniformly illuminated aperture of the same size [21]. With a log-periodic feed, a gain of 75 percent of uniform aperture gain has been reported [6].

The large magnitude of E_θ in the vicinity of a conductor will generate a high sidelobe level in the parabolic reflector antenna pattern. Theoretical solutions predict a 17-dB sidelobe level [34] and this level has almost been obtained in practice [21].

The front/back ratio for the feed pattern is equal to $\cot^2 (\theta_o /2)$ and is given in Table 14 as a function of the parabolic reflector F/D ratio.

Table 14
CONICAL TRANSMISSION LINE FEED FRONT/BACK RATIO

F/D RATIO	θ_o	FEED F/B RATIO IN dB
0.3	81^o	2.7
0.35	72^o	5.5
0.4	65^o	7.8
0.45	59^o	10.6
0.5	53^o	12.1

The feed-back radiation contributes to the sidelobe radiation of the reflector antenna. It is shown in Section 5.3 that feed radiation equals or exceeds reflector edge diffraction (far-out sidelobes) when the feed front/back ratio is lower than 10 dB. Therefore, the conical transmission line feed will give a high sidelobe level far out from the mainlobe as well as close in.

A.3 APERTURE BLOCKAGE EFFECTS

It is assumed in this section that the LOFT antenna has a trapezoidal tooth feed and that eight of the front tension stays are conducting strips which could be used for a transmission line feed as a backup to the primary trapezoidal tooth feed.

The field reflected from the parabola will induce currents in the transmission line conductors. These induced currents also produce a field which must be included. This effect is called aperture blockage, because the transmission line conductors shadow the aperture field, to use optical terminology.

Since the conductors lie in the direction of propagation of the field produced by the trapezoidal tooth feed, it is assumed that this incident field is undisturbed. After reflection from the parabola, the component of field tangential to each of the eight equispaced (45°) conductors was determined. The current induced in the conductors by this tangentially applied field was then derived [35]. Finally, the far-field radiation pattern produced by the eight induced line currents , E_{cond}, was computed using vector potential theory [36]. The resulting field equations were too complicated for convenient hand computation but are available for programming on a computer. In the direction of the reflector main beam, the field due to the currents induced in the transmission line feed is maximum, and its magnitude relative to the field of an isotropic radiator is:

$$\frac{E_{cond}}{E_{iso}} = \frac{2.06}{i + 0.635 \ln \frac{2.76\lambda}{w}} \qquad \text{when } \theta_0 = 53^\circ \text{ (F/D = 0.5)}$$

where

λ = wavelength

ω = conductor width

Thus, the maximum field radiated by currents induced in the eight conductors is independent of reflector diameter or conductor length. At first, one might think that the field should increase with increasing conductor length, because the beamwidth of the conductor's radiation pattern decreases. However, this effect is cancelled by the reduced current magnitude per unit length as conductor length and reflector diameter are increased.

The field strength on axis due to conductor radiation, E_{cond}, is compared to the field strength of the mainlobe reflector radiation, E_{ml}, in Table 15 for various conductor widths and frequencies. E_{iso} is the field strength of an isotropic radiator. The parabolic antenna gain for a 100-meter-diameter reflector is given by $20 \log_{10}\left(\frac{E_{ml}}{E_{iso}}\right)$

It can be seen that the field scattered in the direction of the mainlobe by the conducting wires is small relative to the mainlobe field of the reflector. It can also be shown, by similar calculations, that the sidelobe level of the reflector would not be significantly affected by scattering from the transmission line field.

If the eight conductors were excited as a transmission line feed, the aperture blockage field strength would be slightly different from that calculated with a log-periodic feed, because the reflector illumination is different. Even so, the sidelobe level computed by Hughes, neglecting aperture blockage [20,21], is higher than the aperture blockage mainlobe level in Table 15. Therefore, aperture blockage sidelobe level caused by a transmission line feed is much lower than the sidelobe levels calculated by Hughes and blockage of the transmission line feed is negligibly small.

Table 15

CONDUCTOR APERTURE BLOCKAGE FIELD STRENGTH RELATIVE TO ISOTROPIC AND MAINLOBE FIELD STRENGTHS

100-METER-DIAMETER REFLECTOR
EIGHT-CONDUCTOR CONICAL TRANSMISSION LINE
TRAPEZOIDAL TOOTH ANTENNA FEED
CONDUCTOR WIDTH IN METERS

CONDUCTOR WIDTH (m)	FREQUENCY (MHz)	E_{cond}/E_{iso}* (dB)	E_{ml}/E_{iso}* (dB)	E_{ml}/E_{cond}* (dB)
$\omega' = 0.01$	15	-8.5	22.2	30.7
	30	-7.7	28.3	36.0
	72	-6.7	35.9	42.6
	150	-5.8	42.0	47.8
$\omega' = 0.1$	15	-5.8	22.2	28.0
	30	-4.7	28.3	33.0
	72	-3.3	35.9	39.2
	150	-1.8	42.0	43.8
$\omega' = 1$	15	-2.3	22.2	24.5
	30	-0.2	28.3	28.5
	72	0.9	35.9	35.0
	150	2.9	42.0	39.1

*THE ENTRIES IN THE TABLE ARE EQUAL TO 20 LOG_{10} (X), WHERE X IS THE APPROPRIATE FIELD RATIO.

Appendix B
DESCRIPTION OF COMPUTER PROGRAMS

B.1 INTRODUCTION

Two computer programs were used for pattern computations during the program. The first centered around a previously written and verified program by W.V.T. Rusch [37-40] and was obtained through personal correspondence [41] with one of the authors [Clark]. This program evaluates a single-surface integral (the integral in the other dimension having been performed analytically) on an axisymmetric surface. Programmer usage is described in Section B.4.3 and input/output (I/O) data in Section B.4.4.

The second program, described in Appendix B.5, was developed during this study, and used some of the procedures of the first program, thus keeping the input/output data very similar. The second program evaluates a double-surface integral and accurately accounts for nonaxisymmetric surface perturbations such as thermal and torsional disturbances in the LOFT antenna. Programmer usage is described in Section B.5.3. Both programs can accomodate either a perfectly conducting or grid reflector.

B.2 COORDINATE SYSTEM AND ANGULAR DEFINITIONS

Figure 40 illustrates the spherical coordinate system common to both programs and the integration and far-field point angular definitions. For the case of a parabolic surface, S_o , the origin is located at the focal point of the paraboloid, with the z-axis as the axis of symmetry toward the main beam. For an electric field polarized in the x-direction (always true for the feeds studied in this report), the scattered field in the x-z or E-plane will consist entirely of a θ component; for the y-z or H-plane, the scattered field will be entirely a ϕ component. For nonprincipal planes (containing the z-axis but neither x or y), the fields are best expressed as

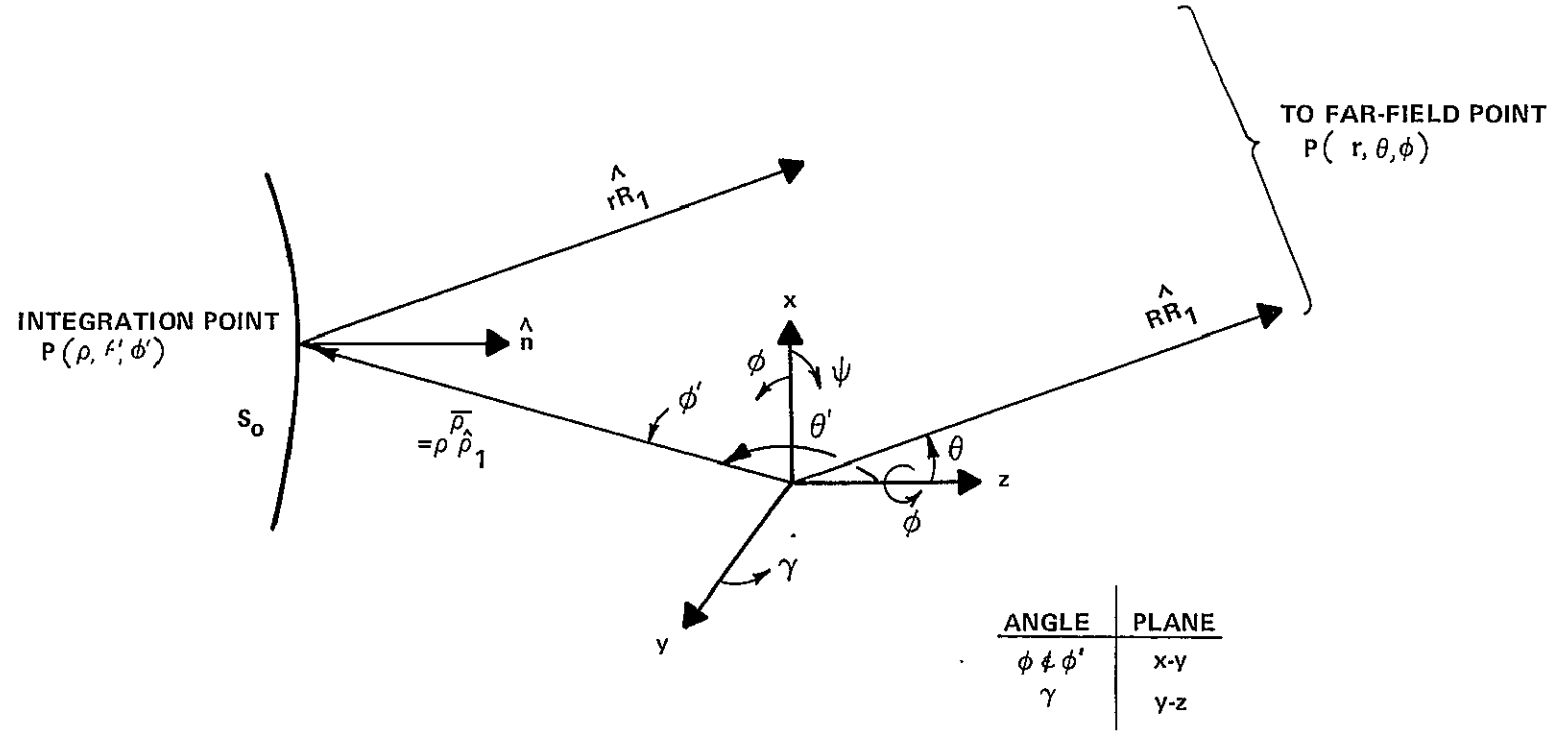

Figure 40 COORDINATE SYSTEM ANGULAR DEFINITIONS

ψ and γ components (Figure 40), which are termed the principal and cross-polarized components, respectively.

B.3 INTEGRATION OF SURFACE CURRENTS

In computing a far-zone scattered field by the physical optics technique, one essentially integrates the transverse components of the currents induced on the reflector by the feed radiation; these currents are determined by geometrical optics. In terms of the coordinates of Figure 40, the transverse components of the far-zone scattered field are given by:

$$\bar{E}_s = \frac{-i\omega\mu}{2\pi R} e^{-ikR} \iint_{S_0} (\hat{n} \times \bar{H}_i) e^{+ik\bar{\rho}\cdot\hat{R}_1} \, dS \tag{B-1}$$

($e^{+i\omega t}$ time dependence, $i = \sqrt{-1}$, is assumed in Appendix B)

For the single-integral program, the ϕ' dependence of dS is previously integrated analytically to give series of bessel functions; the program numerically integrates over θ'. For the double-integral program, numerical integration is performed over both θ' and ϕ'.

B.4 SINGLE-INTEGRAL PROGRAM

This program is valid only for axisymmetric reflectors but can accomodate any type of feed pattern having no radial field component. Once certain coefficients are computed, they can be reused, as often as desired, to compute the field pattern in any given plane through the axis of symmetry, resulting in a saving of considerable processing time.

B.4.1 Mathematical Background*

*This discussion of the analytical development for the axisymmetric case is purposely meant to be brief. For a more detailed explanation, see References 1-4.

3

B.4.1.1 Incident and Scattered Field Definition

The field radiated by the feed is assumed to be a Fourier series of the form

$$\bar{E}_i(\theta',\varphi') = \frac{e^{-ik\rho}}{\rho}\left\{\sum_{m=m_1}^{m_2}\left[A_m(\theta')\sin m\varphi' + B_n(\theta')\cos m\varphi'\right]\hat{a}_{\theta'}\right. \\ \left. + \sum_{m=m_1}^{m_2}\left[C_m(\theta')\sin m\varphi' + D_m(\theta')\cos m\varphi'\right]\hat{a}_{\varphi'}\right\} \tag{B-2}$$

$$\bar{H}_i(\theta',\varphi') = \frac{1}{-i\omega\mu}\nabla\times\bar{E}_i(\theta',\varphi') \tag{B-3}$$

where θ' and φ' indicate evaluation on the reflector surface. The coefficients (A,B,C, and D) are, in general, complex, encompassing linear, circular or elliptical polarization and phase errors of the feed. They can be specified in the input data or computed via a subroutine. The total field is computed from the direct feed contribution $\bar{E}_i(\theta,\varphi)$ plus the scattered field given in the same form of equation (B-2) by

$$\bar{E}_s(\theta,\varphi) = \frac{e^{-ikR}}{R}\left\{\sum_{m=m_1}^{m_2}\left[F_m(\theta)\sin m\varphi + G_m(\theta)\cos m\varphi\right]\hat{a}_\theta\right. \\ \left. + \sum_{m=m_1}^{m_2}\left[H_m(\theta)\sin m\varphi + K_m(\theta)\cos m\varphi\right]\hat{a}_\varphi\right\} \tag{B-4}$$

The F,G,H and K coefficients are integrals over the angle θ', whose integrands are sinusoidal and bessel functions in cross produces with the A,B,C and D coefficients of the illuminating source. The bessel functions in the integrand arise from the φ' integration performed analytically.

B.4.1.2 Feed Fourier Coefficients

For a point source feed polarized in the x-direction (E-plane), the Fourier coefficients of the feed are constants given by

$$B_1(\theta') = C_1(\theta') = \text{constant},$$

all others being identically zero. For the more general feeds studied during the program, the coefficients were evaluated by a subroutine which numerically integrated the feed pattern in φ' for a fixed θ'. The A and C integrals are

$$A_m(\theta') = \frac{-\sqrt{60 P_T G_f}\, A(\theta') \cos\theta' e^{-i\psi_5(\theta')}}{\pi} R_{\theta'}(\theta') \int_{-\pi}^{+\pi} \frac{D(\theta',\varphi') e^{-i\psi_6(\theta')\cos 2\varphi'} \cos\varphi'}{\sqrt{1-\sin^2\theta'\cos^2\varphi'}} \sin m\varphi' d\varphi' \tag{B-5}$$

$$C_m(\theta') = \frac{\sqrt{60 P_T G_f}\, A(\theta') e^{-i\psi_5(\theta')}}{\pi} R_{\varphi'}(\theta') \int_{-\pi}^{+\pi} \frac{D(\theta',\varphi') e^{-i\psi_6(\theta')\cos 2\varphi'} \sin\varphi'}{\sqrt{1-\sin^2\theta'\cos^2\varphi'}} \sin m\varphi' d\varphi' \tag{B-6}$$

The B and D terms are orthogonal to the A and B terms, containing $\cos m\varphi'$ in place of $\sin m\varphi'$. For the feeds studied, only B_m and C_m (for m odd) were nonzero, thus reducing the computation time. The coefficients are computed in subroutine FABCD and punched on cards to save on a rerun. The several variables in these expressions are explained in the following two sections.

B.4.1.3 Feed Amplitude Functions

The amplitude of the feed pattern incident on the reflector surface is given by

$$E_i(\theta',\varphi') = \frac{\sqrt{60 P_T G_f}}{\rho(\theta',\varphi')} A(\theta')\, D(\theta',\varphi') \tag{B-7}$$

where

P_T = Input power to the feed (W)
G_f = Gain of the feed over isotropic (linear units)
$A(\theta')$ = Weighting factor in the θ' direction (=1 for $\theta' = \pi$)
$D(\theta', \varphi')$ = Pattern shape

and is derived from

$$\frac{1}{2} \cdot \frac{E_i^2}{120\pi} = \frac{P_T G_f}{4\pi\rho^2} \tag{B-8}$$

For an isotropic feed in the far field, $\rho \rightarrow R$, $G_f = 1$; then $E_{iso} = \sqrt{60 P_T}/R$. If the total scattered field is desired relative to isotropic (as was always the case), division of E_i by E_{iso} drops the radical. Thus, in the program, P_T was set equal to 1/60 to give gain over isotropic. Two types of feeds were studied: the trapezoidal tooth and the log-periodic dipole antenna. Table 16 gives their characteristics, which apply to equations (B-5) and (B-6).

B.4.1.4 Feed Phase Function

The terms S_E and S_H in Table 16 specify the feed phase center displacement relative to the focal point as a function of frequency in the E- and H-planes (S in Figure 3). They are used to compute ψ_5 and ψ_6 in equations (B-5) and (B-6) given by

$$\psi_5(\theta') = \frac{1}{2}(\psi_1 - \psi_2 + \psi_3 - \psi_4) \tag{B-9}$$

$$\psi_6(\theta') = \frac{1}{2}(\psi_1 - \psi_2 - \psi_3 + \psi_4) \tag{B-10}$$

where

$$\psi_1 = k\sqrt{\rho^2(\theta') + S_E^2 - 2S_E\rho(\theta')\cos\theta'} \tag{B-11}$$

Table 16
FEED CHARACTERISTICS

	POINT SOURCE	TRAPEZOIDAL TOOTH (TT)	LOG-PERIODIC DIPOLE (LPD)
G_f	1.0	9.1	5.28
$A(\theta')$	1.0	$\cos^2\theta'$	$\dfrac{\cos\left(\frac{\pi}{2}\sin\theta'\cos\varphi'\right)}{\sqrt{1-\sin^2\theta'\cos^2\varphi'}}$
$D(\theta', \varphi')$	1.0	$\cos^2\left[0.6(\pi-\theta')\right]$	$\dfrac{\cos\left(\frac{\pi}{2}\sin\theta'\cos\varphi'\right)}{\sqrt{1-\sin^2\theta'\cos^2\varphi'}}$
$S_E(\lambda's)$	0.0	$0.5 - 0.8/\lambda$	$0.72 - 2.0/\lambda$
$S_H(\lambda's)$	0.0	$0.3 - 0.8/\lambda$	$0.72 - 2.0/\lambda$

$$\psi_2 = k \left[\rho(\theta') + S_E \right] \tag{B-12}$$

$$\psi_3 = k \sqrt{\rho^2(\theta') + S_H^2 - 2 S_H \rho(\theta') \cos\theta'} \tag{B-13}$$

$$\psi_4 = k \left[\rho(\theta') + S_H \right] \qquad , \qquad k = \frac{2\pi}{\lambda} \tag{B-14}$$

B.4.1.5 Axisymmetric Reflector Surface Definition

A function $g(\theta')$ is defined as

$$g(\theta') = \frac{-1}{k\rho(\theta')} \quad , \tag{B-15}$$

which completely describes the reflecting surface. To remove the wavelength dependence of $g(\theta')$, a new normalized function is defined as

$$g_1(\theta') = g(\theta') \cdot C \ , \tag{B-16}$$

where C is some convenient constant containing the wavelength dependence. Its choice is dependent on the form of $\rho(\theta')$. For the present cases involving a paraboloid and conics, it was convenient to let $C = kD$, where D is the total reflector diameter in meters.

Figure 41 is an axial cut showing the breakup of the reflector surface into two inner cones and an outer parabola. The edges (intersection) of these surfaces are defined by a subscripted θ'.

The equations for computing the above angles and the reflector geometry were taken from Reference 39. Table 17 presents these equations for the three surface sectors.

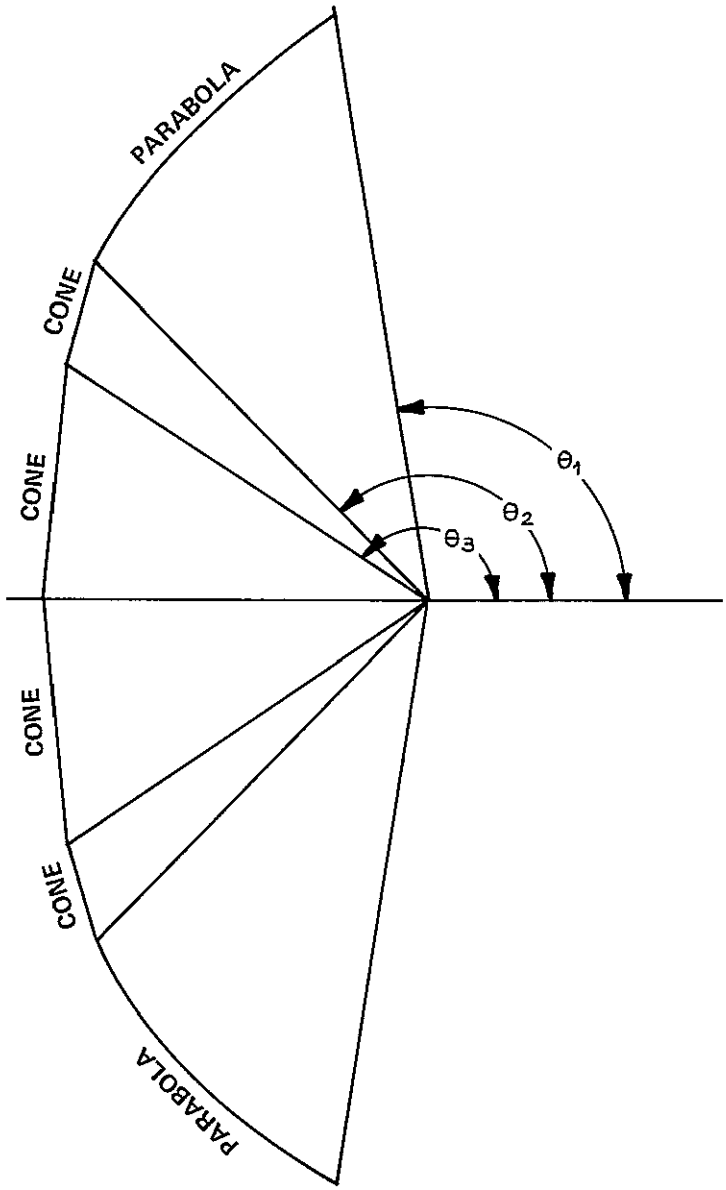

Figure 41 REFLECTOR CONIC AND PARABOLIC SURFACES

Table 17

REFLECTOR DEFINITION

RANGE OF θ'	$g_1(\theta') = \frac{-1}{k\rho} \cdot kD$	$g_1'(\theta')$
$\theta_1 = \pi - \sin^{-1}\left[\frac{1}{\sqrt{1+\left(2f-\frac{1}{8}\right)^2}}\right]$ TO $\theta_2 = \pi - \sin^{-1}\left[\frac{1}{\sqrt{1+\frac{8}{f}\left(f-\frac{5}{160}\right)^2}}\right]$	$\frac{\cos\theta' - 1}{2f}$ (PARABOLA)	$\frac{-\sin\theta'}{2f}$
θ_2 TO $\theta_3 = \pi - \sin^{-1}\left[\frac{1}{\sqrt{1+\frac{12.5}{f}\left(f-\frac{3}{160}\right)^2}}\right]$	$\frac{\cos\theta' - \frac{5}{\sqrt{800f}}\sin\theta'}{f+\frac{5}{160}}$ (CONE)	$\frac{-\sin\theta' - \frac{5}{\sqrt{800f}}\cos\theta'}{f+\frac{5}{160}}$
θ_3 TO π	$\frac{\cos\theta' - \left(\frac{4-\sqrt{2}}{\sqrt{800f}}\right)\sin\theta'}{f+\frac{34-16\sqrt{2}}{1600}}$ (CONE)	$\frac{-\sin\theta' - \left(\frac{4-\sqrt{2}}{\sqrt{800f}}\right)\cos\theta'}{f+\frac{34-16\sqrt{2}}{1600}}$

where f = F/D is the reflector F/D ratio, and $g'(\theta')$ implies a derivative with respect to θ'. The values of θ_1 through θ_4 and $g(\theta')$, $g'(\theta')$ and θ' are inputs to the main computer program. They are computed and punched on cards by subroutine FIX or may be read in from preexisting cards.

B.4.1.6 Grid Reflection Coefficients

In equations (B-5) and (B-6), the grid voltage reflection coefficients are $R_{\theta'}(\theta')$ for the θ' field component ($R_{//}$ in equation (3), Section 3); $R_{\varphi'}(\theta')$ for the φ' field component ($R_{\perp}$ in equation (1), Section 3). These coefficients are computed in subroutine FABCD, which calls subroutine GRID to obtain the grid spacings. If a solid, perfectly conducting reflector is desired, both reflection coefficients are set to unity.

B.4.2 Functional Flow

The functional flow of the single-integral programs is outlined in Figure 42. The figure shows the general processing flow, subroutine subordination and recycle paths. The acquisition of the reflector profile ($g_1(\theta')$, etc.) and feed definition data ($A_m(\theta')$, etc.) deserves a more detailed explanation. If data cards containing this information are available, they are simply read in at the beginning of the program; if not, the data are computed by subroutines FIX and perhaps FABCD, and punched on cards for future use. If a recycle involves a change of F/D ratio (focal length to diameter), then new reflector and feed data are required; but if a recycle involves only a frequency change and the feed has a phase error or the reflector is a grid, then only new feed data are read or computed and the reflector data from the first cycle are reused. The computation of new feed data on a recycle requires that the reflector be defined in the same number and size of angular increments in θ' as that desired for the feed. Feed data from the first cycle are reused, if a frequency change is made and no feed phase error or grid is used.

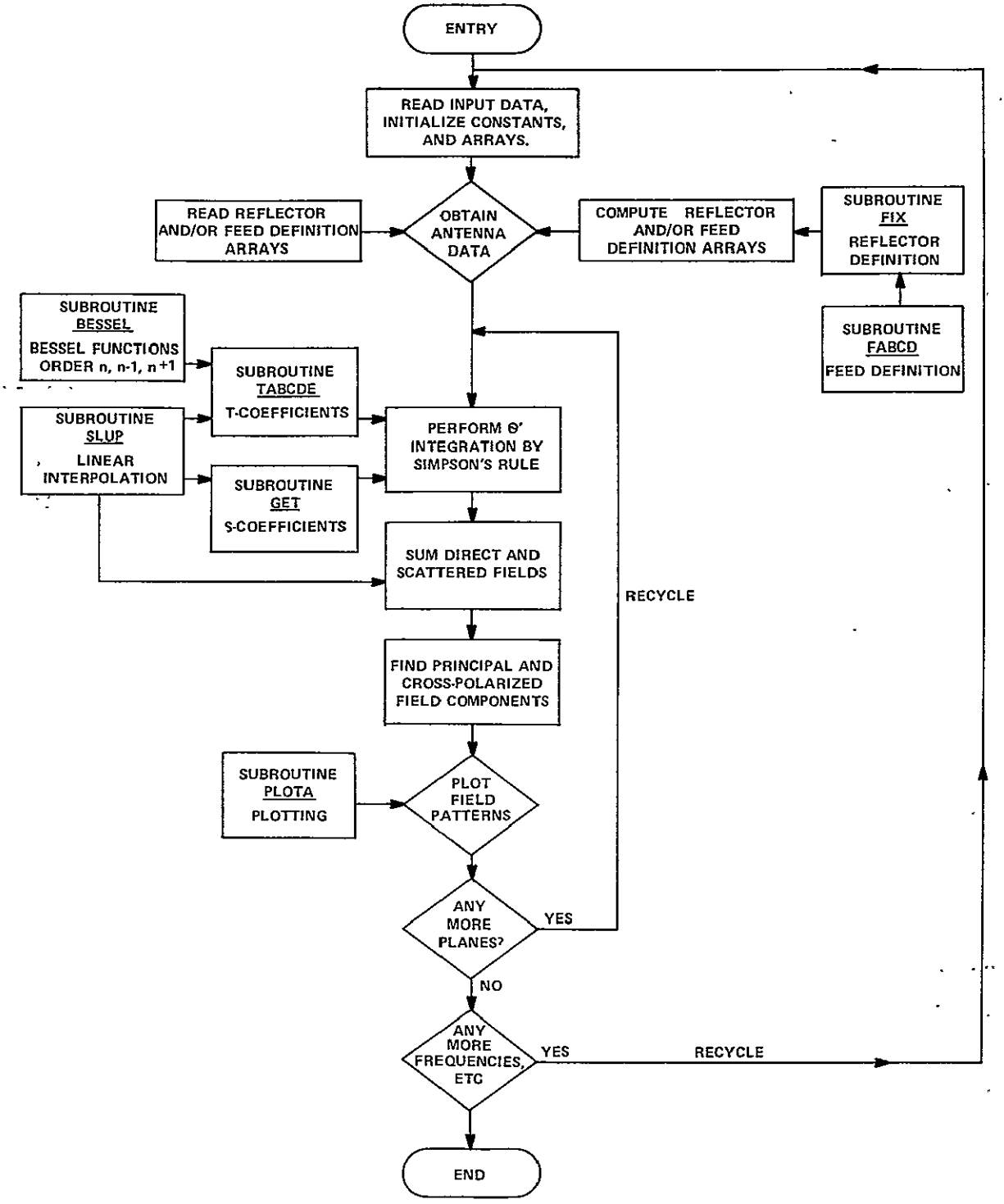

Figure 42 FUNCTIONAL FLOW, SINGLE-INTEGRAL PROGRAM

Subroutine FIX, which computes the reflector data, can be modified or replaced to change the reflector construction. One version of FIX is used for a parabolic-conical surface and another for a purely parabolic surface.

B.4.3 Program Usage

With the exception of the reflector and feed data discussed in Section B.4.2 and an initial identification card, all input data cards which provide data and control parameters are read on FORTRAN namelists and grouped according to their commonality. It will be sufficient to briefly describe each namelist variable in order of appearance at the head of the main program. The initial value of the variables, if applicable, is shown in closed brackets.

B.4.3.1 Namelist NAM 1

XKC — that number such that $g_1(\theta') = g(\theta') \cdot$ XKC (equation B-15, Section B.4.1.3)

Y1 — initial value of the observation angle θ . (Figure 41)

DY — increment in θ

X1...X4 — $\theta_1' \ldots \theta_4'$ as defined in Figure 41, Section B.4.1.4

P1 — initial value of the observation angle ϕ (Figure 41)

DP — increment in ϕ

FOD — F/D ratio (focal length/diameter)

DOL — d/λ ratio (diameter/wavelength)

B.4.3.2 Namelist NAM 2

M1,M2 — lower and upper summation limits in equation (B-2), Section B.4.1

N1,N2,N3 — the number of integration intervals between X1 to X2, X2 to X3, and X3 to X4 (each must be even)

NY — number of θ observation angles less 1

NP — number of ϕ observation angles less 1

IFN — number of $g_1(\theta')$'s, etc. on cards; if zero, they are computed by FIX

IAR — number of $A_m(\theta')$'s, etc. on cards; if zero, they are computed by FABCD

ISPOT — print code, = 1: print intermediate calculation results, = 0: no print

IFREQ — number of program cycles due to frequency change.

B.4.3.3 Namelist NAM 3

GMAX — maximum dB level of plotting abscissa

GMIN — minimum dB level of plotting abscissa

XMAX — maximum θ value of plotting ordinate.

B.4.3.4 Namelist NAM 4

TH — reflector grid thickness in meters [0.]

SIG — reflector grid conductivity in mho/meter [0.]

FREQ — frequency in the case of a grid (mHz) [0.]

SE — E-plane feed phase error (Section B.4.1.4) [0.]

SH — H-plane feed phase error (Section B.4.1.4) [0.]

IFEED — feed code

= 1: Trapezoidal Tooth, = 3: 1/2 wave dipole
= 2: Log Periodic Dipole (LPD), = 4: point source

NPHI — number of φ' integration points in equations (B-5) and (B-6), Section B.4.1.2

ISC — surface code, = 1: perturbation, = 0: no perturbation in surface as function of φ' (an approximate result is obtained)

B.4.3.5 Namelist NAM 5 (fox subroutine FIX)

N1,N2,N3 the number of intervals for which the reflector and feed data are to be computed between X1 to X2, X2 to X3, X3 to X4

B.4.3.6 Namelist NAM 6 (for subroutine GRID)

DP grid φ' dimension (meters)

DT grid θ' dimension (meters)

WP grid φ' spacing (meters)

WT grid θ' spacing (meters)

B.4.4 Sample Output

Figure 43 shows the computer printout for a typical run having no feed phase error, a solid paraboloid reflector (no grid), no surface perturbation and already available feed and reflection data read from cards. The namelists are printed first, followed by reflector and feed data. The feed data are printed as a function of θ' for each Fourier coefficient M1 to M2. Finally, the resulting θ , φ , γ and ψ field components are printed as gain over isotropic in dB units and a function of each observation angle θ for the plane specified by the observation angle. The S,T and U,V columns are the real and imaginary parts of the θ and φ total field components in volts [Reference 39] and indicate the electrical phase of these two components. Typical output plots are produced at CAL on the Xerox-LDX plotter (8-1/2" x 11"). For identification purposes, the contents of a comment card appearing in the input data before each namelist group are written on the plot page and on the printed output.

B.5 DOUBLE-INTEGRAL PROGRAM

This program was used as a check on the results of the single-integral program and also to calculate the effects of reflector surface perturbations

THE RUSCH INTEGRALS

```
&NAM1
XKC=  62.831848     ,YI= 0.0            ,DY= 0.50000000     ,XI=  2.0243931     ,X2=  2.5964861     ,X3=  2.7028809     ,X4=
  3.1415930     ,P1= 0.0            ,DP=  45.000000     ,FOO= 0.39999998     ,DUL=  10.000000
&END
&NAM2
M1=          1,M2=          5,N1=         20,N2=          4,N3=         18,NY=         60,NP=          0,IFN=         43,IAR=
        43,ISPOT=          0,IFREQ=          1
&END
&NAM3
GMAX=  45.000000     ,GMIN= -30.000000     ,XMAX=  30.000000
&END
&NAM4
TH= 0.0           ,SIG= 0.0           ,FREQ= 0.0           ,SE= 0.0           ,SH= 0.0           ,IFEED=          1,NPHI=
        31,ISC=          0
&END
PARABOLOID, TRAP. TOOTH FEED, D/L=10., F/D=0.4

THE F(X) FUNCTION FOLLOWS

   -0.1797750E 01    -0.1829662E 01    -0.1861100E 01    -0.1892037E 01    -0.1922448E 01    -0.1952311E 01    -0.1981598E 01
   -0.2010286E 01    -0.2038353F 01    -0.2065775F 01    -0.2092529E 01    -0.2118594E 01    -0.2143948E 01    -0.2168571E 01
   -0.2192443E 01    -0.2215543F 01    -0.2237852E 01    -0.2259355F 01    -0.2280031E 01    -0.2299864E 01    -0.2318840E 01
   -0.2335698E 01    -0.2351790E 01    -0.2367102F 01    -0.2381623E 01    -0.2394228E 01    -0.2406151E 01    -0.2417389E 01
   -0.2427933E 01    -0.2437778F 01    -0.2446916E 01    -0.2455344E 01    -0.2463056E 01    -0.2470046E 01    -0.2476313E 01
   -0.2481852F 01    -0.2486656E 01    -0.2490728E 01    -0.2494063E 01    -0.2496659E 01    -0.2498514F 01    -0.2499628E 01
   -0.2500000E 01

THE G(X) FUNCTION FOLLOWS

   -0.1123596E 01    -0.1107470E 01    -0.1090438E 01    -0.1072515E 01    -0.1053713E 01    -0.1034049E 01    -0.1013540E 01
   -0.9922008E 00    -0.9700503E 00    -0.9471061E 00    -0.9233868E 00    -0.8989122E 00    -0.8737021E 00    -0.8477773E 00
   -0.8211578E 00    -0.7938673E 00    -0.7659274F 00    -0.7373610E 00    -0.7081911E 00    -0.6784418E 00    -0.6481365E 00
   -0.6194816E 00    -0.5903875E 00    -0.5608756E 00    -0.5309670E 00    -0.5032319E 00    -0.4751969E 00    -0.4468796E 00
   -0.4182969E 00    -0.3894656E 00    -0.3604042F 00    -0.3311275E 00    -0.3016541E 00    -0.2720016E 00    -0.2421875E 00
   -0.2122295E 00    -0.1821466E 00    -0.1519544E 00    -0.1216719E 00    -0.9131706E-01    -0.6090811E-01    -0.3046289E-01
   -0.8192341E-06

THE INDEPENDENT VARIABLE OF F(X),G(X)

    0.2024393E 01     0.2052998E 01     0.2081602E 01     0.2110207E 01     0.2138811E 01     0.2167416E 01     0.2196020E 01
    0.2224626E 01     0.2253230E 01     0.2281835E 01     0.2310439E 01     0.2339044E 01     0.2367648E 01     0.2396253E 01
    0.2424858E 01     0.2453463E 01     0.2482067E 01     0.2510672E 01     0.2539276E 01     0.2567881E 01     0.2596486E 01
    0.2623084E 01     0.2649683E 01     0.2676282E 01     0.2702881E 01     0.2727253E 01     0.2751626E 01     0.2775999E 01
    0.2800372E 01     0.2824745E 01     0.2849117E 01     0.2873490E 01     0.2897863E 01     0.2922236E 01     0.2946609E 01
    0.2970983E 01     0.2995355F 01     0.3019728E 01     0.3044101E 01     0.3068474E 01     0.3092847E 01     0.3117220E 01
    0.3141592E 01
```

Figure 43 COMPUTER PRINTOUT FOR A TYPICAL RUN (SHEET 1 OF 5)

```
THE INPUT FUNCTIONS  AR,AI,....DR,DI WITH M=     1

BR FUNCTION
    0.4410523E 00     0.5054256E 00     0.5735856E 00     0.6452952E 00     0.7202985E 00     0.7983228E 00     0.8790793E 00
    0.9622769E 00     0.1047592E 01     0.1134719E 01     0.1223317E 01     0.1313059E 01     0.1403606E 01     0.1494617E 01
    0.1585752E 01     0.1676661E 01     0.1767005E 01     0.1856438E 01     0.1944644E 01     0.2031271E 01     0.2116005E 01
    0.2192820E 01     0.2267469E 01     0.2339720E 01     0.2409339E 01     0.2470623E 01     0.2529346E 01     0.2585339E 01
    0.2638460E 01     0.2688568E 01     0.2735521E 01     0.2779192E 01     0.2819481E 01     0.2856258E 01     0.2889431E 01
    0.2918908E 01     0.2944626E 01     0.2966512E 01     0.2984480E 01     0.2998518E 01     0.3008564E 01     0.3014619E 01
    0.3016625E 01

BI FUNCTION
   -0.5285669E-05    -0.6057133E-05    -0.3436988E-05    -0.3866680E-05    -0.4316108E-05    -0.4783638E-05    -0.1053508E-04
   -0.5766070E-05    -0.6277291E-05    -0.1359873E-04    -0.1466051E-04    -0.1573599E-04    -0.8410570E-05    -0.8955916E-05
   -0.9502008E-05    -0.2009346E-04    -0.1058809E-04    -0.2224797E-04    -0.2330504E-04    -0.1217161E-04    -0.1267934E-04
   -0.1313962E-04    -0.1358693E-04    -0.1401987E-04    -0.1443703E-04    -0.2960848E-04    -0.1515611E-04    -0.3098328E-04
   -0.1580994E-04    -0.1611019E-04    -0.1639154E-04    -0.3330644E-04    -0.3378930E-04    -0.3423003E-04    -0.3462758E-04
   -0.1749041E-04    -0.3528903E-04     0.0              -0.1788333E-04    -0.3593491E-04    -0.1802764E-04     0.0
    0.0

CR FUNCTION
    0.6718964E 00     0.7472885E 00     0.8248969E 00     0.9044403E 00     0.9856192E 00     0.1068158E 01     0.1151771E 01
    0.1236175E 01     0.1321103E 01     0.1406277E 01     0.1491445E 01     0.1576336E 01     0.1660697E 01     0.1744287E 01
    0.1826870E 01     0.1908200E 01     0.1988055E 01     0.2066210E 01     0.2142454E 01     0.2216599E 01     0.2288417E 01
    0.2352966E 01     0.2415204E 01     0.2474997E 01     0.2532212E 01     0.2582273E 01     0.2629971E 01     0.2675218E 01
    0.2717947E 01     0.2758049E 01     0.2795486E 01     0.2830173E 01     0.2862046E 01     0.2891058E 01     0.2917164E 01
    0.2940291E 01     0.2960427E 01     0.2977532E 01     0.2991543E 01     0.3002488E 01     0.3010314E 01     0.3014997E 01
    0.3016575E 01

CI FUNCTION
   -0.8052156E-05    -0.8955673E-05    -0.4942875E-05    -0.5419507E-05    -0.5905940E-05    -0.6400526E-05    -0.1380308E-04
   -0.7407297E-05    -0.7916199E-05    -0.1685313E-04    -0.1787380E-04    -0.1889115E-04    -0.9951083E-05    -0.1045196E-04
   -0.1094681E-04    -0.2286829E-04    -0.1191265E-04    -0.2476192E-04    -0.2567566E-04    -0.1328211E-04    -0.1371245E-04
   -0.1409924E-04    -0.1447218E-04    -0.1483046E-04    -0.1517330E-04    -0.3094654E-04    -0.1575905E-04    -0.3206040E-04
   -0.1628624E-04    -0.1652652E-04    -0.1675087E-04    -0.3391741E-04    -0.3429940E-04    -0.3464708E-04    -0.3495994E-04
   -0.1761854E-04    -0.3547841E-04     0.0              -0.1792565E-04    -0.3598249E-04    -0.1803813E-04     0.0
    0.0
```

Figure 43 COMPUTER PRINTOUT FOR A TYPICAL RUN (SHEET 2 OF 5)

```
THE INPUT FUNCTIONS  AR,AI,....DR,DI WITH M=     3

BR FUNCTION
    0.9493786E-01     0.1014006E 00     0.1071904E 00     0.1122482E 00     0.1165298E 00     0.1200029E 00     0.1226488E 00
    0.1244596E 00     0.1254388E 00     0.1255988E 00     0.1249619E 00     0.1235574E 00     0.1214232E 00     0.1186028E 00
    0.1151446E 00     0.1111026E 00     0.1065354E 00     0.1015037E 00     0.9607196E-01     0.9030598E-01     0.8427262E-01
    0.7848191E-01     0.7257277E-01     0.6660056E-01     0.6061957E-01     0.5517525E-01     0.4980598E-01     0.4455095E-01
    0.3944701E-01     0.3452916E-01     0.2983195E-01     0.2538608E-01     0.2122233E-01     0.1736872E-01     0.1385140E-01
    0.1069074E-01     0.7909317E-02     0.5524304E-02     0.3552605E-02     0.2005443E-02     0.8934638E-03     0.2223417E-03
   -0.1299232E-05

BI FUNCTION
   -0.1137756E-05    -0.1215208E-05    -0.6422966E-06    -0.6726037E-06    -0.6982598E-06    -0.7190710E-06    -0.1469851E-05
   -0.7457762E-06    -0.7516434E-06    -0.1505203E-05    -0.1497569E-05    -0.1480740E-05    -0.7275816E-06    -0.7106811E-06
   -0.6899591E-06    -0.1331478E-05    -0.6383721E-06    -0.1216444E-05    -0.1151348E-05    -0.5411237E-06    -0.5049710E-06
   -0.4702727E-06    -0.4348643E-06    -0.3990783E-06    -0.3632393E-06    -0.6612321E-06    -0.2984427E-06    -0.5339087E-06
   -0.2363708E-06    -0.2069024E-06    -0.1787563E-06    -0.3042324E-06    -0.2543333E-06    -0.2081505E-06    -0.1659983E-06
   -0.6406009E-07    -0.9478697E-07     0.0              -0.2128759E-07    -0.2403368E-07    -0.5353733E-08     0.0
    0.0

CR FUNCTION
    0.1179438E 00     0.1239494E 00     0.1290947E 00     0.1333485E 00     0.1366922E 00     0.1391214E 00     0.1406416E 00
    0.1412685E 00     0.1410272E 00     0.1399510E 00     0.1380787E 00     0.1354566E 00     0.1321355E 00     0.1281713E 00
    0.1236224E 00     0.1185511E 00     0.1130210E 00     0.1070980E 00     0.1008498E 00     0.9434187E-01     0.8764285E-01
    0.8130038E-01     0.7490206E-01     0.6850171E-01     0.6214736E-01     0.5640959E-01     0.5078787E-01     0.4531925E-01
    0.4003718E-01     0.3497249E-01     0.3015787E-01     0.2561828E-01     0.2138252E-01     0.1747430E-01     0.1391693E-01
    0.1072967E-01     0.7929556E-02     0.5533956E-02     0.3556371E-02     0.2005710E-02     0.8923782E-03     0.2215903E-03
   -0.2239884E-05

CI FUNCTION
   -0.1413464E-05    -0.1485438E-05    -0.7735501E-06    -0.7990391E-06    -0.8190749E-06    -0.8336310E-06    -0.1685480E-05
   -0.8464970E-06    -0.8450507E-06    -0.1677203E-05    -0.1654765E-05    -0.1623342E-05    -0.7917710E-06    -0.7680168E-06
   -0.7407593E-06    -0.1420743E-05    -0.6772344E-06    -0.1283486E-05    -0.1208607E-05    -0.5653074E-06    -0.5251658E-06
   -0.4871613E-06    -0.4488218E-06    -0.4104701E-06    -0.3723939E-06    -0.6760249E-06    -0.3043263E-06    -0.5431160E-06
   -0.2399072E-06    -0.2095590E-06    -0.1807093E-06    -0.3070151E-06    -0.2562529E-06    -0.2094159E-06    -0.1667835E-06
   -0.6429332E-07    -0.9502952E-07     0.0              -0.2131015E-07    -0.2403688E-07    -0.5347228E-08     0.0
    0.0
```

Figure 43 COMPUTER PRINTOUT FOR A TYPICAL RUN (SHEET 3 OF 5)

```
THE INPUT FUNCTIONS  AR,AI,....OR,OI WITH M=    5

BR FUNCTION
    0.2869244E-01     0.2868613E-01     0.2836100E-01     0.2775051E-01     0.2689047E-01     0.2581804E-01     0.2457063E-01
    0.2318467E-01     0.2169579E-01     0.2013626E-01     0.1853716E-01     0.1692596E-01     0.1532753E-01     0.1376392E-01
    0.1225289E-01     0.1081093E-01     0.9449892E-02     0.8179497E-02     0.7007129E-02     0.5936854E-02     0.4970796E-02
    0.4165314E-02     0.3448687E-02     0.2818300E-02     0.2270289E-02     0.1835768E-02     0.1462579E-02     0.1146127E-02
    0.8809625E-03     0.6634127E-03     0.4873788E-03     0.3479733E-03     0.2400257E-03     0.1592906E-03     0.1012958E-03
    0.6039663E-04     0.3396794E-04     0.1633550E-04     0.7501894E-05     0.3682415E-05     0.2404271E-05     0.9271967E-06
    0.1751644E-05

BI FUNCTION
   -0.3438566E-06    -0.3437810E-06    -0.1699423E-06    -0.1662841E-06    -0.1611307E-06    -0.1547045E-06    -0.2944599E-06
   -0.1389251E-06    -0.1300035E-06    -0.2413173E-06    -0.2221533E-06    -0.2028445E-06    -0.9184430E-07    -0.8247491E-07
   -0.7342067E-07    -0.1295605E-06    -0.5662482E-07    -0.9802494E-07    -0.8397501E-07    -0.3557430E-07    -0.2978557E-07
   -0.2495904E-07    -0.2066492E-07    -0.1668757E-07    -0.1360382E-07    -0.2200024E-07    -0.8763930E-08    -0.1373545E-07
   -0.5278824E-08    -0.1975241E-08    -0.2920428E-08    -0.4170190E-08    -0.2876523E-08    -0.1908974E-08    -0.1213951E-08
   -0.3619032E-09    -0.4070790E-09     0.0              -0.4495215E-10    -0.4413088E-10    -0.1440666E-10     0.0
    0.0

CR FUNCTION
    0.3323221E-01     0.3285405E-01     0.3215029E-01     0.3116345E-01     0.2993686E-01     0.2851341E-01     0.2693454E-01
    0.2524002E-01     0.2346686E-01     0.2164915E-01     0.1981711E-01     0.1799932E-01     0.1621828E-01     0.1449596E-01
    0.1284809E-01     0.1128920E-01     0.9829920E-02     0.8477442E-02     0.7237304E-02     0.6112024E-02     0.5102035E-02
    0.4264090E-02     0.3522280E-02     0.2870843E-02     0.2307259E-02     0.1862847E-02     0.1481469E-02     0.1158893E-02
    0.8899728E-03     0.6690007E-03     0.4905618E-03     0.3498544E-03     0.2406898E-03     0.1594980E-03     0.1005389E-03
    0.5949644E-04     0.3293408E-04     0.1607130E-04     0.7391444E-05     0.3407607E-05     0.1492814E-05     0.1013383E-05
    0.9352295E-06

CI FUNCTION
   -0.3982622E-06    -0.3937303E-06    -0.1926481E-06    -0.1867348E-06    -0.1793850E-06    -0.1708556E-06    -0.3227896E-06
   -0.1512410E-06    -0.1406160E-06    -0.2594481E-06    -0.2374926E-06    -0.2157078E-06    -0.9718173E-07    -0.8686141E-07
   -0.7698719E-07    -0.1352922E-06    -0.5890199E-07    -0.1015956E-06    -0.8673345E-07    -0.3662395E-07    -0.3057198E-07
   -0.2555091E-07    -0.2110590E-07    -0.1720241E-07    -0.1382536E-07    -0.2232477E-07    -0.8877116E-08    -0.1388844E-07
   -0.5332815E-08    -0.4008722E-08    -0.2939501E-08    -0.4192731E-08    -0.2884480E-08    -0.1911460E-08    -0.1204880E-08
   -0.3565090E-09    -0.3946894E-09     0.0              -0.4429034E-10    -0.4083753E-10    -0.8945105E-11     0.0
    0.0

THE INDEP. VARIABLE FOR THE AR,.....,OI
    0.2024393E 01     0.2052998E 01     0.2081602E 01     0.2110207E 01     0.2138811E 01     0.2167416E 01     0.2196020E 01
    0.2224626E 01     0.2253230E 01     0.2281835E 01     0.2310439E 01     0.2339044E 01     0.2367648E 01     0.2396253E 01
    0.2424858E 01     0.2453463E 01     0.2482067E 01     0.2510672E 01     0.2539276E 01     0.2567881E 01     0.2596486E 01
    0.2623084E 01     0.2649683E 01     0.2676282E 01     0.2702881E 01     0.2727253E 01     0.2751626E 01     0.2775999E 01
    0.2800372E 01     0.2824745E 01     0.2849117E 01     0.2873490E 01     0.2897863E 01     0.2922236E 01     0.2946609E 01
    0.2970983E 01     0.2995355E 01     0.3019728E 01     0.3044101E 01     0.3068474E 01     0.3092847E 01     0.3117220E 01
    0.3141592E 01
```

Figure 43 COMPUTER PRINTOUT FOR A TYPICAL RUN (SHEET 4 OF 5)

THE VALU OF P= 0.0

0.0 PARABOLOID, TRAP. TOOTH FEED, D/L=10., F/D=0.4

Y	S	T	U	V	THETA C (DB)	PHI C (DB)	GAMMA C (DB)	PSI C. (DB)
0.0	0.6545305E-03	0.2588123E 02	0.1000000E-19	0.1000000E-19	0.2825969E 02	-0.3969897E 03	-0.3969897E 03	0.2825969E 02
0.5000	-0.1475642E-01	0.2571371E 02	0.1000000E-19	0.1000000E-19	0.2820329E 02	-0.3969897E 03	-0.1426705E 03	0.2820329E 02
1.0000	-0.5992474E-01	0.2521640E 02	0.1000000E-19	0.1000000E-19	0.2803368E 02	-0.3969897E 03	-0.1368199E 03	0.2803368E 02
1.5000	-0.1313205E 00	0.2440446E 02	0.1000000E-19	0.1000000E-19	0.2774950E 02	-0.3969897E 03	-0.1335827E 03	0.2774950E 02
2.0000	-0.2239794E 00	0.2330267E 02	0.1000000E-19	0.1000000E-19	0.2734850E 02	-0.3969897E 03	-0.1314857E 03	0.2734850E 02
2.5000	-0.3309620E 00	0.2194420E 02	0.1000000E-19	0.1000000E-19	0.2682738E 02	-0.3969897E 03	-0.1300697E 03	0.2682738E 02
3.0000	-0.4444029E 00	0.2036929E 02	0.1000000E-19	0.1000000E-19	0.2618158E 02	-0.3969897E 03	-0.1291330E 03	0.2618158E 02
3.5000	-0.5560953E 00	0.1862364E 02	0.1000000E-19	0.1000000E-19	0.2540514E 02	-0.3969897E 03	-0.1285719E 03	0.2540514E 02
4.0000	-0.6580239E 00	0.1675658E 02	0.1000000E-19	0.1000000E-19	0.2449039E 02	-0.3969897E 03	-0.1283285E 03	0.2449039E 02
4.5000	-0.7428086E 00	0.1481913E 02	0.1000000E-19	0.1000000E-19	0.2342735E 02	-0.3969897E 03	-0.1283704E 03	0.2342735E 02
5.0000	-0.8045572E 00	0.1286199E 02	0.1000000E-19	0.1000000E-19	0.2220311E 02	-0.3969897E 03	-0.6521123E 02	0.2220311E 02
5.5000	-0.8388264E 00	0.1093370E 02	0.1000000E-19	0.1000000E-19	0.2080081E 02	-0.3969897E 03	-0.1292583E 03	0.2080081E 02
6.0000	-0.8435474E 00	0.9078845E 01	0.1000000E-19	0.1000000E-19	0.1919794E 02	-0.3969897E 03	-0.1301080E 03	0.1919794E 02
6.5000	-0.8185700E 00	0.7336596E 01	0.1000000E-19	0.1000000E-19	0.1736360E 02	-0.3969897E 03	-0.1312498E 03	0.1736360E 02
7.0000	-0.7659987E 00	0.5739450E 01	0.1000000E-19	0.1000000E-19	0.1525408E 02	-0.3969897E 03	-0.1327187E 03	0.1525408E 02
7.5000	-0.6896576E 00	0.4312417E 01	0.1000000E-19	0.1000000E-19	0.1280408E 02	-0.3969897E 03	-0.1345726E 03	0.1280408E 02
8.0000	-0.5950705E 00	0.3072434E 01	0.1000000E-19	0.1000000E-19	0.9909583E 01	-0.3969897E 03	-0.1369099E 03	0.9909583E 01
8.5000	-0.4889164E 00	0.2028323E 01	0.1000000E-19	0.1000000E-19	0.6388019E 01	-0.3969897E 03	-0.1399085E 03	0.6388019E 01
9.0000	-0.3783320E 00	0.1181071E 01	0.1000000E-19	0.1000000E-19	0.1869743E 01	-0.3969897E 03	-0.1439343E 03	0.1869743E 01
9.5000	-0.2705367E 00	0.5243511E 00	0.1000000E-19	0.1000000E-19	-0.4582533E 01	-0.3969897E 03	-0.1499210E 03	-0.4582533E 01
10.0000	-0.1722547E 00	0.4550326E-01	0.1000000E-19	0.1000000E-19	-0.1498362E 02	-0.3969897E 03	-0.1598808E 03	-0.1498362E 02
10.5000	-0.8910519E-01	-0.2733158E 00	0.1000000E-19	0.1000000E-19	-0.1082803E 02	-0.3969897E 03	-0.1553060E 03	-0.1082803E 02
11.0000	-0.2531727E-01	-0.4538589E 00	0.1000000E-19	0.1000000E-19	-0.6848089E 01	-0.3969897E 03	-0.1509267E 03	-0.6848089E 01
11.5000	0.1655445E-01	-0.5204010E 00	0.1000000E-19	0.1000000E-19	-0.5668845E 01	-0.3969897E 03	-0.1493664E 03	-0.5668845E 01
12.0000	0.3590424E-01	-0.4982654E 00	0.1000000E-19	0.1000000E-19	-0.6028291E 01	-0.3969897E 03	-0.1493614E 03	-0.6028291E 01
12.5000	0.3378428E-01	-0.4125801E 00	0.1000000E-19	0.1000000E-19	-0.7660810E 01	-0.3969897E 03	-0.1506447E 03	-0.7660810E 01
13.0000	0.1301544E-01	-0.2870121E 00	0.1000000E-19	0.1000000E-19	-0.1083307E 02	-0.3969897E 03	-0.1534820E 03	-0.1083307E 02
13.5000	-0.2223459E-01	-0.1427533E 00	0.1000000E-19	0.1000000E-19	-0.1680417E 02	-0.3969897E 03	-0.1591311E 03	-0.1680417E 02
14.0000	-0.6684476E-01	0.2211269E-02	0.1000000E-19	0.1000000E-19	-0.2349390E 02	-0.3969897E 03	-0.1655110E 03	-0.2349390E 02
14.5000	-0.1151275E 00	0.1336316E 00	0.1000000E-19	0.1000000E-19	-0.1507075E 02	-0.3969897E 03	-0.1567894E 03	-0.1507075E 02
15.0000	-0.1614578E 00	0.2412075E 00	0.1000000E-19	0.1000000E-19	-0.1074431E 02	-0.3969897E 03	-0.8870465E 02	-0.1074431E 02
15.5000	-0.2005214E 00	0.3186632E 00	0.1000000E-19	0.1000000E-19	-0.8484612E 01	-0.3969897E 03	-0.1496373E 03	-0.8484612E 01
16.0000	-0.2279782E 00	0.3633225E 00	0.1000000E-19	0.1000000E-19	-0.7352357E 01	-0.3969897E 03	-0.1482362E 03	-0.7352357E 01
16.5000	-0.2405930E 00	0.3758403E 00	0.1000000E-19	0.1000000E-19	-0.7008391E 01	-0.3969897E 03	-0.1476322E 03	-0.7008391E 01
17.0000	-0.2366014E 00	0.3594609E 00	0.1000000E-19	0.1000000E-19	-0.7323771E 01	-0.3969897E 03	-0.1476957E 03	-0.7323771E 01
17.5000	-0.2157151E 00	0.3193965E 00	0.1000000E-19	0.1000000E-19	-0.8281361E 01	-0.3969897E 03	-0.1484091E 03	-0.8281361E 01
18.0000	-0.1791547E 00	0.2620707E 00	0.1000000E-19	0.1000000E-19	-0.9966367E 01	-0.3969897E 03	-0.1498574E 03	-0.9966367E 01
18.5000	-0.1294671E 00	0.1943991E 00	0.1000000E-19	0.1000000E-19	-0.1263183E 02	-0.3969897E 03	-0.1522929E 03	-0.1263183E 02
19.0000	-0.7029253E-01	0.1231571E 00	0.1000000E-19	0.1000000E-19	-0.1696616E 02	-0.3969897E 03	-0.1564039E 03	-0.1696616E 02
19.5000	-0.6013110E-02	0.5438843E-01	0.1000000E-19	0.1000000E-19	-0.2523709E 02	-0.3969897E 03	-0.1644577E 03	-0.2523709E 02
20.0000	0.5863693E-01	-0.6955281E-02	0.1000000E-19	0.1000000E-19	-0.2457588E 02	-0.3969897E 03	-0.1635854E 03	-0.2457588E 02
20.5000	0.1189296E 00	-0.5732362E-01	0.1000000E-19	0.1000000E-19	-0.1758696E 02	-0.3969897E 03	-0.1563911E 03	-0.1758696E 02
21.0000	0.1706005E 00	-0.9461778E-01	0.1000000E-19	0.1000000E-19	-0.1419564E 02	-0.3969897E 03	-0.1527997E 03	-0.1419564E 02
21.5000	0.2100835E 00	-0.1182554E 00	0.1000000E-19	0.1000000E-19	-0.1235678E 02	-0.3969897E 03	-0.1507659E 03	-0.1235678E 02
22.0000	0.2348729E 00	-0.1289114E 00	0.1000000E-19	0.1000000E-19	-0.1143975E 02	-0.3969897E 03	-0.1496589E 03	-0.1143975E 02
22.5000	0.2436060E 00	-0.1283380E 00	0.1000000E-19	0.1000000E-19	-0.1120248E 02	-0.3969897E 03	-0.1492363E 03	-0.1120248E 02
23.0000	0.2361584E 00	-0.1190131E 00	0.1000000E-19	0.1000000E-19	-0.1155306E 02	-0.3969897E 03	-0.1494062E 03	-0.1155306E 02
23.5000	0.2136132E 00	-0.1038365E 00	0.1000000E-19	0.1000000E-19	-0.1248623E 02	-0.3969897E 03	-0.1501629E 03	-0.1248623E 02
24.0000	0.1780913E 00	-0.8577514E-01	0.1000000E-19	0.1000000E-19	-0.1408113E 02	-0.3969897E 03	-0.1515855E 03	-0.1408113E 02
24.5000	0.1326141E 00	-0.6754994E-01	0.1000000E-19	0.1000000E-19	-0.1654636E 02	-0.3969897E 03	-0.1538824E 03	-0.1654636E 02
25.0000	0.8070070E-01	-0.5136745E-01	0.1000000E-19	0.1000000E-19	-0.2038521E 02	-0.3969897E 03	-0.1575569E 03	-0.2038521E 02
25.5000	0.2616187E-01	-0.3878208E-01	0.1000000E-19	0.1000000E-19	-0.2659854E 02	-0.3969897E 03	-0.1636095E 03	-0.2659854E 02
26.0000	-0.2717328E-01	-0.3066828E-01	0.1000000E-19	0.1000000E-19	-0.2774649E 02	-0.3969897E 03	-0.1646002E 03	-0.2774649E 02
26.5000	-0.7587767E-01	-0.2715306E-01	0.1000000E-19	0.1000000E-19	-0.2187439E 02	-0.3969897E 03	-0.1585745E 03	-0.2187439E 02
27.0000	-0.1170552E 00	-0.2762660E-01	0.1000000E-19	0.1000000E-19	-0.1839676E 02	-0.3969897E 03	-0.1549465E 03	-0.1839676E 02
27.5000	-0.1485432E 00	-0.3103993E-01	0.1000000E-19	0.1000000E-19	-0.1637733E 02	-0.3969897E 03	-0.1527799E 03	-0.1637733E 02
28.0000	-0.1690706E 00	-0.3594691E-01	0.1000000E-19	0.1000000E-19	-0.1524662E 02	-0.3969897E 03	-0.1515051E 03	-0.1524662E 02
28.5000	-0.1782447E 00	-0.4077891E-01	0.1000000E-19	0.1000000E-19	-0.1475810E 02	-0.3969897E 03	-0.1508755E 03	-0.1475810E 02
29.0000	-0.1764845E 00	-0.4399862E-01	0.1000000E-19	0.1000000E-19	-0.1480411E 02	-0.3969897E 03	-0.1507833E 03	-0.1480411E 02
29.5000	-0.1650502E 00	-0.4429131E-01	0.1000000E-19	0.1000000E-19	-0.1534620E 02	-0.3969897E 03	-0.8771965E 02	-0.1534621E 02

Figure 43 COMPUTER PRINTOUT FOR A TYPICAL RUN (SHEET 5 OF 5)

in the ϕ' direction on the antenna pattern.

B.5.1 Mathematical Background

The feed field equation used in the double-integral program was of the form

$$E_{ff} = \frac{e^{-ik\rho(\theta',\phi') - i\psi_z(\theta') - i\psi_0(\theta')\cos 2\phi'}}{\rho(\theta',\phi')} \left[E_\theta(\theta',\phi')\,\bar{a}_\theta + E_\phi(\theta',\phi')\,\bar{a}_\phi \right] \tag{B-16}$$

The $\underline{\theta}$ and $\underline{\phi}$ components of the scattered field are

$$\bar{a}_\theta \cdot \bar{E}_s = \frac{e^{-ikR}}{R} \frac{i}{2\pi} \int_{\theta_1'}^{\theta_4'} \int_0^{2\pi} \frac{e^{-i\Phi}\,\sin\theta'}{g^2}\, \bar{a}_\theta \cdot (\bar{n} \times \bar{h})\, d\phi'\, d\theta' \tag{B-17}$$

$$\bar{a}_\phi \cdot \bar{E}_s = \frac{e^{-ikR}}{R} \frac{i}{2\pi} \int_{\theta_1'}^{\theta_4'} \int_0^{2\pi} \frac{e^{-i\Phi}\,\sin\theta'}{g^2}\, \bar{a}_\phi \cdot (\bar{n} \times \bar{h})\, d\phi'\, d\theta' \tag{B-18}$$

where

$$\begin{aligned} \bar{a}_\theta \cdot (\bar{n} \times \bar{h}) = \frac{1}{\sqrt{g_s}} \Big(& E_\theta \left\{ g' \left[\sin\theta' \cos\theta \cos(\phi' - \phi) - \cos\theta' \sin\theta \right] \right. \\ & \left. - g \left[\cos\theta' \cos\theta \cos(\phi' - \phi) + \sin\theta' \sin\theta \right] \right\} \\ & + E_\phi\, g \cos\theta \sin(\phi' - \phi) \Big) \end{aligned} \tag{B-19}$$

$$\begin{aligned} \bar{a}_\phi \cdot (\bar{n} \times \bar{h}) = \frac{1}{\sqrt{g_s}} \Big(& E_\theta \left\{ g' \sin\theta' \sin(\phi' - \phi) \right. \\ & \left. - g \cos\theta' \sin(\phi' - \phi) \right\} - E_\phi\, g \cos(\phi' - \phi) \Big) \end{aligned} \tag{B-20}$$

$$\Phi(\theta', \phi', \theta, \phi) = \frac{2\pi}{\lambda} \left(\rho(\theta') + S(\theta', \phi') \right) \left(1 - \cos\theta \cos\theta' - \sin\theta \sin\theta' \cos(\phi' - \phi) \right)$$

where $S(\theta' \phi')$ is the reflector surface perturbation relative to the surface defined in Table 17.

B.5.2 Functional Flow

The functional flow of the double integral program is outlined in Figure 44. The figure shows the general processing flow, subroutine subordination and recycle paths. As in the single-integral program, the data cards containing the reflector profile information are read in at the beginning of the program. If the cards are not available, the reflector profile data are computed in subroutine AFIX. One version of AFIX is used for a parabolic-conical surface and another for a purely parabolic surface.

The subroutines SIMP and FIELD are called every time θ' is incremented in the main program. These routines perform a Simpson's rule integration over ϕ' and this is the main difference between the single- and double-integral programs. In the single-integral program, the ϕ' integration is previously performed analytically to give a series of Bessel functions.

Subroutine SURF brings in different surface perturbations according to the namelist parameter ICODE. The possibilities are: torsional perturbations only, thermal only or torsional plus thermal.

B.5.3 Program Usage

With the exception of the reflection data discussed in Section B.4.2 and an initial identification card, all input data and control parameters are read on FORTRAN namelists. The namelist variables in order of appearance will be briefly described.

B.5.3.1 Namelist NAM 1

Y1	initial value of the observation angle θ (Figure 41)
DY	increment in θ
X1...X4	θ_1' ... θ_4' as defined in Figure 41, Section B.4.1.4
P1	initial value of the observation angle ϕ (Figure 41)
DP	increment in ϕ

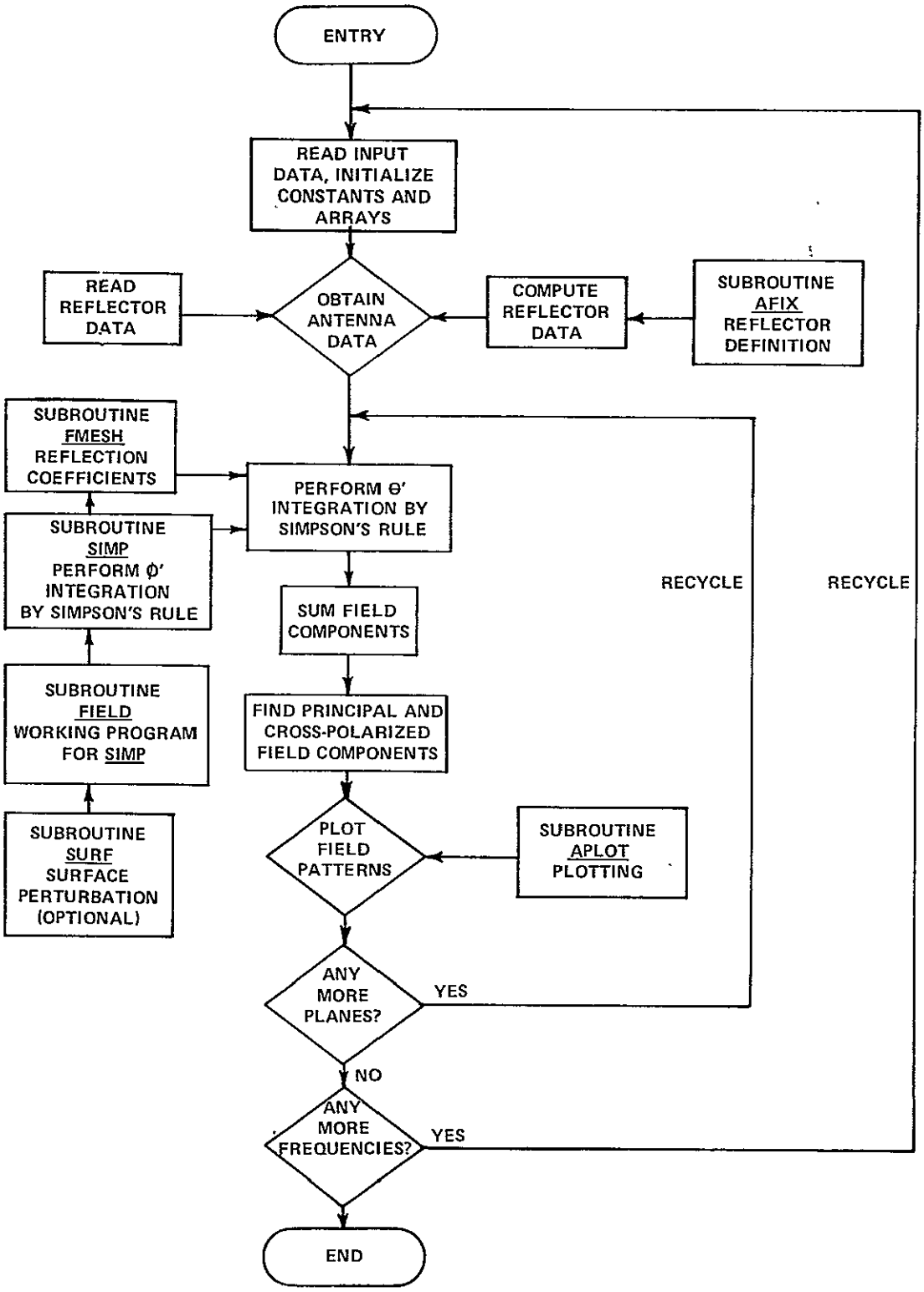

Figure 44 FUNCTIONAL FLOW, DOUBLE-INTEGRAL PROGRAM

B.5.3.2 Namelist NAM 2

N1,N2,N3 the number of integration intervals from X1 to X2, X2 to X3, and X3 to X4 (each must be even because Simpson's rule is used)

NY number of θ observation angles minus 1

NP number of ϕ observation angles minus 1

IFN number of $g_1(\theta')$'s etc. on cards; if zero, they are computed by AFIX

ISPOT print code, if equal to 1: print intermediate results; if equal to zero: no print

INFREQ number of program cycles due to frequency change

B.5.3.3 Namelist NAM 3

DOL D/λ ratio (diameter/wavelength)

FOD F/D ratio (focal length/diameter)

L1,L2 determine the number of integration intervals in the ϕ' loop (must be even because Simpson's rule is used)

B.5.3.4 Namelist NAM 4

GMAX maximum dB level of plotting abscissa

GMIN minimum dB level of plotting abscissa

XMAX maximum θ value of plotting ordinate

B.5.3.5 Namelist NAM 5

TH reflector grid thickness in meters

SIG reflector grid conductivity in mho/meter

FREQ frequency if a grid is used (mHz)

SE E-plane feed phase error (Section B.4.1.4)

SH H-plane feed phase error (Section B.4.1.4)

ISC surface code, if equal to 1: perturb surface, if equal to 0: no perturbation

B.5.3.6 Namelist NAM 6 (for subroutine AFIX)

N1,N2,N3 the number of intervals for which the reflector data are to be computed from X1 to X2, X2 to X3, X3 to X4

B.5.3.7 Namelist NAM 7 (for subroutine GRID)

DPG grid ϕ' dimension (meters)

DTG grid θ' dimension (meters)

WPH grid ϕ' spacing (meters)

WTH grid θ' spacing (meters)

B.5.3.8 Namelist NAM 8 (for subroutine SURF)

ICODE the value of ICODE determines the type of surface perturbation to be used; torsion only, thermal only to torque and thermal

B.5.4 Sample Output

Figure 45 shows a typical computer output having feed phase error, a solid paraboloid reflector (no grid), surface perturbation and already available reflector data read from cards. The namelists read in the main program are printed out first, followed by reflector data. The resulting θ , ϕ , γ and ψ field components are printed as gain over isotropic in dB units as a function of each observation angle θ . The columns labeled FIRST SUM, SECOND SUM and THIRD SUM are the real and imaginary parts of the three regions of θ' integration X1 to X2, X2 to X3 and X3 to X4, respectively.

THE DOUBLE INTEGRALS

```
PARA., CONICS, TRAP. TOOTH, D/L=24,F/D=.443,SE=.308,SH=.108,DINT,PP=0
&NAM1
Y1= 0.0           ,DY= 0.25000000    ,X1=  2.1140194    ,X2=  2.6223793    ,X3=  2.7239494    ,X4=  3.1415892    ,PI=
  90.000000    ,DP= 0.0
&END
&NAM2
N1=          44,N2=          12,N3=          40,NY=          60,NP=           0,IFN=          97,ISPOT=           1,IFREQ=
&END
&NAM3
DOL=  24.000000    ,FOD= 0.44299996    ,L1=           6,L2=          10
&END
&NAM4
GMAX=  45.000000    ,GMIN= -30.000000    ,XMAX=  15.000000
&END
&NAM5
TH= 0.0           ,SIG= 0.0          ,FREQ=  150.00000    ,SE= 0.99999964E-01,SH=-0.99999964E-01,IFEED=           1,ISC=
&END

THE F(X) FUNCTION FOLLOWS

  -0.1712083E 01   -0.1723206E 01   -0.1734249E 01   -0.1745214E 01   -0.1756095E 01   -0.1766891E 01   -0.1777603E 01
  -0.1788231E 01   -0.1798767E 01   -0.1809216E 01   -0.1819572E 01   -0.1829839E 01   -0.1840010E 01   -0.1850086E 01
  -0.1860065E 01   -0.1869948E 01   -0.1879733E 01   -0.1889417E 01   -0.1898995E 01   -0.1908478E 01   -0.1917851E 01
  -0.1927121E 01   -0.1936284E 01   -0.1945339E 01   -0.1954287E 01   -0.1963122E 01   -0.1971848E 01   -0.1980458E 01
  -0.1988956E 01   -0.1997340E 01   -0.2005610E 01   -0.2013760E 01   -0.2021791E 01   -0.2029704E 01   -0.2037498E 01
  -0.2045169E 01   -0.2052717E 01   -0.2060143E 01   -0.2067446E 01   -0.2074621E 01   -0.2081673E 01   -0.2088593E 01
  -0.2095389E 01   -0.2102055E 01   -0.2108591E 01   -0.2113256E 01   -0.2117769E 01   -0.2122130E 01   -0.2126341E 01
  -0.2130399E 01   -0.2134301E 01   -0.2138054E 01   -0.2141653E 01   -0.2145099E 01   -0.2148390E 01   -0.2151526E 01
  -0.2154510E 01   -0.2160891E 01   -0.2167032E 01   -0.2172939E 01   -0.2178610E 01   -0.2184042E 01   -0.2189237E 01
  -0.2194192E 01   -0.2198909E 01   -0.2203384E 01   -0.2207622E 01   -0.2211617E 01   -0.2215372E 01   -0.2218884E 01
  -0.2222156E 01   -0.2225184E 01   -0.2227971E 01   -0.2230515E 01   -0.2232818E 01   -0.2234875E 01   -0.2236689E 01
  -0.2238256E 01   -0.2239591E 01   -0.2240664E 01   -0.2241502E 01   -0.2242095E 01   -0.2242442E 01   -0.2242549E 01
  -0.2242407E 01   -0.2242023E 01   -0.2241393E 01   -0.2240520E 01   -0.2239403E 01   -0.2238040E 01   -0.2236434E 01
  -0.2234584E 01   -0.2232492E 01   -0.2230156E 01   -0.2227574E 01   -0.2224752E 01   -0.2221688E 01

THE G(X) FUNCTION FOLLOWS

  -0.9661877E 00   -0.9593832E 00   -0.9524503E 00   -0.9453900E 00   -0.9382038E 00   -0.9308926E 00   -0.9234568E 00
  -0.9158977E 00   -0.9082164E 00   -0.9004143E 00   -0.8924915E 00   -0.8844495E 00   -0.8762895E 00   -0.8680125E 00
  -0.8596204E 00   -0.8511128E 00   -0.8424916E 00   -0.8337579E 00   -0.8249137E 00   -0.8159586E 00   -0.8068945E 00
  -0.7977228E 00   -0.7884454E 00   -0.7790620E 00   -0.7695745E 00   -0.7599844E 00   -0.7502927E 00   -0.7405018E 00
  -0.7306111E 00   -0.7206230E 00   -0.7105387E 00   -0.7003604E 00   -0.6900877E 00   -0.6797229E 00   -0.6692674E 00
  -0.6587234E 00   -0.6480907E 00   -0.6373714E 00   -0.6265669E 00   -0.6156790E 00   -0.6047097E 00   -0.5936587E 00
  -0.5825286E 00   -0.5713207E 00   -0.5600370E 00   -0.5421703E 00   -0.5242628E 00   -0.5063176E 00   -0.4883364E 00
  -0.4703220E 00   -0.4522719E 00   -0.4341894E 00   -0.4160759E 00   -0.3979344E 00   -0.3797676E 00   -0.3615634E 00
  -0.6221793E 00   -0.5996510E 00   -0.5770571E 00   -0.5544004E 00   -0.5316834E 00   -0.5089082E 00   -0.4860780E 00
  -0.4631943E 00   -0.4402602E 00   -0.4172782E 00   -0.3942508E 00   -0.3711803E 00   -0.3480694E 00   -0.3249204E 00
  -0.3017362E 00   -0.2785189E 00   -0.2552715E 00   -0.2319961E 00   -0.2086955E 00   -0.1853719E 00   -0.1620284E 00
  -0.1386670E 00   -0.1152905E 00   -0.9190184E-01   -0.6850260E-01   -0.4509640E-01   -0.2169493E-01   0.1728783E-02
   0.2514237E-01    0.4855304E-01    0.7195860E-01    0.9535635E-01    0.1187437E 00    0.1421180E 00    0.1654767E 00
   0.1888173E 00    0.2121376E 00    0.2354348E 00    0.2587062E 00    0.2819493E 00    0.3051620E 00

THE INDEPENDENT VARIABLE OF F(X),G(X)

   0.2114029E 01    0.2125582E 01    0.2137136E 01    0.2148689E 01    0.2160242E 01    0.2171794E 01    0.2183350E 01
   0.2194902E 01    0.2206456E 01    0.2218010E 01    0.2229564E 01    0.2241117E 01    0.2252670E 01    0.2264224E 01
   0.2275778E 01    0.2287332E 01    0.2298884E 01    0.2310439E 01    0.2321992E 01    0.2333546E 01    0.2345098E 01
   0.2356652E 01    0.2368205E 01    0.2379760E 01    0.2391314E 01    0.2402865E 01    0.2414420E 01    0.2425974E 01
   0.2437528E 01    0.2449080E 01    0.2460634E 01    0.2472188E 01    0.2483742E 01    0.2495296E 01    0.2506848E 01
   0.2518401E 01    0.2529956E 01    0.2541510E 01    0.2553062E 01    0.2564616E 01    0.2576170E 01    0.2587724E 01
   0.2599277E 01    0.2610830E 01    0.2622384E 01    0.2630949E 01    0.2639314E 01    0.2647779E 01    0.2656242E 01
   0.2664706E 01    0.2673172E 01    0.2681637E 01    0.2690102E 01    0.2698565E 01    0.2707029E 01    0.2715494E 01
   0.2723960E 01    0.2734401E 01    0.2744842E 01    0.2755281E 01    0.2765722E 01    0.2776163E 01    0.2786605E 01
   0.2797046E 01    0.2807487E 01    0.2817926E 01    0.2828367E 01    0.2838808E 01    0.2849250E 01    0.2859691E 01
   0.2870131E 01    0.2880571E 01    0.2891012E 01    0.2901454E 01    0.2911895E 01    0.2922336E 01    0.2932775E 01
   0.2943216E 01    0.2953657E 01    0.2964099E 01    0.2974540E 01    0.2984981E 01    0.2995420E 01    0.3005861E 01
   0.3016302E 01    0.3026744E 01    0.3037185E 01    0.3047626E 01    0.3058065E 01    0.3068506E 01    0.3078947E 01
   0.3089389E 01    0.3099830E 01    0.3110271E 01    0.3120710E 01    0.3131151E 01    0.3141593E 01
```

Figure 45 COMPUTER PRINTOUT, DOUBLE-INTEGRAL PROGRAM (SHEET 1 OF 3)

THE VALU OF P= 0.8999994E 02

0.8999994E 02 PARA., CONICS, TRAP. TOOTH, D/L=24,F/D=.443,SE=.308,SH=.108,DINT,PP=0

THETA	FIRST SUM		SECOND SUM		THIRD SUM		THETA C (DB)	PHI C (DB)	GAMMA C (DB)	PSI C (DB)
0.0	-0.105E 01	0.715E 00	0.633E-02	-0.545E-01	0.411E-01	0.205E-01	-0.100E 01	0.790E 00	0.211E 01	0.211E 01
0.0	=0.650E-01	-0.105E 02	0.243E 00	-0.471E 00	-0.210E 01	0.342E 01	-0.192E 01	-0.751E 01	0.178E 02	0.178E 02
0.25	-0.943E 00	0.644E 00	0.877E-02	0.582E-01	0.418E-01	0.177E-01	-0.893E 00	0.720E 00	0.119E 01	0.119E 01
0.25	-0.478E-01	-0.116E 02	0.258E 00	-0.361E 00	-0.213E 01	0.328E 01	-0.192E 01	-0.869E 01	0.190E 02	0.190E 02
0.50	-0.797E 00	0.566E 00	0.116E-01	0.612E-01	0.425E-01	0.146E-01	-0.743E 00	0.642E 00	-0.164E 00	-0.164E 00
0.50	-0.219E 00	-0.124E 02	0.274E 00	-0.240E 00	-0.213E 01	0.313E 01	-0.208E 01	-0.951E 01	0.198E 02	0.198E 02
0.75	-0.615E 00	0.484E 00	0.148E-01	0.636E-01	0.429E-01	0.113E-01	-0.557E 00	0.559E 00	-0.206E 01	-0.206E 01
0.75	-0.570E 00	-0.128E 02	0.293E 00	-0.112E 00	-0.212E 01	0.298E 01	-0.240E 01	-0.992E 01	0.202E 02	0.202E 02
1.00	-0.408E 00	0.399E 00	0.182E-01	0.654E-01	0.433E-01	0.780E-02	-0.346E 00	0.473E 00	-0.464E 01	-0.464E 01
1.00	-0.108E 01	-0.127E 02	0.316E 00	0.210E-01	-0.210E 01	0.282E 01	-0.286E 01	-0.988E 01	0.202E 02	0.202E 02
1.25	-0.119E 00	0.104E 00	-0.263E-01	0.511E-01	0.303E-01	-0.328E-02	-0.115E 00	0.152E 00	-0.144E 02	-0.144E 02
1.25	-0.617E 00	-0.107E 02	0.332E 00	0.108E 01	-0.297E 01	0.241E 01	-0.326E 01	-0.725E 01	0.180E 02	0.180E 02
1.50	0.493E-01	0.777E-01	-0.274E-01	0.517E-01	0.297E-01	-0.659E-02	0.516E-01	0.123E 00	-0.175E 02	-0.175E 02
1.50	-0.157E 01	-0.975E 01	0.315E 00	0.119E 01	-0.295E 01	0.229E 01	-0.420E 01	-0.627E 01	0.176E 02	0.176E 02
1.75	0.215E 00	0.639E-01	-0.279E-01	0.521E-01	0.290E-01	-0.994E-02	0.216E 00	0.106E 00	-0.124E 02	-0.124E 02
1.75	-0.255E 01	-0.839E 01	0.302E 00	0.130E 01	-0.290E 01	0.217E 01	-0.515E 01	-0.492E 01	0.170E 02	0.170E 02
2.00	0.370E 00	0.609E-01	-0.276E-01	0.522E-01	0.282E-01	-0.133E-01	0.370E 00	0.998E-01	-0.832E 01	-0.832E 01
2.00	-0.347E 01	-0.671E 01	0.295E 00	0.139E 01	-0.284E 01	0.205E 01	-0.602E 01	-0.327E 01	0.167E 02	0.167E 02
2.25	0.507E 00	0.667E-01	-0.268E-01	0.521E-01	0.271E-01	-0.166E-01	0.508E 00	0.102E 00	-0.572E 01	-0.572E 01
2.25	-0.429E 01	-0.482E 01	0.293E 00	0.147E 01	-0.277E 01	0.193E 01	-0.676E 01	-0.142E 01	0.168E 02	0.168E 02
2.50	0.621E 00	0.786E-01	-0.253E-01	0.518E-01	0.259E-01	-0.199E-01	0.621E 00	0.110E 00	-0.400E 01	-0.400E 01
2.50	-0.493E 01	-0.283E 01	0.298E 00	0.153E 01	-0.268E 01	0.181E 01	-0.731E 01	0.510E 00	0.173E 02	0.173E 02
2.75	0.705E 00	0.932E-01	-0.233E-01	0.513E-01	0.246E-01	-0.231E-01	0.706E 00	0.121E 00	-0.290E 01	-0.290E 01
2.75	-0.535E 01	-0.852E 00	0.308E 00	0.157E 01	-0.257E 01	0.168E 01	-0.761E 01	0.241E 01	0.180E 02	0.180E 02
3.00	0.756E 00	0.107E 00	-0.209E-01	0.505E-01	0.230E-01	-0.263E-01	0.758E 00	0.132E 00	-0.227E 01	-0.227E 01
3.00	-0.552E 01	0.994E 00	0.323E 00	0.159E 01	-0.245E 01	0.156E 01	-0.765E 01	0.414E 01	0.188E 02	0.188E 02
3.25	0.772E 00	0.118E 00	-0.180E-01	0.495E-01	0.213E-01	-0.292E-01	0.776E 00	0.138E 00	-0.207E 01	-0.207E 01
3.25	-0.541E 01	0.260E 01	0.341E 00	0.159E 01	-0.232E 01	0.143E 01	-0.739E 01	0.562E 01	0.194E 02	0.194E 02
3.50	0.754E 00	0.122E 00	-0.148E-01	0.483E-01	0.194E-01	-0.321E-01	0.758E 00	0.138E 00	-0.226E 01	-0.226E 01
3.50	-0.503E 01	0.387E 01	0.363E 00	0.155E 01	-0.218E 01	0.130E 01	-0.685E 01	0.673E 01	0.196E 02	0.196E 02
3.75	0.586E 00	0.144E 00	-0.277E-02	0.316E-01	0.201E-01	-0.345E-01	0.604E 00	0.141E 00	-0.415E 01	-0.415E 01
3.75	-0.559E 01	0.253E 01	-0.149E 00	-0.389E 00	-0.199E 01	0.141E 01	-0.773E 01	0.356E 01	0.186E 02	0.186E 02
4.00	0.475E 00	0.128E 00	-0.415E-02	0.291E-01	0.186E-01	-0.374E-01	0.490E 00	0.119E 00	-0.595E 01	-0.595E 01
4.00	-0.499E 01	0.273E 01	-0.185E 00	-0.553E 00	-0.179E 01	0.128E 01	-0.696E 01	0.346E 01	0.178E 02	0.178E 02
4.25	0.342E 00	0.106E 00	-0.550E-02	0.266E-01	0.169E-01	-0.402E-01	0.354E 00	0.920E-01	-0.874E 01	-0.874E 01
4.25	-0.419E 01	0.248E 01	-0.226E 00	-0.729E 00	-0.157E 01	0.114E 01	-0.599E 01	0.289E 01	0.165E 02	0.165E 02
4.50	0.194E 00	0.779E-01	-0.682E-02	0.241E-01	0.151E-01	-0.427E-01	0.203E 00	0.592E-01	-0.135E 02	-0.135E 02
4.50	-0.325E 01	0.180E 01	-0.272E 00	-0.913E 00	-0.136E 01	0.994E 00	-0.488E 01	0.188E 01	0.144E 02	0.144E 02
4.75	0.384E-01	0.448E-01	-0.811E-02	0.216E-01	0.131E-01	-0.450E-01	0.434E-01	0.214E-01	-0.263E 02	-0.263E 02
4.75	-0.223E 01	0.739E 00	-0.326E 00	-0.110E 01	-0.114E 01	0.838E 00	-0.370E 01	0.474E 00	0.114E 02	0.114E 02
5.00	-0.118E 00	0.698E-02	-0.936E-02	0.193E-01	0.110E-01	-0.471E-01	-0.116E 00	-0.208E-01	-0.186E 02	-0.186E 02
5.00	-0.120E 01	-0.623E 00	-0.387E 00	-0.129E 01	-0.921E 00	0.672E 00	-0.251E 01	-0.124E 01	0.894E 01	0.894E 01
5.25	-0.267E 00	-0.348E-01	-0.106E-01	0.171E-01	0.874E-02	-0.489E-01	-0.269E 00	-0.666E-01	-0.111E 02	-0.111E 02
5.25	-0.220E 00	-0.219E 01	-0.457E 00	-0.148E 01	-0.704E 00	0.497E 00	-0.138E 01	-0.317E 01	0.108E 02	0.108E 02
5.50	-0.403E 00	-0.794E-01	-0.117E-01	0.151E-01	0.640E-02	-0.505E-01	-0.408E 00	-0.115E 00	-0.746E 01	-0.746E 01
5.50	0.649E 00	-0.384E 01	-0.536E 00	-0.167E 01	-0.493E 00	0.313E 00	-0.380E 00	-0.520E 01	0.143E 02	0.143E 02
5.75	-0.518E 00	-0.126E 00	-0.128E-01	0.132E-01	0.397E-02	-0.518E-01	-0.527E 00	-0.164E 00	-0.516E 01	-0.516E 01
5.75	0.136E 01	-0.546E 01	-0.625E 00	-0.184E 01	-0.289E 00	0.121E 00	0.444E 00	-0.718E 01	0.171E 02	0.171E 02
6.00	-0.409E 00	-0.344E 00	0.371E-01	0.207E-02	0.128E-02	-0.554E-01	-0.371E 00	-0.397E 00	-0.530E 01	-0.530E 01
6.00	0.183E 01	-0.491E 01	-0.515E 00	-0.964E 00	0.164E 00	-0.105E 01	0.148E 01	-0.692E 01	0.170E 02	0.170E 02
6.25	-0.450E 00	-0.385E 00	0.381E-01	-0.370E-02	-0.164E-02	-0.559E-01	-0.413E 00	-0.444E 00	-0.434E 01	-0.434E 01
6.25	0.187E 01	-0.598E 01	-0.635E 00	-0.118E 01	0.296E 00	-0.123E 01	0.153E 01	-0.839E 01	0.186E 02	0.186E 02
6.50	-0.463E 00	-0.421E 00	0.384E-01	-0.939E-02	-0.453E-02	-0.560E-01	-0.429E 00	-0.486E 00	-0.376E 01	-0.376E 01
6.50	0.171E 01	-0.674E 01	-0.770E 00	-0.139E 01	0.415E 00	-0.142E 01	0.135E 01	-0.955E 01	0.197E 02	0.197E 02
6.75	-0.449E 00	-0.451E 00	0.382E-01	-0.149E-01	-0.737E-02	-0.559E-01	-0.418E 00	-0.522E 00	-0.350E 01	-0.350E 01
6.75	0.138E 01	-0.716E 01	-0.920E 00	-0.158E 01	0.519E 00	-0.162E 01	0.979E 00	-0.104E 02	0.203E 02	0.203E 02
7.00	-0.409E 00	-0.474E 00	0.373E-01	-0.202E-01	-0.101E-01	-0.554E-01	-0.382E 00	-0.550E 00	-0.349E 01	-0.349E 01
7.00	0.925E 00	-0.720E 01	-0.108E 01	-0.176E 01	0.606E 00	-0.181E 01	0.448E 00	-0.108E 02	0.207E 02	0.207E 02
7.25	-0.349E 00	-0.489E 00	0.358E-01	-0.253E-01	-0.128E-01	-0.547E-01	-0.326E 00	-0.569E 00	-0.367E 01	-0.367E 01
7.25	0.389E 00	-0.689E 01	-0.126E 01	-0.191E 01	0.676E 00	-0.200E 01	-0.191E 00	-0.108E 02	0.207E 02	0.207E 02
7.50	-0.272E 00	-0.496E 00	0.338E-01	-0.299E-01	-0.153E-01	-0.536E-01	-0.259E 00	-0.580E 00	-0.398E 01	-0.398E 01

Figure 45 COMPUTER PRINTOUT, DOUBLE-INTEGRAL PROGRAM (SHEET 2 OF 3)

7.50	-0.175E 00	-0.623E 01	-0.144E 01	-0.204E 01	0.727E 00	-0.219E 01	-0.887E 00	-0.105E 02	0.204E 02	0.204E 02
7.75	-0.183E 00	-0.495E 00	0.312E-01	-0.341E-01	-0.176E-01	-0.523E-01	-0.170E 00	-0.582E 00	-0.435E 01	-0.435E 01
7.75	-0.718E 00	-0.531E 01	-0.163E 01	-0.214E 01	0.759E 00	-0.237E 01	-0.159E 01	-0.982E 01	0.200E 02	0.200E 02
8.00	-0.898E-01	-0.486E 00	0.281E-01	-0.379E-01	-0.198E-01	-0.508E-01	-0.815E-01	-0.575E 00	-0.472E 01	-0.472E 01
8.00	-0.120E 01	-0.417E 01	-0.182E 01	-0.221E 01	0.770E 00	-0.255E 01	-0.225E 01	-0.893E 01	0.193E 02	0.193E 02
8.25	0.310E-02	-0.470E 00	0.245E-01	-0.411E-01	-0.218E-01	-0.491E-01	0.586E-02	-0.560E 00	-0.503E 01	-0.503E 01
8.25	-0.159E 01	-0.292E 01	-0.201E 01	-0.224E 01	0.760F 00	-0.272E 01	-0.283E 01	-0.789E 01	0.185E 02	0.185E 02
8.50	0.392E-01	-0.322E 00	0.119E-01	-0.200E-01	-0.207E-01	-0.437E-01	0.305E-01	-0.386E 00	-0.825E 01	-0.825E 01
8.50	-0.282E 01	-0.169E 01	-0.150E 01	-0.210E 01	0.414E 00	-0.196E 01	-0.391E 01	-0.575E 01	0.168F 02	0.168E 02
8.75	0.134E 00	-0.310E 00	0.115E-01	-0.225E-01	-0.218E-01	-0.417E-01	0.124E 00	-0.374E 00	-0.808E 01	-0.808E 01
8.75	-0.303E 01	-0.568E 00	-0.160E 01	-0.205E 01	0.405E 00	-0.211E 01	-0.422E 01	-0.473E 01	0.160E 02	0.160E 02
9.00	0.213E 00	-0.294E 00	0.108E-01	-0.249E-01	-0.227E-01	-0.397E-01	0.202E 00	-0.359E 00	-0.771E 01	-0.771E 01
9.00	-0.310E 01	0.424E 00	-0.169E 01	-0.197E 01	0.376E 00	-0.226E 01	-0.441F 01	-0.380E 01	0.153E 02	0.153E 02
9.25	0.273E 00	-0.275E 00	0.998F-02	-0.271E-01	-0.233E-01	-0.376E-01	0.260E 00	-0.340E 00	-0.737E 01	-0.737E 01
9.25	-0.305E 01	0.123E 01	-0.176E 01	-0.187E 01	0.329E 00	-0.238E 01	-0.448E 01	-0.302E 01	0.147E 02	0.147E 02
9.50	0.312E 00	-0.253E 00	0.894F-02	-0.290E-01	-0.237E-01	-0.355E-01	0.297E 00	-0.317E 00	-0.724E 01	-0.724E 01
9.50	-0.292E 01	0.180E 01	-0.181E 01	-0.175E 01	0.263F 00	-0.250E 01	-0.447E 01	-0.244E 01	0.141E 02	0.141E 02
9.75	0.329E 00	-0.227E 00	0.772E-02	-0.308E-01	-0.239F-01	-0.334E-01	0.313E 00	-0.291E 00	-0.739E 01	-0.739E 01
9.75	-0.271E 01	0.213F 01	-0.184E 01	-0.160E 01	0.181E 00	-0.260E 01	-0.438E 01	-0.207E 01	0.137E 02	0.137E 02
10.00	0.325E 00	-0.198E 00	0.634E-02	-0.324F-01	-0.239F-01	-0.314E-01	0.308E 00	-0.261E 00	-0.788E 01	-0.788F 01
10.00	-0.248E 01	0.221E 01	-0.186E 01	-0.145E 01	0.828E-01	-0.268E 01	-0.425E 01	-0.192F 01	0.134F 02	0.134E 02
10.25	0.303E 00	-0.166E 00	0.481E-02	-0.337E-01	-0.237E-01	-0.295E-01	0.284E 00	-0.229E 00	-0.875E 01	-0.875E 01
10.25	-0.223E 01	0.206E 01	-0.184E 01	-0.128E 01	-0.291E-01	-0.275E 01	-0.410E 01	-0.196E 01	0.132F 02	0.132E 02
10.50	0.266E 00	-0.133E 00	0.313E-02	-0.349E-01	-0.233E-01	-0.277F-01	0.245E 00	-0.196F 00	-0.101E 02	-0.101E 02
10.50	-0.200E 01	0.173F 01	-0.181E 01	-0.110F 01	-0.153E 00	-0.279E 01	-0.396E 01	-0.217E 01	0.131F 02	0.131E 02
10.75	0.217E 00	-0.993E-01	0.137E-02	-0.358E-01	-0.228E-01	-0.260E-01	0.195F 00	-0.161E 00	-0.119E 02	-0.119E 02
10.75	-0.180E 01	0.125E 01	-0.175E 01	-0.919E 00	-0.287E 00	-0.282E 01	-0.383E 01	-0.249E 01	0.132E 02	0.132E 02
11.00	0.156E 00	-0.120E 00	-0.761E-02	-0.500E-01	-0.234E-01	-0.251E-01	0.125E 00	-0.195F 00	-0.127E 02	-0.127E 02
11.00	-0.430E 00	0.211E 01	-0.168E 01	-0.369F 00	-0.492F 00	-0.332F 01	-0.260E 01	-0.157E 01	0.965E 01	0.965E 01
11.25	0.112E 00	-0.772E-01	-0.107E-01	-0.493E-01	-0.229E-01	-0.236E-01	0.779E-01	-0.150E 00	-0.154E 02	-0.154E 02
11.25	-0.394E 00	0.130E 01	-0.152E 01	-0.172E 00	-0.674F 00	-0.329E 01	-0.259E 01	-0.217E 01	0.106E 02	0.106E 02
11.50	0.635F-01	-0.368E-01	-0.137E-01	-0.483E-01	-0.224E-01	-0.222F-01	0.274E-01	-0.107F 00	-0.191E 02	-0.191E 02
11.50	-0.403E 00	0.470E 00	-0.134E 01	0.956E-02	-0.857E 00	-0.325E 01	-0.760E 01	-0.277E 01	0.116E 02	0.116E 02
11.75	0.155E-01	-0.616E-03	-0.164E-01	-0.470F-01	-0.219E-01	-0.210E-01	-0.230E-01	-0.687E-01	-0.228E 02	-0.228E 02
11.75	-0.438E 00	-0.317F 00	-0.115E 01	0.173E 00	-0.104E 01	-0.318E 01	-0.263E 01	-0.332E 01	0.125E 02	0.125E 02
12.00	-0.296E-01	0.299E-01	-0.194E-01	-0.455F-01	-0.214E-01	-0.200E-01	-0.704E-01	-0.355E-01	-0.221E 02	-0.221E 02
12.00	-0.478E 00	-0.107E 01	-0.945E 00	0.314E 00	-0.122E 01	-0.308E 01	-0.264E 01	-0.378F 01	0.133E 02	0.133E 02
12.25	-0.696E-01	0.536E-01	-0.220E-01	-0.437E-01	-0.209E-01	-0.191E-01	-0.112E 00	-0.913E-02	-0.190E 02	-0.190E 02
12.25	-0.499E 00	-0.159F 01	-0.736F 00	0.431E 00	-0.139E 01	-0.296E 01	-0.263E 01	-0.412E 01	0.138E 02	0.138E 02
12.50	-0.103E 00	0.696E-01	-0.246F-01	-0.416E-01	-0.204F-01	-0.183E-01	-0.148E 00	0.961E-02	-0.166E 02	-0.166E 02
12.50	-0.482E 00	-0.203F 01	-0.523E 00	0.523E 00	-0.155E 01	-0.281E 01	-0.256E 01	-0.431E 01	0.140E 02	0.140E 02
12.75	-0.128E 00	0.771E-01	-0.269E-01	-0.394F-01	-0.201E-01	-0.177E-01	-0.175F 00	0.201E-01	-0.151E 02	-0.151E 02
12.75	-0.414E 00	-0.232F 01	-0.315E 00	0.588E 00	-0.170E 01	-0.264F 01	-0.243E 01	-0.437E 01	0.140E 02	0.140E 02
13.00	-0.145E 00	0.761E-01	-0.291F-01	-0.369E-01	-0.199E-01	-0.172E-01	-0.194E 00	0.221E-01	-0.142F 02	-0.142E 02
13.00	-0.289E 00	-0.247E 01	-0.114E 00	0.628E 00	-0.184E 01	-0.246E 01	-0.724E 01	-0.430E 01	0.137E 02	0.137E 02
13.25	-0.166E 00	0.122F 00	-0.322E-01	-0.327E-01	-0.228E-01	-0.157F-01	-0.221E 00	0.740F-01	-0.126E 02	-0.126E 02
13.25	-0.505E-01	-0.227E 01	-0.598E 00	0.529E 00	-0.172E 01	-0.202E 01	-0.237E 01	-0.377E 01	0.130E 02	0.130E 02
13.50	-0.148E 00	0.920E-01	-0.340E-01	-0.298E-01	-0.230E-01	-0.150F-01	-0.205F 00	0.472E-01	-0.135E 02	-0.135E 02
13.50	0.197F 00	-0.222E 01	-0.394E 00	0.545E 00	-0.179F 01	-0.183E 01	-0.198E 01	-0.351E 01	0.121F 02	0.121E 02
13.75	-0.125E 00	0.549E-01	-0.356E-01	-0.266E-01	-0.232E-01	-0.142F-01	-0.184F 00	0.140E-01	-0.147E 02	-0.147E 02
13.75	0.425E 00	-0.214F 01	-0.203F 00	0.538F 00	-0.183F 01	-0.163E 01	-0.161E 01	-0.323F 01	0.112E 02	0.112E 02
14.00	-0.988E-01	0.133E-01	-0.369E-01	-0.232F-01	-0.236E-01	-0.135E-01	-0.159F 00	-0.233E-01	-0.159E 02	-0.159E 02
14.00	0.611F 00	-0.203E 01	-0.272E-01	0.510E 00	-0.186E 01	-0.143E 01	-0.128E 01	-0.295F 01	0.102E 02	0.102E 02
14.25	-0.726E-01	-0.302E-01	-0.379E-01	-0.195E-01	-0.242E-01	-0.126E-01	-0.135E 00	-0.623E-01	-0.166E 02	-0.166E 02
14.25	0.739E 00	-0.191E 01	0.129E 00	0.463F 00	-0.187E 01	-0.123E 01	-0.100E 01	-0.268E 01	0.913F 01	0.913E 01
14.50	-0.481E-01	-0.730E-01	-0.385E-01	-0.157E-01	-0.248F-01	-0.116E-01	-0.111E 00	-0.100E 00	-0.165E 02	-0.165E 02
14.50	0.795E 00	-0.178F 01	0.263E 00	0.402E 00	-0.186E 01	-0.103E 01	-0.803E 00	-0.241E 01	0.808E 01	0.808E 01
14.75	-0.267E-01	-0.113E 00	-0.387E-01	-0.116E-01	-0.255E-01	-0.104E-01	-0.909F-01	-0.135E 00	-0.158F 02	-0.158E 02
14.75	0.773E 00	-0.163E 01	0.372E 00	0.331F 00	-0.183E 01	-0.837E 00	-0.687E 00	-0.213E 01	0.700E 01	0.700E 01
15.00	-0.935E-02	-0.147F 00	-0.385E-01	-0.746E-02	-0.263E-01	-0.901E-02	-0.741F-01	-0.163E 00	-0.149E 02	-0.149E 02
15.00	0.676E 00	-0.145F 01	0.455E 00	0.255E 00	-0.179E 01	-0.651F 00	-0.655E 00	-0.185E 01	0.584E 01	0.584F 01

Figure 45. COMPUTER PRINTOUT, DOUBLE-INTEGRAL PROGRAM (SHEET 3 OF 3)

Appendix C
APERTURE BLOCKAGE AND FEED SCATTERING

The aperture blockage theory used in Section 4.5 is subject to criticism, because it relies heavily on geometric optic concepts, and it considers the power intercepted by the feed as being absorbed rather than scattered. A more complete theory would employ the scattering pattern of the feed. However, the scattering properties of log-periodic antennas are generally unknown at present and would be very difficult to theoretically calculate. As an approximation to scattering by the feed, the scattering of a shorted half-wave dipole will be used. This analysis should provide a reasonable estimate of the scattering from a log-periodic feed, as only a few active half-wave elements are present at a given frequency [10]. At high frequencies, the longer log-periodic antenna elements may be active scatterers in the $1.5\text{-}\lambda$, $2.5\text{-}\lambda$, $3.5\text{-}\lambda$, etc. mode. However, the scattering cross section of wire elements in these modes is only slightly larger than the cross section of a $0.5\text{-}\lambda$ long wire [42]. The half-wave dipole scattering is admittedly less applicable to log-periodic antenna scattering as frequency increases, but it will be shown that half-wave dipole scattering decreases with increasing frequency, so the error involved would have to be very large to make high-frequency scattering as severe as low-frequency scattering.

Consider the LOFT as a transmitting antenna. The Poynting vector power density S at the focal point of the parabolic reflector is:

$$S = \frac{P_t G_f}{4\pi F^2}$$

where

P_t = transmitter power

G_f = log-periodic feed gain

F = reflector focal distance

Therefore, the power P_d received by a matched half-wave dipole placed at the focal point is

$$P_d = \frac{S\lambda^2 G_d}{4\pi} = P_t G_f G_d \left(\frac{\lambda}{4\pi F}\right)^2$$

where

G_d = gain of half-wave dipole ($G_r = 1.64$)

λ = wavelength

The power density scattered into the far-field S_d by a shorted half-wave dipole at the focal point is

$$S_d = 4\left(\frac{P_d G_d}{4\pi R^2}\right)\left[\frac{\cos\left(\frac{\pi}{2}\sin\theta\right)}{\cos\theta}\right]^2$$

where

R = range to far-field observation point

θ = polar angle measured from the reflector axis

The factor 4 in the numerator arises because the current induced in a shorted half-wave is twice that for a matched half-wave dipole, and scattered power is proportional to the square of the induced dipole current. The term involving θ is the power pattern of a half-wave dipole.

The far-field power density S_i of an isotropic radiator with transmitter power P_t is

$$S_i = \frac{P_t}{4\pi R^2}$$

Therefore, the scattered power density relative to isotropic at $\theta = 0°$ is

$$\frac{S_d}{S_i} = \frac{4 G_d P_d}{P_t} = 4 G_f G_d^2 \left(\frac{\lambda}{4\pi F}\right)^2$$

Substituting

G_f = 9.1, gain of trapezoidal tooth feed

G_d = 1.64, gain of half-wave dipole

$$\frac{S_d}{S_i} = 0.623 \left(\frac{\lambda}{F}\right)^2$$

S_d / S_i in dB as a function of frequency and F/D ratio for a 100-meter reflector (D = 100) is tabulated below:

Scattered Power Relative to Isotropic (dB)

Frequency (MHz)	F/D RATIO		
	0.3	0.4	0.5
15	- 5.6	- 8.1	-10.0
30	-11.6	-14.1	-16.0
72	-19.2	-21.7	-23.6
150	-25.6	-28.1	-30.0

The trapezoidal tooth feed has a gain of 9.6 dB relative to isotropic. Assuming a front/back ratio of 10 to 15 dB for the feed pattern [10], the direct radiation of the feed in the direction of the LOFT antenna mainlobe is -0.4 dB to -5.4 dB relative to isotropic. Therefore, direct feed radiation dominates over feed-scattered radiation computed from the half-wave dipole scattering theory, especially at higher frequencies. Thus, inclusion of an exact feed scattering theory would not be expected to significantly change the LOFT antenna far-field patterns from those presented in this report.

Appendix D

GEOMETRIC DIFFRACTION THEORY

Geometric diffraction theory (GDT) can be used to calculate the sidelobe pattern of an antenna which has a sharp-edged reflector. Sidelobe radiation is treated as an edge diffraction problem; only the incident field strength, polarization, angle of arrival at the edge, and the radius of curvature of the edge need be known. The reflector surface current distribution is not used by GDT. The advantages of using GDT over surface integral theory are: (1) GDT computations are much simpler, and (2) surface current distribution is not known with sufficient accuracy to compute sidelobe levels using surface integral theory in angular regions far from the mainlobe, due mainly to edge effects. During the course of the present investigation, it was found that the two theories yielded the same sidelobe level even in the angular region close to the mainlobe when the reflector aperture phase error was small.

GDT equations for the sidelobe level for any direction were derived. The resulting equations are complicated [43] and no significant effects were noted that cannot be covered with E- and H-plane patterns. Therefore, simplified GDT equations valid only in the E- and H-planes will be treated here.

Figure 46A shows the incident and diffracted rays relative to a perfectly conducting thin plane. The diffracted fields derived by Keller [44] are,

E-field parallel to edge

$$E_D = \frac{-E_i e^{-i\left(ks+\frac{\pi}{4}\right)}}{2\sqrt{2\pi k}\,\sqrt{s(1+s/\rho_1)}}\left[\sec\frac{1}{2}(\psi-\alpha)+\csc(\psi+\alpha)\right] \qquad \text{(D-1)}$$

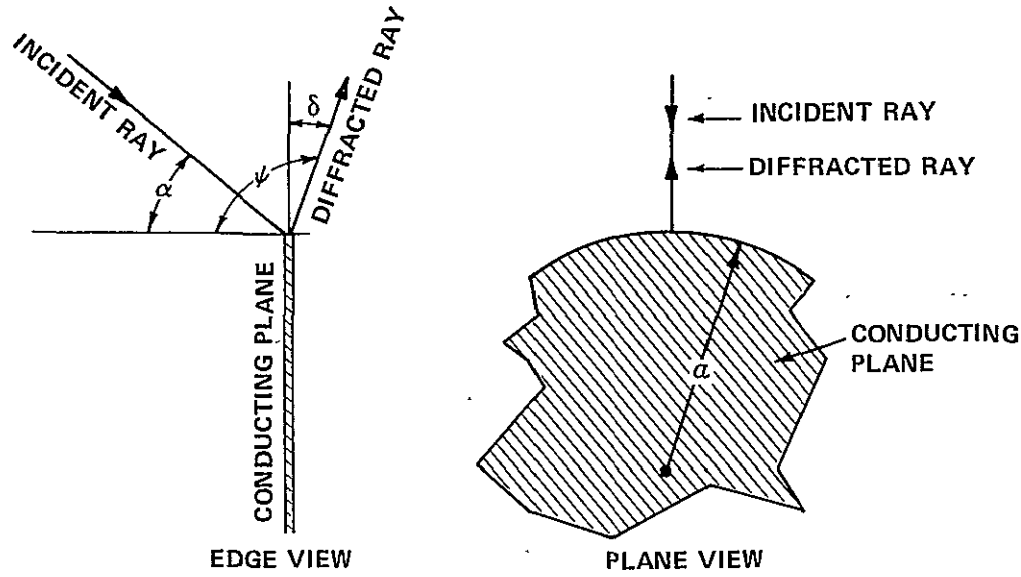

(A) KELLER'S NOTATION

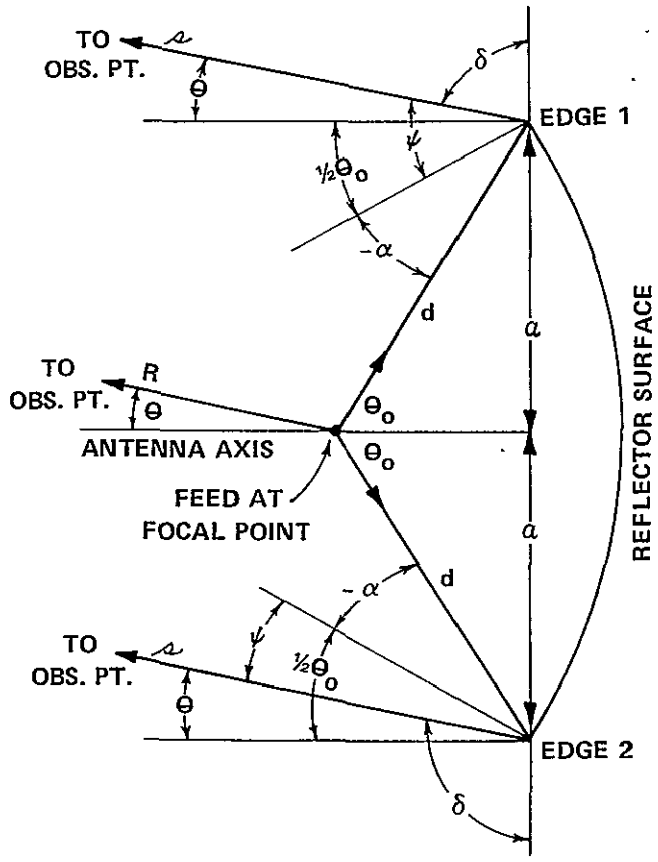

(B) PARABOLIC REFLECTOR EDGE DIFFRACTION

Figure 46 COORDINATE SYSTEM GEOMETRIC DIFFRACTION THEORY

H-field parallel to edge

$$H_D = \frac{-H_i e^{-i(ks+\frac{\pi}{4})}}{2\sqrt{2\pi k}\sqrt{s(1+s/\rho_1)}} \left[\sec\frac{1}{2}(\psi-\alpha) - \csc\frac{1}{2}(\psi+\alpha)\right] \qquad \text{(D-2)}$$

where

E_D = Diffracted electric field

H_D = Diffracted magnetic field

E_i = Incident electric field tangent to edge

H_i = Incident magnetic field tangent to edge

i = $\sqrt{-1}$

k = $\frac{2\pi}{\lambda}$, λ wavelength

s = distance from edge to far-field observation point

ψ = angle of diffracted ray (Figure 46A)

α = angle of incident ray (Figure 46A)

and

ρ_1 = $\frac{a}{\cos\delta}$

where

a = radius of curvature of edge

δ = angle between the plane of the edge and the diffracted ray.

The coordinate system for edge diffraction from a parabolic antenna is shown in Figure 46B. The far-field observation point is at range R away from the focal point, and in the angular direction θ relative to the antenna axis. The reflector has a raduis "a" and subtends an angle $2\theta_0$. Edge diffraction occurs at two diametrically opposite points on the reflector edge in the plane containing the antenna axis and the far-field observation point. The notation used in Figure 46A is also shown. The following relations are evident from Figure 46B.

Edge 1	Edge 2
$\psi = \frac{1}{2}\theta_o + \theta$	$\psi = \frac{1}{2}\theta_o - \theta$
$\alpha = -\frac{1}{2}\theta_o$	$\alpha = -\frac{1}{2}\theta_o$
$\delta = \frac{\pi}{2} - \theta$	$\delta = \frac{\pi}{2} + \theta$
$s = R + d\cos(\theta_o + \theta)$	$s = R + d\cos(\theta_o - \theta)$
$= R + d\cos\theta_o\cos\theta - a\sin\theta$	$= R + d\cos\theta_o\cos\theta + a\sin\theta$
$\sqrt{s(1+s/\rho_1)} \approx \frac{R}{\rho_1} = R\sqrt{\frac{\cos\delta}{a}} = R\sqrt{\frac{\sin\theta}{a}}$	$\sqrt{s(1+s/\rho_1)} \approx R\sqrt{\frac{\cos\delta}{a}} = -iR\sqrt{\frac{\sin\theta}{a}}$

Substituting into Equations (D-1) and (D-2).

$$E_D = \frac{-E_i\sqrt{a\lambda}}{4\pi R} D_H e^{-i\beta} \qquad \text{(D-3)}$$

$$H_D = \frac{-H_i\sqrt{a\lambda}}{4\pi R} D_E e^{-i\beta} \qquad \text{(D-4)}$$

where

$$D_E = \frac{\left[\sec\frac{1}{2}(\theta+\theta_o) + \csc\frac{1}{2}\theta\right] e^{ika\sin\theta} + \left[\sec\frac{1}{2}(\theta-\theta_o) - \csc\frac{1}{2}\theta\right] e^{-ika\sin\theta}}{\sqrt{\sin\theta}}$$

$$D_H = \frac{\left[\sec\frac{1}{2}(\theta+\theta_o) - \csc\frac{1}{2}\theta\right] e^{ika\sin\theta} + \left[\sec\frac{1}{2}(\theta-\theta_o) + \csc\frac{1}{2}\theta\right] e^{-ika\sin\theta}}{\sqrt{\sin\theta}}$$

$$\beta = kR + kd\cos\theta_o\cos\theta + \frac{\pi}{4}$$

Equations (D-3) and (D-4) give respectively the H- and E-field diffraction patterns. These equations will now be normalized to give field strength relative to the field of an isotropic radiator. Assume a transmitter with power output P_t is driving the LOFT feed. The feed field incident on the reflector edge in the H- and E-planes is

$$E_i = \sqrt{2\sqrt{\frac{\mu}{\epsilon}}\frac{P_t G_f}{4\pi d^2}} f_H(\theta_o) e^{-ikd} = \frac{\sqrt{60 P_t G_f} f_H(\theta_o)}{d} e^{-ikd} \qquad \text{(H-plane)}$$

$$H_i = \sqrt{2\sqrt{\frac{\epsilon}{\mu}}\frac{P_t G_f}{4\pi d^2}}\, f_E(\theta_o)\, e^{-ikd} = \sqrt{\frac{P_t G_f}{240\pi^2}}\,\frac{f_E(\theta_o)}{d}\, e^{-ikd} \qquad \text{(E-plane)}$$

where

G_f = feed gain

$\sqrt{\frac{\mu}{\epsilon}}$ = 120π = free-space wave impedance

$f_H(\theta_o)$ = H-plane feed field strength in directions θ_o divided by feed field strength on axis

$f_E(\theta_o)$ = E-plane feed field strength in direction θ_o divided by field strength on axis

The far-field strength of an isotropic radiator with transmitter power output P_t is,

$$E_{iso} = \sqrt{2\sqrt{\frac{\mu}{\epsilon}}\frac{P_t}{4\pi R^2}} = \frac{\sqrt{60 P_t}}{R}$$

$$H_{iso} = \sqrt{2\sqrt{\frac{\epsilon}{\mu}}\frac{P_t}{4\pi R^2}} = \frac{1}{R}\sqrt{\frac{P_t}{240\pi^2}}$$

Therefore, the diffracted field strength relative to isotropic (omitting phase term) is,

H-Plane $$\frac{E_D}{E_{iso}} = \frac{\sqrt{a\lambda}\, D_H}{4\pi R}\,\frac{\sqrt{60 P_t G_f}\, f_H(\theta_o)}{d}\,\frac{R}{\sqrt{60 P_t}} = \frac{\sin\theta_o}{4\pi}\sqrt{\frac{G_f \lambda}{a}}\, f_H(\theta_o)\, D_H \qquad \text{(D-5)}$$

E-Plane $$\frac{H_o}{H_{iso}} = \frac{\sqrt{a\lambda}\, D_E}{4\pi R}\sqrt{\frac{P_t G_f}{240\pi^2}}\,\frac{f_E(\theta_o)}{d}\, R\sqrt{\frac{240\pi^2}{P_t}} = \frac{\sin\theta_o}{4\pi}\sqrt{\frac{G_f \lambda}{a}}\, f_E(\theta_o)\, D_E \qquad \text{(D-6)}$$

For the LOFT reflector, a = 50 meters. The angle θ_o, in terms of reflector F/D ratio is,

$$\sin\theta_o = \frac{8(F/D)}{1+16(F/D)^2}$$

REFERENCES

1. William M. Robbins, Jr., "Some Preliminary Design Studies for a Very Large Orbiting Radiotelescope," Astro Research Corporation, NASA Report No. CR-573, September 1966.

2. William M. Robbins, Jr., "The Feasibility of an Orbiting 1500-Meter Radiotelescope," Astro Research Corporation, NASA Report No. CR-792, June 1967.

3. "Study of an Orbiting Low Frequency Radio Telescope," Astro Research Corporation, prepared for NASA under Contract No. NAS7-426 Mod 3, Report No. ARC-R-262, November 22, 1967.

4. H.O. Schuerch and J.M. Hedgepeth, "Large Low-Frequency Orbiting Radiotelescope," Astro Research Corporation, NASA Report No. CR-1201, October 1968.

5. Robert L. Carrel, "Analysis and Design of the Log-Periodic Dipole Antenna," University of Illinois, Urbana, Illinois, Antenna Laboratory Report No. 52, July 1961.

6. R.H. Duhamel and F.R. Ore, "Log-Periodic Feeds for Lens and Reflectors," IRE National Convention Record, Pt 1, 1959, pp. 128-137.

7. American Electronic Laboratories Catalog, AEL Model APX 1250, Crossed LP Dipole Array.

8. Claes T. Elfving, "Foreshortened Log-Periodic Dipole Array," IRE WESCON Convention Record, Pt 1, 1963.

9. P.E. Mayes and R.L. Carrel, "High Gain Log-Periodic Antennas," Tenth Annual Symposium on the U.S.A.F. Research and Development Program, University of Illinois, 1960.

10. R.H. Duhamel and F.R. Ore, "Logarithmically Periodic Antenna Designs," IRE National Convention Record, Pt 1, 1958, pp. 139-151.

11. Telephone contact with Merton Bushong, Collins Radio Company, Dallas, Texas.

12. Claes T. Elfving, "Design Criteria for Log-Periodic Antennas," IRE WESCON Convention Record, Pt 1, 1961.

13. Sam C. Kuo and Paul E. Mayes, "An Experimental Study and the Design of the Log-Periodic Zig Zag Antenna," AFAL-TR-65-328, February 1966.

14. John D. Dyson, "The Characteristics and Design of the Conical Log-Spiral Antenna," IEEE PGAP, July 1965, pp. 488-499.

15. Telephone contact with John D. Dyson, University of Illinois at Urbana, Illinois and Kenneth K. Mei, University of California at Berkley, California.

16. Carl W. Gerst and Robert A. Worden, "Helix Antennas Take Turn for Better," Electronics, 22 August 1966, pp. 100-110.

17. Telephone contact with Robert Greenaugh, Syracuse University Research Corporation, Syracuse, New York.

18. Charkamol Lumjiak, "An Experimental Study of the Quadrifilar Helical Antenna," MS in EE Thesis, Syracuse University, November 1969.

19. James J. Campbell and William R. Jones, "Impedance Characteristics of a Class of Multiconductor Transmission Lines," IEEE PGMTT, February 1969, pp. 101-107.

20. Private Communication with William R. Jones, Hughes Aircraft Company, Fullerton, California.

21. Hughes Aircraft Company Proposal for Constant Beamwidth Antenna System, FP67-14-300, 14 September 1967.

22. Anzac Electronics models JBG7750, JBH7160, HBH6850.

23. G.J. v.d. Broek and J. v.d. Vooren, "On the Reflection Properties of a Periodically Supported Metallic Wire Grating with Rectangular Mesh Showing Small Sag Due to Its Own Weight," National Lucht-En Ruimtervaartlaboratorium, TN-W, 34, National Aerospace Laboratory, The Netherlands.

24. S. Ramo and R. Whinney, Fields and Waves in Modern Radio, Second Edition, p. 237.

25. William M. Robbins, Jr., "The Feasibility of an Orbiting 1500-Meter Radiotelescope," Astro Research Corporation, NASA Report No. CR-792, June 1967, Sections 6.09 and 6.10.

26. Reference Data for Radio Engineers, ITT Handbook, Fifth Edition, p. 4-21.

27. William M. Robbins, Jr., "Spinning Parabolical Tension Networks," Astro Research Corporation, NASA Report No. CR-873, September 1967.

28. Equations for the Conic Surfaces were obtained from John Hedgepeth, Astro Research Corporation in a private communication.

29. J.A. Joseph and R.A. Pollock, "Dynamic Studies of the 50-Meter LOFT," The MacNeal-Schwendler Corporation, Los Angeles, California, Report No. MS-83, December 1969.

30. Private Communication, Dr. Hedgepeth, Astro Research Corporation.

31. E.L. Patrick, "Unmanned Low Frequency Orbiting Radio Telescope Feed Antenna Definition Study," Aero Geo Astro, Final Report, Section 7, October 1969.

32. John Ruze, "Antenna Tolerance Theory - A Review," Proc. IEEE, April 1966, pp. 633-640.

33. H.N. Kritikos, "The Extended Aperture Method for the Determination of the Shadow Region Radiation of Parabolic Reflectors," IEEE PGAP, July 1963, pp. 400-404.

34. R.H. Duhamel, et al., "Frequency Independent Conical Feeds for Lens and Reflectors," IEEE PTGAP Int. Symposium, 1968, pp. 414-418.

35. James R. Wait, "Reflection at Arbitrary Incidence from a Parallel Wire Grid," Applied Science Research Section B V4 N6, 1955, pp. 393-400, Equation 9.

36. S. Ramo and J. Whinney, Fields and Waves in Modern Radio, Second Edition, Section 12:09.

37. W.V.T. Rusch, "Scattering of a Spherical Wave by an Arbitrary Truncated Surface of Revolution," JPL Technical Report No. 32-434, May 1963.

38. W.V.T. Rusch and H.L. Strachman, "Application of a Comprehensive Computer Program to the Analysis of Axisymmetric Microwave Reflector-Antenna System," TRW Systems Group, Redondo Beach, California, presented at the 1968 NEREM meeting in Boston.

39. W.V.T. Rusch, "Scattering of an Arbitrary Spherical Wave by an Arbitrary Surface of Revolution," JPL Program Statement for Digital Computer Program 5513, September 1964.

40. A. Ludwig, "Computer Programs for Antenna Feed System Design and Analysis," JPL Technical Report No. 32-979, Volumes I and II.

41. Personal Correspondence with W.V.T. Rusch, 27 September and 3 December 1968, 9 April and 25 March 1970.

42. Roger F. Harrington, "Matrix Methods for Field Problems," Proc. IEEE, February 1967, Figure 8, p. 147.

43. J.O. Clark, "Application of Quasi-Optical Scattering Theory to a Paraboloid Antenna," Cornell Aeronautical Laboratory, Inc., Report No. UA-2707-E-1, April 1969.

44. Joseph B. Keller, "Diffraction by an Aperture," New York University, Pt 1, Report EM-92, June 1956, and Pt 2, Report EM-96, August 1956.